

AD-A087 434 UTAH UNIV. SALT LAKE CITY DEPARTMENT OF METEOROLOGY
DEVELOPMENT OF THE MICROWAVE RADIATIVE TRANSFER PROG...ETC.(U)
SEP 79 LIOU, KUO-NAN F19628-78-C-0144

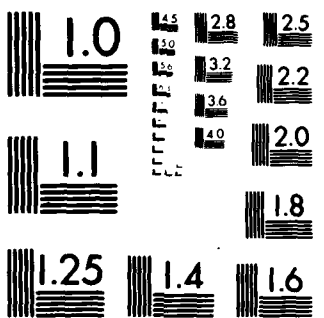
F/G 20/13

UNCLASSIFIED

PROJ. 7670 TASK 13 AFCL TR-80-0051

N/I

1 2
2 3 4 5 6 7 8 9 10 11 12 13 14 15 16 17 18 19 20 21 22 23 24 25 26 27 28 29 30 31 32 33 34 35 36 37 38 39 40 41 42 43 44 45 46 47 48 49 50 51 52 53 54 55 56 57 58 59 60 61 62 63 64 65 66 67 68 69 70 71 72 73 74 75 76 77 78 79 80 81 82 83 84 85 86 87 88 89 90 91 92 93 94 95 96 97 98 99 100



MICROCOPY RESOLUTION TEST CHART

NATIONAL BUREAU

**INVESTIGATION OF THE INFRARED INFRATE TRANSFER PHENOMENON
AND ITS APPLICATIONS TO
INFRARED SENSORS**

**John A. East, Paul T. Misko, Grant C. Aufderhaar
and Han-Young Yeh**

**Department of Meteorology
University of Utah
Salt Lake City, Utah 84112**

30 December 1979

**Final Report for Period
1 June 1978 to 30 September 1979**

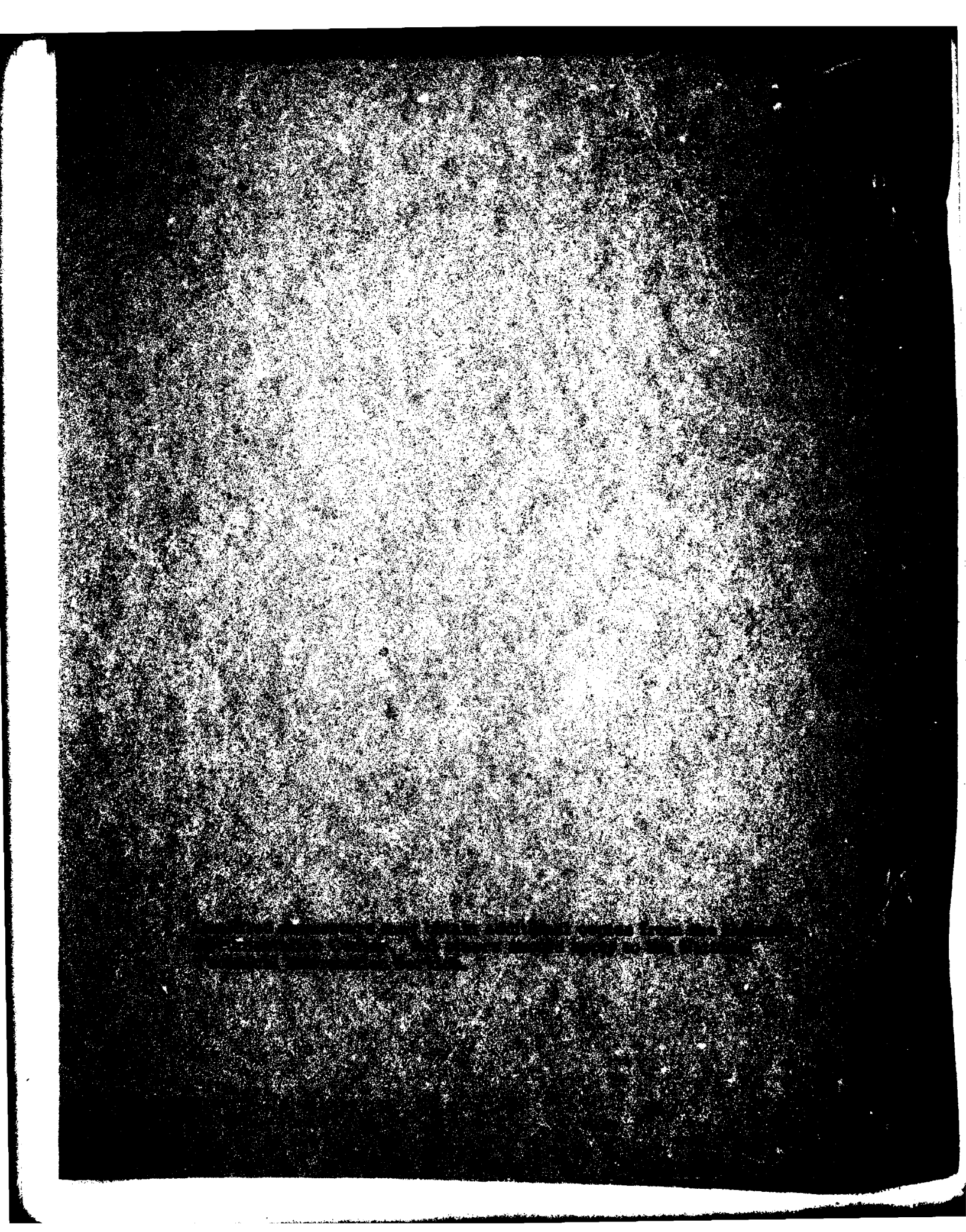
Approved for public release; distribution unlimited

AIR FORCE RESEARCH LABORATORY

RESEARCH AND TECHNOLOGY DIVISION

INFRARED SENSORS SECTION

ARL-TR-79-100



Unclassified

SECURITY CLASSIFICATION OF THIS PAGE (When Data Entered)

REPORT DOCUMENTATION PAGE		READ INSTRUCTIONS BEFORE COMPLETING FORM						
1. REPORT NUMBER AFGL-TR-80-0051	2. GOVT ACCESSION NO.	3. PECIFICNT'S CATALOG NUMBER						
4. TITLE (and Subtitle) DEVELOPMENT OF THE MICROWAVE RADIATIVE TRANSFER PROGRAM FOR CLOUDY ATMOSPHERES: APPLICATION TO DMSP SSM/T CHANNELS		5. TYPE OF REPORT & PERIOD COVERED Final Report 6/1/78 - 9/30/79						
7. AUTHOR(s) Kuo-Nan Liou, Paul T. Nipko, Grant C. AufderHaar, Hwa-Young Yeh		6. PERFORMING ORG. REPORT NUMBER F19628-78-C-0144						
9. PERFORMING ORGANIZATION NAME AND ADDRESS Department of Meteorology University of Utah Salt Lake City, Utah 84112		10. PROGRAM ELEMENT, PROJECT, TASK AREA & WORK UNIT NUMBERS 62101F 767013AA						
11. CONTROLLING OFFICE NAME AND ADDRESS Air Force Geophysics Laboratory Hanscom AFB, Massachusetts 01731 Contract Monitor: Vincent Falcone/OPI		12. REPORT DATE 30 December 1979						
		13. NUMBER OF PAGES 120						
14. MONITORING AGENCY NAME & ADDRESS (if different from Controlling Office)		15. SECURITY CLASS. (of this report) Unclassified						
		15a. DECLASSIFICATION/DOWNGRADING SCHEDULE						
16. DISTRIBUTION STATEMENT (of this Report) Approved for public release; distribution unlimited								
17. DISTRIBUTION STATEMENT (of the abstract entered in Block 20, if different from Report)								
18. SUPPLEMENTARY NOTES								
19. KEY WORDS (Continue on reverse side if necessary and identify by block number) <table style="width: 100%; border-collapse: collapse;"> <tr> <td style="width: 45%; vertical-align: top;">Microwave Radiation</td> <td style="width: 45%; vertical-align: top;">Defense Meteorological Satellite Program (DMSP)</td> </tr> <tr> <td>Remote Sensing</td> <td>Passive Microwave Temperature Sounder (SSM/T)</td> </tr> <tr> <td>Radiative Transfer</td> <td>Cloud and Precipitation</td> </tr> </table>			Microwave Radiation	Defense Meteorological Satellite Program (DMSP)	Remote Sensing	Passive Microwave Temperature Sounder (SSM/T)	Radiative Transfer	Cloud and Precipitation
Microwave Radiation	Defense Meteorological Satellite Program (DMSP)							
Remote Sensing	Passive Microwave Temperature Sounder (SSM/T)							
Radiative Transfer	Cloud and Precipitation							
20. ABSTRACT (Continue on reverse side if necessary and identify by block number) <p style="margin-left: 20px;">A microwave radiative transfer program for cloudy and precipitating atmospheres applicable to the DMSP SSM/T channels has been developed. The microwave transfer program takes into account the simultaneous contributions of multiple scattering and absorption by hydrometeors and absorption due to molecular oxygen and water vapor in the atmosphere. Sensitivity analyses have been carried out to investigate the effects of the rainfall rate, cloud thickness, and cloud location on the upwelling brightness temperature over land and</p>								

Unclassified

SECURITY CLASSIFICATION OF THIS PAGE(When Data Entered)

20. (cont.)

ocean surfaces for two different atmospheric profiles. Over the land surface, it is shown that increasing the cloud liquid water content and cloud thickness significantly reduces the brightness temperatures for SSM/T channels 1 - 3. Over the ocean surface, however, the brightness temperatures for channels 1 - 3 are increased as the cloud liquid water content increases and reach to maximum values depending on the cloud thickness involved. Moreover, we show the importance of the cloud position and the atmospheric temperature profile on the brightness temperature values. In addition, investigation of the effects of precipitation on the temperature retrieval using both the theoretically simulated values and real SSM/T data has also been carried out on the basis of a statistical method. The hypothetical retrieval experiments reveal that the temperatures close to the surface suffer increased degradation as the rainfall rate increases. This finding is further supported by the analysis employing the real SSM/T data for a number of case studies in which temperature profiles from radiosondes are available for comparisons.

Unclassified

SECURITY CLASSIFICATION OF THIS PAGE(When Data Entered)

TABLE OF CONTENTS

	<u>Page</u>
ABSTRACT	
ACKNOWLEDGMENTS	v
Section 1 INTRODUCTORY REMARKS	1
Section 2 THEORY OF MICROWAVE RADIATIVE TRANSFER IN PLANE-PARALLEL ATMOSPHERES	3
2.1 Microwave Radiative Transfer in Clear Atmospheres	3
2.2 Microwave Radiative Transfer in Scattering Cloudy Atmospheres	6
Section 3 APPLICATION OF MICROWAVE RADIATIVE TRANSFER TO DMSP BLOCK 5D SSM/T CHANNELS	12
3.1 Characteristics of DMSP Block 5D SSM/T Channels	12
3.2 Atmospheric Absorption and Scattering Parameters for SSM/T Frequencies	15
3.2.1 Absorption due to gaseous constituents	15
3.2.2 Scattering and absorption due to cloud droplets	19
3.3 Atmospheric Profile and Cloud Models Used	22
Section 4 SENSITIVITY ANALYSES ON THE EFFECTS OF CLOUD AND PRECIPITATION ON THE DMSP SSM/T CHANNELS	36

	<u>Page</u>
4.1 Dependence on Layer Thickness and Rainfall Rate	41
4.2 Dependence on Layer Location and Atmospheric Profile	44
4.3 Interpretation of Results	54
Section 5 TEMPERATURE PROFILE RETRIEVAL EXERCISES	63
5.1 Temperature Profile Retrieval Using Simulated Brightness Temperatures	63
5.2 Temperature Profile Retrieval Using DMSP SSM/T Data	68
Section 6 CONCLUSION	74
REFERENCES	77
APPENDIX LISTING OF THE MICROWAVE TRANSFER PROGRAM	79

ACKNOWLEDGEMENTS

We would like to thank Vince Falcone, our contract monitor, for providing the transmittance routine for the DMSP SSM/T frequencies and for many helpful discussions. Appreciation is also extended to Dr. Jean F. King for his constant encouragement on our research work. The cooperation of Captain Joseph Gahlingher of the Air Force Global Weather Central for providing the timely DMSP data is gratefully appreciated. The research work reported here was supported by the Air Force Geophysics Laboratory, Air Force Systems Command under contract F19628-78-C-0144.

SECTION 1

INTRODUCTORY REMARKS

The first microwave sounder intended for operational use was flown aboard the Air Force Defense Meteorological Satellite Program (DMSP) Block 5D satellite system launched in June, 1979. The microwave sensor (SSM/T) is a 7-channel scanning radiometer in the 50-60 GHz oxygen band region. The prime objective of SSM/T is to provide data for deriving global basis temperature profiles in the troposphere and lower stratosphere. Channel 1 (50.5 GHz) is a window channel responding strongly to the earth's surface characteristics, dense clouds, and precipitation. Moreover, the peaks of weighting functions for channels 2, 3, and 4 (53.2, 54.35, and 54.9 GHz) are below about 10 km.

It is known that the prime advantage of microwave over infrared temperature sounders is that the longer wavelength microwaves are much less affected by clouds and precipitation. However, to what degree and quantitative extent will clouds and precipitation influence the brightness temperature values which would have been observed under clear conditions? The objectives of the present project under the sponsorship of the Air Force Geophysics Laboratory have been (1) to develop a program for the transfer of microwave radiation in cloudy and precipitating atmospheres, (2) to compare the theoretical simulated microwave and infrared radiances with

observed values utilizing the required ground truth data when the DMSP microwave and infrared data become available, and (3) to investigate the inference of temperature profiles under all weather conditions.

Within the scope of these objectives and subject to the availability of the DMSP data, this final report first presents the theoretical foundation for the transfer of microwave radiation in clear and cloudy atmospheres. Applications of the microwave program to DMSP SSM/T channels are then described. Sensitivity analyses on the effects of clouds and precipitation on the upwelling brightness temperatures for channels 1 - 4 are subsequently carried out. In addition, we report the results of temperature profile retrieval exercises using the simulated brightness temperatures computed from the microwave radiative transfer program described previously. Lastly, a number of selected case studies utilizing the real SSM/T data recently made available to us are also carried out for the temperature retrieval exercises by means of a statistical method. These case studies cover the conditions for clear, cloudy and precipitating atmospheres.

SECTION 2

THEORY OF MICROWAVE RADIATIVE TRANSFER IN PLANE-PARALLEL ATMOSPHERES

2.1 Microwave Radiative Transfer in Clear Atmospheres

Consider a non-scattering, plane-parallel atmosphere which is in local thermodynamic equilibrium and assume that thermal radiation from the earth atmosphere is independent of the azimuthal angle ϕ , the general equation of transfer may be expressed in the frequency domain as

$$\frac{d I_v(z, \mu)}{\mu k_v \rho dz} = - I_v(z, \mu) + B_v[T(z)], \quad (2.1)$$

where I_v is the radiance at frequency v , k_v is the absorption coefficient, ρ is the density, $\mu = \cos\theta$, θ is the emergent angle, z is the height, and B_v denotes the Planck function. For satellite sounding applications, the observations are normally taken close to the upwelling direction ($\mu \approx 1$). Thus, for the simplicity of discussions on the transfer of thermal radiation in a non-scattering atmosphere, the dependence on μ contained in the radiance expression is omitted.

The radiance solution of Eq. (2.1) at the top of the atmosphere in the upwelling direction is given by

$$I_v(\infty) = I_v(0) T_v(0, \infty) + \int_0^{\infty} B_v[T(z)] \frac{\partial T_v(z, \infty)}{\partial z} dz, \quad (2.2)$$

where $I_v(0)$ represents the radiance contribution from the surface,

and the transmittance $T_v(z, \infty)$ is expressed with respect to the top of the atmosphere in the form

$$T_v(z, \infty) = \exp\left[-\int_z^{\infty} k_v(z') \rho(z') dz'\right]. \quad (2.3)$$

In the microwave region, since the emissivity ϵ_v of the surface is normally less than unity, there will be a reflection contribution from the surface. The radiance emitted from the surface having a temperature T_s would therefore be given by

$$I_v(0) = \epsilon_v B_v(T_s) + (1-\epsilon_v) \int_{\infty}^0 B_v[T(z)] \frac{\partial T_v(0, z)}{\partial z} dz. \quad (2.4)$$

The first terms in the right-hand side of Eq. (2.4) denotes the surface emission contribution, whereas the second term represents the emission contribution from the entire atmosphere to the surface, which is reflected back to the atmosphere at the same frequency. The transmittance $T_v(0, z)$ is now expressed with respect to the surface.

Inserting the lower boundary condition into Eq. (2.2), we find

$$\begin{aligned} I_v(\infty) &= \epsilon_v B_v(T_s) T_v(0, \infty) + (1-\epsilon_v) T_v(0, \infty) \int_{\infty}^0 B_v[T(z)] \frac{\partial T_v(0, z)}{\partial z} dz \\ &\quad + \int_0^{\infty} B_v[T(z)] \frac{\partial T_v(z, \infty)}{\partial z} dz. \end{aligned} \quad (2.5)$$

In the frequency domain, the Planck function is given by

$$B_v(T) = 2h v^3 / [c^2 (e^{hv/KT} - 1)], \quad (2.6)$$

where h is the Planck constant, K is the Boltzmann constant, and c is the velocity of light. Moreover, in the microwave region $hv/KT \ll 1$,

the Planck function may be approximated by

$$B_v(T) \approx (2Kv^2/c^2)T . \quad (2.7)$$

This is the Rayleigh-Jeans law, which states that the Planck radiance is linearly proportional to the temperature. Furthermore, radiometers which measure the thermal emission are usually calibrated with sources at certain reference temperatures. Thus, we may define an equivalent brightness temperature T_B such that

$$I_v = (2Kv^2/c^2)T_B(v) . \quad (2.8)$$

Substituting Eqs. (2.7) and (2.8) into Eq. (2.5), the solution of microwave radiative transfer may now be written in terms of temperature as follows:

$$\begin{aligned} T_B(v) &= \epsilon_v T_s T_v(0, \infty) + (1-\epsilon_v) T_v(0, \infty) \int_0^\infty T(z) \frac{\partial T_v(0, z)}{\partial z} dz \\ &+ \int_0^\infty T(z) \frac{\partial T_v(z, \infty)}{\partial z} dz . \end{aligned} \quad (2.9)$$

The transmittance is generally available with respect to the top of the atmosphere; i.e., $T_v(z) = T_v(z, \infty)$. Thus, for computational purposes, it is desirable to express $T_v(0, z)$ in terms of $T_v(z, \infty)$. For monochromatic frequencies, the transmittance is an exponential function of the optical depth as shown in Eq. (2.3). Hence, we may write

$$\begin{aligned} T_v(0, z) &= \exp\left[-\int_0^z k_v(z') \rho(z') dz'\right] \\ &= \exp\left[-\int_0^\infty k_v(z') \rho(z') dz' + \int_z^\infty k_v(z') \rho(z') dz'\right] \\ &= T_v(0, \infty) / T_v(z, \infty) . \end{aligned} \quad (2.10)$$

Moreover, since $T_v(0, \infty)$, the transmittance of the entire atmosphere, is a constant value, we also find

$$\frac{\partial T_v(0, z)}{\partial z} = - \frac{T_v(0, \infty)}{[T_v(z, \infty)]^2} \frac{\partial T_v(z, \infty)}{\partial z} . \quad (2.11)$$

Substituting Eq. (2.11) into Eq. (2.9), rearranging terms, and letting $T_v(z, \infty) = T_v(z)$, Eq. (2.9) may be rewritten to yield

$$T_B(v) = \epsilon_v T_s T_v(0) + \int_0^\infty J_v(z) \frac{\partial T_v(z)}{\partial z} dz , \quad (2.12)$$

where the atmospheric source term is given by

$$J_v(z) = \{1 + (1-\epsilon_v)[T_v(0)/T_v(z)]^2\} T(z) . \quad (2.13)$$

2.2 Microwave Radiative Transfer in Scattering Cloudy Atmospheres

The basic equation of transfer for a plane-parallel cloud layer consisting of absorbing gases in local thermodynamic equilibrium may be written in the form

$$\begin{aligned} \frac{d I_v(\tau, \mu)}{d\tau} &= I_v(\tau, \mu) - \frac{\tilde{\omega}_v}{2} \int_{-1}^1 P_v(\mu, \mu') I_v(\tau, \mu') d\mu' \\ &\quad - (1-\tilde{\omega}_v) B_v[T(\tau)] . \end{aligned} \quad (2.14)$$

In Eq. (2.14), I_v represents the monochromatic radiance of frequency v , μ the cosine of the emergent angle with respect to the zenith, τ the optical depth for cloud particles and gases within the cloud, P_v the normalized axially symmetrical scattering phase function, T the cloud temperature, and the single scattering albedo

$$\tilde{\omega}_v = \frac{\beta_{s,v}}{\beta_{s,v} + \beta_{a,v} + k_v p} , \quad (2.15)$$

where $\beta_{s,v}$ and $\beta_{a,v}$ denote the volume scattering and absorption cross sections, respectively, for cloud particles at frequency v . The normalized phase function can be expressed as a Legendre polynomial of finite terms. By approximating the integration in Eq. (2.14) utilizing Gauss' quadrature formula, a set of first order inhomogeneous differential equations can be derived. Upon searching the homogeneous and particular solutions of the differential equations as outlined by Chandrasekhar (1950), the complete solution of the scattered intensity from an isothermal cloud having a temperature T_c at a given discrete stream can be expressed as

$$I_v(\tau, \mu_i) = \sum_m L_m \phi_m(\mu_i) \exp(-k_m \tau) + B_v(T_c) , \quad (2.16)$$

where m is the number of discrete streams employed, ϕ_m and k_m represent eigenfunctions and eigenvalues for the differential equations, and are associated with the scattering phase function and single-scattering albedo, and L_m are a set of constants of proportionality which can be determined from the radiation boundary conditions above and below the cloud layer.

In the previous subsection, we pointed out that in the microwave region, the Planck function is normally expressed in terms of the temperature and the measured radiance is given by an equivalent brightness temperature. Thus, using Eqs. (2.7) and (2.8), Eq. (2.14) may be written in terms of the brightness temperature as follows:

$$\frac{d T_B(v, \tau; \mu)}{d\tau} = T_B(v, \tau; \mu) - \frac{\tilde{\omega}_v}{2} \int_{-1}^{+1} P_v(\mu, \mu') T_B(v, \tau; \mu') d\mu' - (1 - \tilde{\omega}_v) T(\tau) . \quad (2.17)$$

The solution of Eq. (2.17) can be derived in a manner similar to that of Eq. (2.14) and is given by

$$T_B(v, \tau; \mu_i) = \sum_m L'_m \phi_m(\mu_i) \exp(-k_m \tau) + T_c . \quad (2.18)$$

Here the constants of proportionality L'_m differ from those given in Eq. (2.16) and are to be evaluated from the radiation boundary conditions described below. Note that T_c , the cloud temperature, is independent of frequency v .

The inhomogeneous and nonisothermal structure of a cloud layer may be taken into consideration by dividing the cloud layer into a number of sublayers, each of which has a mean isothermal temperature and is homogeneous with respect to the cloud composition. At the cloud top, the downward brightness temperature is equal to the brightness contributions from every point in the atmosphere above the cloud top. This can be expressed by

$$T_B(v, z_t; -\mu_i) = \int_{z=z_t}^{\infty} T(z) d\pi_v(z, z_t; -\mu_i) , \quad (2.19)$$

where z_t is the height at the cloud top and the negative sign on μ_i simply indicates downward transfer. Note here that we change the τ -coordinate to the height coordinate for the convenience of discussion. The transmittance in this equation is

$$T_v(z_t, z; \mu_i) = T_v(z, z_t; -\mu_i) = \exp\left[-\frac{1}{\mu_i} \int_{z_t}^z k_v(z') \rho(z') dz'\right], \quad (2.20)$$

and in terms of transmittance with respect to the top of the atmosphere, we find

$$\begin{aligned} T_v(z_t, z; \mu_i) &= T_v(z_t, \infty; \mu_i) / T_v(z, \infty; \mu_i) \\ &= T_v(z_t; \mu_i) / T_v(z; \mu_i), \quad z_t > z. \end{aligned} \quad (2.21)$$

Within the cloud layer, where scattering occurs, continuity of brightness values from all directions is required. Thus,

$$T_B(v, z_\ell; \mu_i) = T_B(v, z_{\ell+1}; \mu_i), \quad \ell = 1, 2, \dots, N-1, \quad (2.22)$$

where N is the total number of sublayers within the cloud.

At the lower boundary of the cloud, three brightness contributions are immediately apparent. These include (a) the surface contribution, (b) the direct atmospheric contribution from below the cloud, and (c) the reflected atmospheric contribution from below the cloud. A fourth, and perhaps less obvious, brightness contribution at the lower boundary must be considered. Since the reflection of downward brightness by the earth's surface is significant for microwave radiation, the emergent brightness at the cloud bottom will contribute to the lower boundary condition. That is to say, the solution to the radiative transfer through the cloud affects the boundary conditions used to obtain the solution. This suggests that an iterative approach to the correct solution is required. Practically, this is accomplished by assuming initially that the top-down throughput

of the cloud equals one. The emergent intensity at the cloud bottom obtained by this assumption can then be attenuated by two trips through the atmosphere between the earth's surface and the cloud base and by the reflection at the earth's surface. This value is added to the lower boundary condition and the solution to the radiative transfer equation then produces a new value for the emergent brightness temperature at the cloud bottom. From this solution a new top/down throughput can be calculated and the process is repeated until the new throughput varies from the old by less than one tenth. In all cases examined by this study the iteration halted after only two steps. The lower boundary conditions can then be expressed as

$$\begin{aligned}
 T_B(v, z_b; +\mu_i) = & \epsilon_v T_S T_v(0, z_b; +\mu_i) + \int_{z=0}^{z_b} T(z) dT_v(z, z_b; +\mu_i) \\
 & + (1-\epsilon_v) T_v(0, z_b; +\mu_i) \left[\int_{z=0}^{z_b} T(z) dT_v(0, z; -\mu_i) \right. \\
 & \left. + T_B(v, z_t; -\mu_i) T_v^C(-\mu_i) T_v(z_b, 0; -\mu_i) \right], \quad (2.23)
 \end{aligned}$$

where $T_v^C(\mu_i)$ is defined to be the top/down throughput of the cloud for the stream defined by μ_i and z_b is the height of the cloud base. It is given by

$$T_v^C(\mu_i) = T_B(v, z_b; -\mu_i) / T_B(v, z_t; -\mu_i). \quad (2.24)$$

In Eq. (2.23), all the transmittances can be expressed in reference to the top of the atmosphere. The numerical technique for solving a set of simultaneous linear equations denoted in Eqs. (2.19), (2.22) and (2.23) has been well documented in our previous infrared studies

(Liou et al., 1977; Feddes and Liou, 1977).

The microwave transfer program for cloud layers will give the upward brightness temperature at the cloud top, i.e., $T_B(v, z_t; \mu_i)$. Thus, the upward brightness temperature at the satellite point of view in overcast cloudy conditions may then be written as

$$T_B(v, \infty; \mu_i) = T_B(v, z_t; \mu_i) T_v(z_t, \infty; \mu_i) + \int_{z_t}^{\infty} T(z) dT_v(z, \infty; \mu_i), \quad (2.25)$$

where the first term in the right-hand side of Eq. (2.25) represents the contribution from the cloud top brightness temperature which is being attenuated to the top of the atmosphere, and the remaining term is the atmospheric contribution above the cloud top.

SECTION 3

APPLICATIONS OF MICROWAVE RADIATIVE TRANSFER PROGRAM TO DMSP BLOCK 5D SSM/T CHANNELS

3.1 Characteristics of DMSP Block 5D SSM/T Channels

The Passive Microwave Temperature Sounder (SSM/T) was launched in June, 1979, in a sun-synchronous polar orbit, by the United States Air Force as part of the Defense Meteorological Satellite Program (DMSP) Block 5D package. Other equipment of meteorological interest on board the space craft include visual and infrared imagery channels and a scanning infrared spectroradiometer. The SSM/T sensor is a cross track scanning radiometer, which acquires data at 32 second intervals and at seven angular positions separated by 12 degrees. The "footprints" of a scan for the SSM/T along the satellite subtrack are shown in Figure 1. The horizontal resolution is a near circle of 174 km diameter in the nadir direction, while it is an ellipse with a major axis of 304 km and minor axis of approximately 213 km at the maximum scan angle of 36° from nadir. Seven operational frequencies were chosen in the vicinity of a strong oxygen absorption band in the 50-60 GHz region. Figure 2 depicts the weighting functions ($\partial T / \partial z$) of the SSM/T channels in the nadir direction for a surface emissivity of 0.97. Channel 1, 50.50 GHz, is a "window" channel and senses at or near the earth's surface. Channels 2, 3, and 4 (53.20, 54.35 and 54.90 GHz) have weighting functions that

ORBITAL SUBTRACK

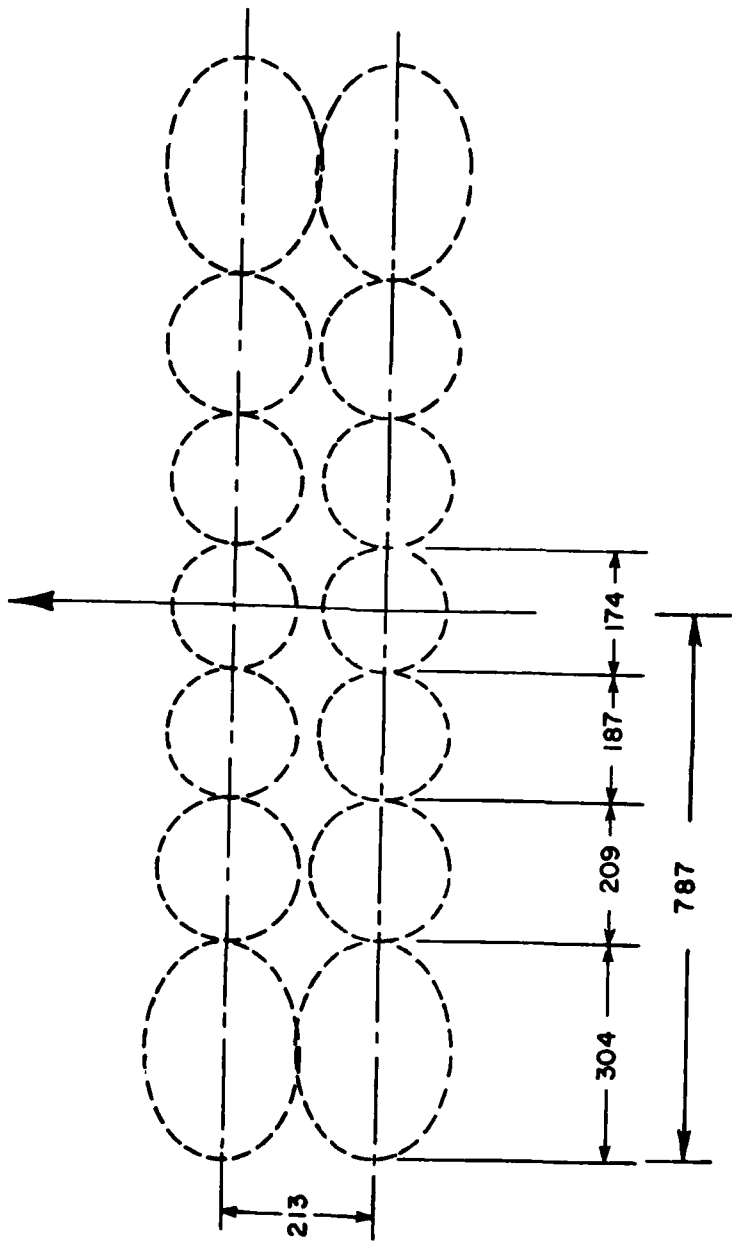


Figure 1. The scan pattern of SSM/T.

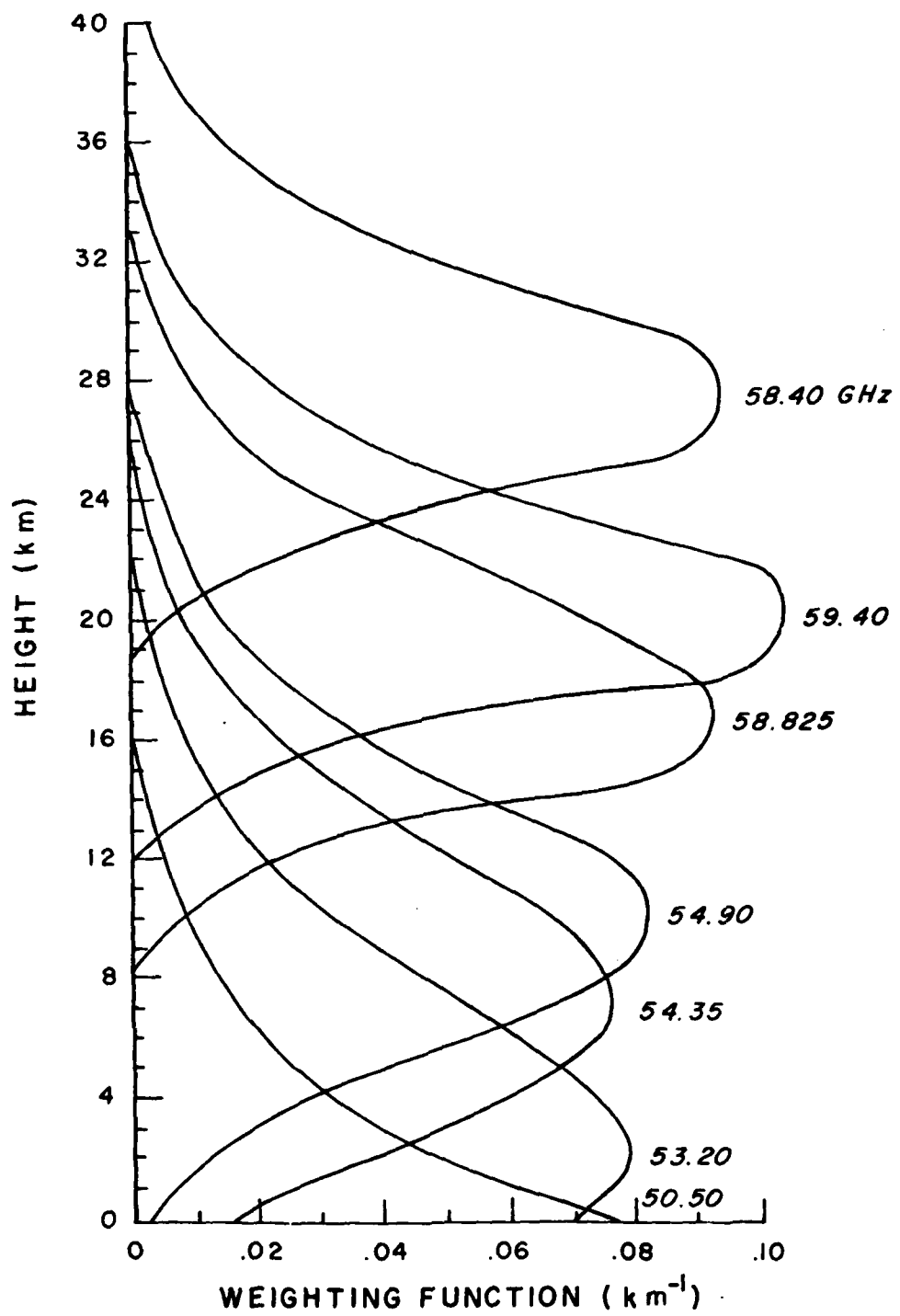


Figure 2. SSM/T weighting functions (nadir) with antenna gain characteristics included for a surface emissivity of 0.97.

peak at increasing heights in the troposphere. The weighting functions of Channels 5, 6 and 7 peak in the stratosphere with Channel 5 peaking highest in the atmosphere near 28 km. The weighting functions result from consideration of atmospheric absorption due to water vapor and molecular oxygen. The peaks of these weighting functions indicate the approximate location in the atmosphere from which most of the energy that reaches the top of the atmosphere originates. The weighting functions presented in Figure 2 also include the transmittance corrections for antenna gain characteristics. The DMSP Block 5D satellite also carries channels in the infrared. The Special Sensor H (SSH) is the infrared temperature-humidity-ozone sounder consisting of six channels in the $15 \mu\text{m}$ CO_2 band, eight channels in the $18\text{-}30 \mu\text{m}$ H_2O rotational band, and one channel in the $9.6 \mu\text{m}$ O_3 band.

3.2 Atmospheric Absorption and Scattering Parameters for SSM/T Frequencies

Microwave frequencies between 50.0 and 60.0 GHz are affected by several different atmospheric constituents. Gases in the atmosphere absorb and emit microwave radiation. Cloud droplets and rain drops not only absorb and emit but also scatter the incoming radiation.

3.2.1 Absorption due to gaseous constituents. The primary gaseous absorbers in the microwave region are H_2O and O_2 . Atmospheric nitrogen gradually becomes a more significant absorber at frequencies greater than 120 GHz, but has little influence in the vicinity of 60 GHz. Other gaseous constituents occur in very low concentrations and, in general, their effects are very small.

The O_2 absorption spectrum in the microwave region is due to the molecule's magnetic dipole moment. Figure 3 presents the absorption coefficient of dry air versus frequency. The absorption coefficient (decibels/km) shows a dramatic peak near 60 GHz and a secondary maximum near 120 GHz. Both peaks are attributable to molecular oxygen. The characteristics of this absorption spectrum were first investigated by Van Vleck (1947). Other investigators have built on his studies, culminating in a paper by Meeks and Lilley (1963). For this study, the absorption coefficients for O_2 were calculated using Meeks and Lilley's parameters.

Water vapor absorption in the microwave is chiefly due to an electric dipole moment. Initial studies were published by Van Vleck (1947), Becker and Autler (1946), and King, et al. (1947). Rosenblum (1961) gave an excellent summary of work done up to 1961. Figure 4 presents water vapor absorption (decibels/km) versus frequency in the microwave region. It is seen that the values of absorption increase gradually through the range of frequencies under investigation. It is apparent that the absorption due to water vapor is less than that of molecular oxygen for all the channels chosen for the SSM/T sounder. Note, however, that even though the absorption coefficients for O_2 are generally higher than those for H_2O , the two values are roughly equivalent for the window channel at 50.50 GHz. H_2O absorption coefficients were calculated using the method of Barrett and Chung (1962). Computer programs for determination of both of these coefficients were kindly provided by Falcone (personal communication).

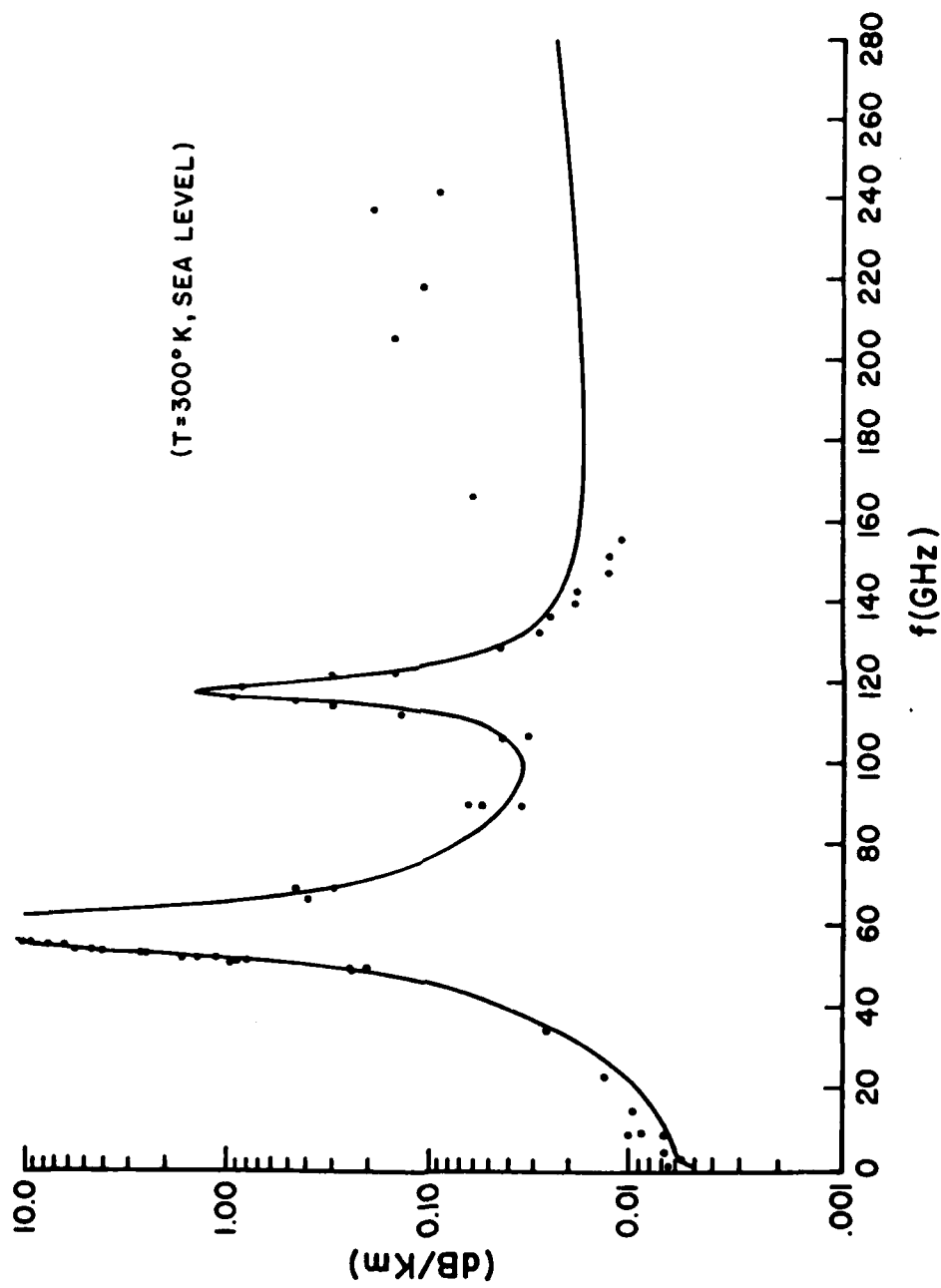


Figure 3. Absorption coefficient (decibels/km) of dry air as a function of frequency (after Meeks and Lilley, 1963). The dots are measured points by Hans Leibe during the period from 1974 to 1976 (courtesy of Rigone).

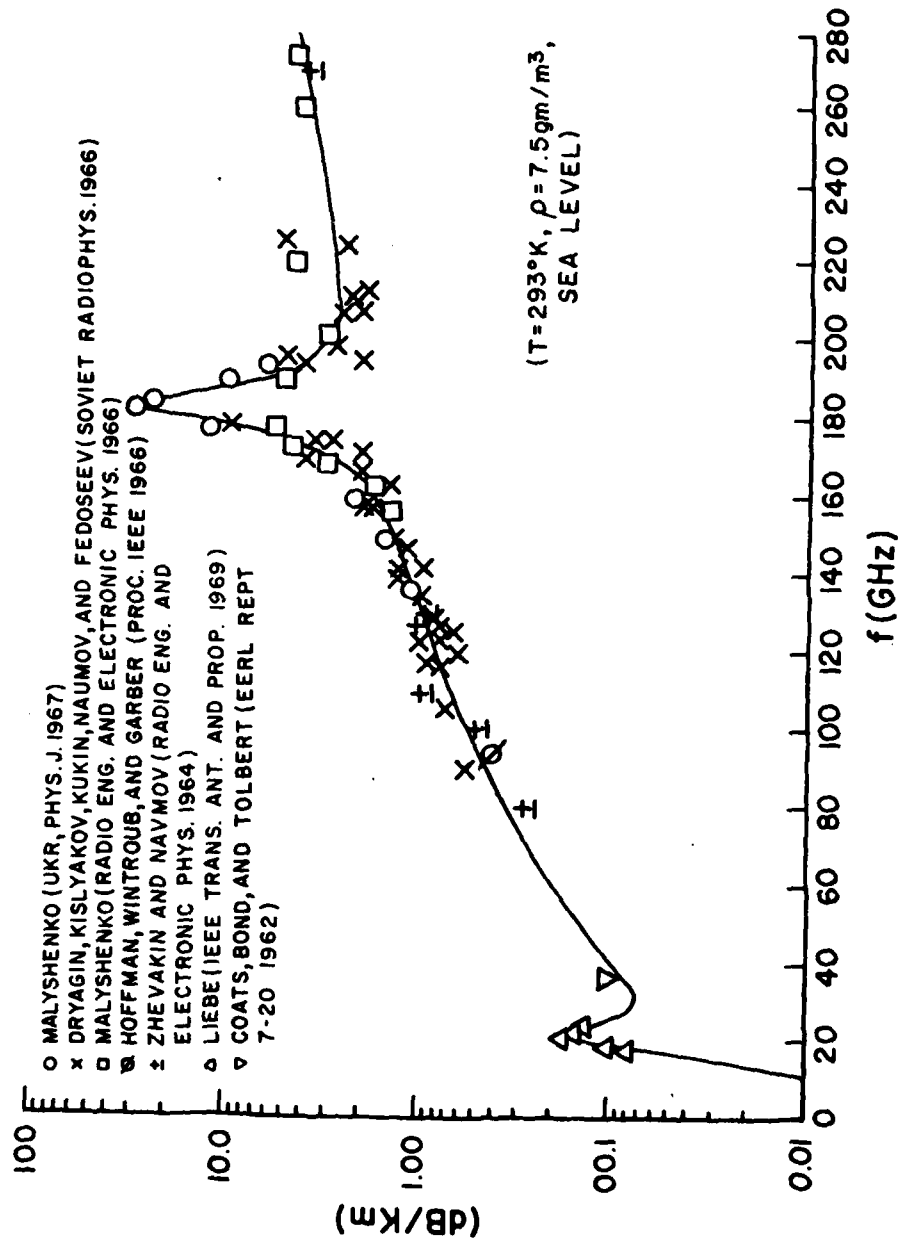


Figure 4. Water vapor absorption (decibels/km) as a function of frequency in the microwave region.

3.2.2 Scattering and absorption due to cloud droplets. The application of Mie scattering theory enables the calculation of optical parameters for assumed spherical particles given the complex index of refraction, wavelength of incident radiation, and particle size distribution. Although larger rain drops are known to deviate somewhat from the spherical shape, Mie theory still remains probably the best currently available theoretical tool for analyzing the effects of cloud droplets and rain in the atmosphere.

The Mie program used for the calculations in this study is a modification for Univac computers of the program by Liou and Hansen (1971). The output of the Mie computations include the coefficients of the Legendre polynomial approximation to the phase function, the extinction coefficient (km^{-1}) and the single scattering albedo. Note that the extinction coefficient and single scattering albedo determined here involve scattering and absorption by the particles as the only mechanisms for extinction. These values are modified to include absorption by the gaseous atmosphere within the cloud prior to their use in the solution of the radiative transfer equation.

The complex indices of refraction for pure liquid water at temperatures of $+10^\circ$ and -10° C have been determined by Savage (1976) for several different frequencies. These values (Table 1) are based on a least squares fit to the data of Saxton and Lane (1962) given by Hollinger (1973). The complex indices of refraction for the SSM/T channels as shown in Table 2 were obtained from Table 1 by linear interpolation in frequency. For the purpose of this study the values for 0° C are used throughout.

Table 1. Refractive index $m = m_r - im_i$ of pure liquid water.

Frequency (GHz)	$T=10^\circ\text{C}$		$T=0^\circ\text{C}$		$T=-10^\circ\text{C}$	
	m_r	m_i	m_r	m_i	m_r	m_i
19.35	5.87	2.96	5.20	2.94	4.64	2.81
37.00	4.32	2.60	3.83	2.37	3.46	2.12
50.30	3.76	2.29	3.37	2.03	3.08	1.78
89.50	3.00	1.67	2.76	1.42	2.60	1.20
100.00	2.89	1.56	2.68	1.31	2.54	1.10
118.00	2.75	1.39	2.58	1.15	2.46	0.96
130.00	2.68	1.30	2.53	1.07	2.43	0.89
183.00	2.49	1.00	2.39	0.81	2.33	0.66
231.00	2.40	0.82	2.33	0.66	2.29	0.53

Table 2. Refractive index of pure liquid water (SSM/T).

Channel Frequencies (GHz)							
	50.50	53.20	54.35	54.90	58.40	58.82	59.40
m_r	3.37	3.32	3.31	3.30	3.24	3.24	3.23
m_i	2.03	1.98	1.97	1.96	1.90	1.90	1.89

Utilizing the wavelength and the associated index of refraction, Mie scattering calculations for single particles may be carried out. Once the absorption and scattering efficiencies for single particles have been determined in terms of effective cross sectional area, the efficiencies for a size distribution of particles can be determined by integrating over the distribution. This area per volume relationship then has dimensions of inverse length and is described as the absorption or scattering coefficient. The extinction coefficient is then the sum of the absorption and scattering coefficients. The drop size distributions used for this study are necessarily numerical models. Two models have been chosen to represent nonprecipitating and precipitating clouds, respectively. Deirmendjian's L-Model cloud (Deirmendjian, 1969) drop size distribution is used for the nonprecipitating case. It is given by

$$N(r) = ar^\alpha \exp(-br^\delta), \quad (3.1)$$

where r is the drop radius in mm and note that $N(r)$ is in units of cm^{-4} . By varying the constants this model can be made to represent a variety of cloud types. For this study, $a=4.975 \times 10^7$, $\alpha=2$, $b=15.1186$, and $\delta=.5$. The selection of the nonprecipitating cloud model here is hypothetical and we fully realize that it is not a representative cloud model for typical clouds occurring in the atmosphere which have normally insignificant effect in the microwave frequencies. For the precipitating case, a theoretical drop size distribution based on rainfall rate is used (Marshall and Palmer, 1948). The distribution is expressed by

$$N(r) = 0.16 \exp(-2r\delta), \quad (3.2)$$

where $\delta = 41 R^{-0.21}$ and R denotes rainfall rate (mm/hr.). This exponential behavior of drop size distribution has been experimentally verified by Gunn and Marshall (1958) and Sekhon and Srivastaval (1970).

The phase function in terms of Legendre polynomial coefficients, extinction coefficients, and single scattering albedos calculated for each SSM/T channel from Mie theory are tabulated in Tables 3-13. Since the extinction coefficient input to the radiative transfer program must be in units of (km^{-1}) , the final values output by the Mie program have been multiplied by the proper constant to obtain these units.

3.3 Atmospheric Profile and Cloud Models Used

Two climatological profiles were used for the sensitivity study. The first profile was derived from the northern hemispheric mid-latitude Spring/Fall climatology contained in the U.S. Standard Atmospheric Supplements, 1966. The second profile was derived from the climatology for 30° north latitude, July, contained in the same source. For both profiles temperature and height values were interpolated to 40 standard pressure levels used for this study. Mixing ratio values for levels below 250 mb were obtained from a Skew-T diagram and hence are saturation values. Above 250 mb a constant mixing ratio of 3 parts per million was used. The profiles for the mid-latitude Spring/Fall and the 30° N latitude, July, are depicted in Figure 5.

To account for the total water within the cloud, the vertical liquid water content is customarily used. For spherical particles the droplet volume per unit volume of atmosphere is given by

Table 3. Optical parameters (Deirmendjian L-Model)

Freq(Ghz)	\bar{w}_0	\bar{w}_1	\bar{w}_2	\bar{w}_3	\bar{w}_4	\bar{w}_5
	\bar{w}_6	\bar{w}_7	\bar{w}_8	\bar{w}_9	\bar{w}_{10}	\bar{w}_{11}
	\bar{w}_{12}	\bar{w}_{13}	\bar{w}_{14}	\bar{w}_{15}	β_{ext}	\bar{w}_{17}
50.50 GHz						
.10000000E+1	.33071515E+0	.49360468E+0	.11251515E+0	-.75388403E-2	-.64620544E-2	
-.61193658E-1	-.19706414E-1	-.72342400E-1	-.21862288E-1	-.73393241E-1	-.21065428E-1	
-.56718646E-1	-.18075541E-1	-.53308599E-1	-.13297797E-1	.19639240E+0	.371442	
53.20 GHz						
.10000000E+1	.36502548E+0	.50176195E+0	.122441376E+0	-.16683441E-2	-.59117595E-2	
-.60990647E-1	-.21526171E-1	-.72936066E-1	-.24082668E-1	-.74087993E-1	-.23228360E-1	
-.67363482E-1	-.19621813E-1	-.53830410E-1	-.14667018E-1	.21121971E+0	.370722	
54.35 GHz						
.10000000E+1	.37639293E+0	.50474406E+0	.126667598E+0	.92690317E-3	-.54816648E-2	
-.60773288E-1	-.22136718E-1	-.73163086E-1	-.24870594E-1	-.74365129E-1	-.24001107E-1	
-.67622238E-1	-.20600170E-1	-.54040190E-1	-.15157736E-1	.21741939E+0	.382306	
54.90 GHz						
.10000000E+1	.38338237E+0	.50662057E+0	.12879932E+0	.22010716E-2	-.53178290E-2	
-.60704117E-1	-.22500922E-1	-.73293393E-1	-.25328362E-1	-.74521266E-1	-.24448897E-1	
-.67767713E-1	-.20985495E-1	-.54157977E-1	-.15441639E-1	.22039172E+0	.383564	
58.40 GHz						
.10000000E+1	.42759183E+0	.519558544E+0	.14307609E+0	.10864534E-1	-.39435839E-2	
-.60144363E-1	-.24772093E-1	-.74167010E-1	-.28268136E-1	-.75591876E-1	-.27337488E-1	
-.68768864E-1	-.23473136E-1	-.54969336E-1	-.17275603E-1	.23852110E+0	.391119	
58.82 GHz						
.10000000E+1	.43064151E+0	.52059478E+0	.14467422E+0	.11900079E-1	-.36744970E-2	
-.60041932E-1	-.24929679E-1	-.74243871E-1	-.28506663E-1	-.75695095E-1	-.27573876E-1	
-.68866560E-1	-.23677469E-1	-.56048812E-1	-.17426715E-1	.24066970E+0	.392445	
59.40 GHz						
.10000000E+1	.43805500E+0	.52296755E+0	.14716554E+0	.13424878E-1	-.33915394E-2	
-.59927715E-1	-.25301872E-1	-.74397610E-1	-.29002240E-1	-.75888122E-1	-.28065275E-1	
-.69047813E-1	-.24101133E-1	-.55195863E-1	-.17739194E-1	.24356932E+0	.393526	

Table 4. Optical parameters (Marshall-Palmer 1mm/hr)

Freq(Ghz)	\bar{w}_0	\bar{w}_1	\bar{w}_2	\bar{w}_3	\bar{w}_4	\bar{w}_5
	\bar{w}_6	\bar{w}_7	\bar{w}_8	\bar{w}_9	\bar{w}_{10}	\bar{w}_{11}
	\bar{w}_{12}	\bar{w}_{13}	\bar{w}_{14}	\bar{w}_{15}	θ_{ext}	\bar{w}_{17}
50.50GHz	.10000000E+1	.19833052E+0	.47688411E+0	.55111832E-1	-.39233125E-1	-.87157051E-2
	-.62096694E-1	-.11531642E-1	-.70222380E-1	-.12313806E-1	-.71009004E-1	-.11824920E-1
	-.64517421E-1	-.10137258E-1	-.51524593E-1	-.74482281E-2	.84232338E-1	.292315
53.20GHz	.10600000E+1	.22402792E+0	.47839620E+0	.59811980E-1	-.37492504E-1	-.95918234E-2
	-.62194212E-1	-.12922219E-1	-.70374822E-1	-.13802233E-1	-.71164137E-1	-.13254064E-1
	-.646559236E-1	-.11362062E-1	-.51639036E-1	-.83415256E-1	.92745402E-1	.304235
54.35GHz	.10000000E+1	.23205810E+0	.47878575E+0	.61910084E-1	-.36678740E-1	-.98396532E-2
	-.62224228E-1	-.13385122E-1	-.70430895E-1	-.14288761E-1	-.71221342E-1	-.13730905E-1
	-.64711583E-1	-.11770879E-1	-.51681400E-1	-.86479728E-1	.96396855E-1	.309626
54.90GHz	.10000000E+1	.23750050E+0	.47918551E+0	.62929877E-1	-.36273642E-1	-.10013095E-1
	-.62247228E-1	-.13680903E+0	-.70468713E-1	-.14615722E-1	-.71259849E-1	-.14035235E-1
	-.64716761E-1	-.12031728E-1	-.51709607E-1	-.86395184E-2	.98139872E-1	.311786
58.40GHz	.10000000E+1	.277220688E+0	.48214605E+0	.69720240E-1	-.33448139E-1	-.11069380E-1
	-.62405476E-1	-.15579456E-1	-.70740126E-1	-.16633212E-1	-.71537185E-1	-.15991775E-1
	-.65000162E-1	-.13708748E-1	-.51914319E-1	-.10071212E-1	.10920593E+0	.324571
58.82GHz	.10000000E+1	.27427582E+0	.48225550E+0	.70554734E-1	-.33082321E-1	-.11109789E-1
	-.62412982E-1	-.157111972E-1	-.70762828E-1	-.16796611E-1	-.71559851E-1	-.16129550E-1
	-.65020926E-1	-.13826951E-1	-.51931131E-1	-.10158213E-1	.11054591E+0	.326468
59.40GHz	.10000000E+1	.28023853E+0	.48286078E+0	.71740599E-1	-.32564901E-1	-.11279653E-1
	-.62442334E-1	-.16023894E-1	-.70815697E-1	-.17148129E-1	-.71613804E-1	-.16467157E-1
	-.65070226E-1	-.14116323E-1	-.51970903E-1	-.10370743E-1	.11236057E+0	.328350

Table 5. Optical parameters (Marshall-Palmer 2mm/hr)

Freq(Ghz)	$\bar{\omega}_0$	$\bar{\omega}_1$	$\bar{\omega}_2$	$\bar{\omega}_3$	$\bar{\omega}_4$	$\bar{\omega}_5$
	$\bar{\omega}_6$	$\bar{\omega}_7$	$\bar{\omega}_8$	$\bar{\omega}_9$	$\bar{\omega}_{10}$	$\bar{\omega}_{11}$
	$\bar{\omega}_{12}$	$\bar{\omega}_{13}$	$\bar{\omega}_{14}$	$\bar{\omega}_{15}$	β_{ext}	$\bar{\omega}_{17}$
50.50GHz						
.10000000E+1	.23305293E+0	.47669795E+0	.69520500E-1	.33475318E-1	.95957994E-2	
.62175845E-1	-.13776946E-1	-.70478158E-1	-.14730295E-1	-.71271311E-1	-.14146668E-1	
.64758072E-1	-.12129186E-1	-.51720168E-1	-.89139807E-2	.17904705E+0	.333189	
53.20GHz						
.10000000E+1	.26325986E+0	.47933453E+0	.75807102E-1	.30618404E-1	.10409493E-1	
.62303234E-1	-.15445792E-1	-.70756236E-1	-.16526853E-1	-.71535191E-1	-.15872090E-1	
.641999290E-1	-.13600205E-1	-.51914898E-1	-.10000476E-1	.19526609E+0	.343557	
54.35GHz						
.10000000E+1	.27304477E+0	.48016100E+0	.78578498E-1	.29300388E-1	.10608633E-1	
.62339826E-1	-.16019093E-1	-.70836625E-1	-.17147537E-1	-.71638278E-1	-.16468370E-1	
.65093569E-1	-.14111549E-1	-.51991134E-1	-.10376438E-1	.20213311E+0	.348307	
54.90GHz						
.10000000E+1	.27938366E+0	.48085325E+0	.79948634E-1	.28644508E-1	.10758894E-1	
.62367953E-1	-.16371191E-1	-.70899995E-1	-.17527962E-1	-.71703261E-1	-.168333152E-1	
.6515969E-1	-.14432824E-1	-.52039092E-1	-.10606620E-1	.20538624E+0	.350154	
58.40GHz						
.10000000E+1	.31965204E+0	.486595885E+0	.89119851E-1	.24116337E-1	.11591706E-1	
.62553437E-1	-.18625856E-1	-.71353265E-1	-.19972884E-1	-.72168952E-1	-.19182567E-1	
.655578578E-1	-.16446644E-1	-.52382578E-1	-.12086596E-1	.22574856E+0	.360992	
58.82GHz						
.10000000E+1	.32229704E+0	.48625726E+0	.90221748E-1	.23540332E-1	.11595119E-1	
.6255937E-1	-.18795815E-1	-.71394044E-1	-.20160143E-1	-.72211288E-1	-.19362601E-1	
.65617340E-1	-.16601176E-1	-.52413899E-1	-.12200346E-1	.22818576E+0	.362670	
59.40GHz						
.10000000E+1	.32915882E+0	.48728307E+0	.91830136E-1	.22720526E-1	.11714991E-1	
.62591200E-1	-.19181183E-1	-.71480898E-1	-.20579983E-1	-.72300772E-1	-.19766032E-1	
.65699129E-1	-.16947077E-1	-.52479871E-1	-.12454616E-1	.23146830E+0	.364242	

Table 6. Optical parameters (Marshall-Palmer 3mm/hr)

Freq(Ghz)	\bar{w}_0	\bar{w}_1	\bar{w}_2	\bar{w}_3	\bar{w}_4	\bar{w}_5
	\bar{w}_6	\bar{w}_7	\bar{w}_8	\bar{w}_9	\bar{w}_{10}	\bar{w}_{11}
	\bar{w}_{12}	\bar{w}_{13}	\bar{w}_{14}	\bar{w}_{15}	\bar{w}_{ext}	\bar{w}_{ν}
50.50GHz	.25862318E+0	.47744717E+0	.79897807E-1	.28583795E-1	-.99653228E-1	
.10000000E+1	-.15418045E-1	-.70739437E-1	-.16511622E-1	-.71540767E-1	-.15858597E-1	
-.62224346E-1	-.13591997E-1	-.51920506E-1	-.9950262E-1	.27303706E+0	.355154	
-.65005033E-1						
53.20GHz	.29162371E+0	.48117814E+0	.8782297E-1	.24840494E-1	-.10646886E-1	
.10000000E+1	-.17266655E-1	-.71090662E-1	-.18513792E-1	-.719011866E-1	-.17782016E-1	
-.62359262E-1	-.15247116E-1	-.52186991E-1	-.11206979E-1	.29677251E+0	.364537	
-.65335110E-1						
54.35GHz	.30252529E+0	.48244693E+0	.90664385R-1	.23128135E-1	-.10770838E-1	
.10000000E+1	-.17909504E-1	-.71230216E-1	-.19219201E-1	-.72046216E-1	-.184600047E-1	
-.62392209E-1	-.15228870E-1	-.52293727E-1	-.11634725E-1	.30640090E+0	.368894	
-.65467230E-1						
54.90GHz	.30941458E+0	.48341050E+0	.92299544E-1	.22275960E-1	-.10883022E-1	
.10000000E+1	-.18297148E-1	-.71315535E-1	-.19642109E-1	-.72134340E-1	-.1886422E-1	
-.6242036E-1	-.16177158E-1	-.52358719E-1	-.11890848E-1	.31094508E+0	.370550	
-.65547707E-1						
58.40GHz	.35308196E+0	.49045007E+0	.10325306E+0	.16426243E-1	-.11419156E-1	
.10000000E+1	-.20771828E-1	-.71920656E-1	-.22359124E-1	-.72761442E-1	-.21478142E-1	
-.62589478E-1	-.18416918E-1	-.52821356E-1	-.13537574E-1	.33915074E+0	.380231	
-.66121005E-1						
58.82GHz	.35609849E+0	.49093359E+0	.10455210E+0	.15689422E-1	-.11379821E-1	
.10000000E+1	-.21385745E-1	-.72091952E-1	-.23042074E-1	-.72821073E-1	-.21687536E-1	
-.6258842E-1	-.18596657E-1	-.52953556E-1	-.13669973E-1	.34249930E+0	.381782	
-.66175624E-1						
59.40GHz	.36350373E+0	.49232587E+0	.10647667E+0	.14636938E-1	-.11438722E-1	
.10000000E+1	-.21385745E-1	-.72091952E-1	-.23042074E-1	-.72940414E-1	-.22135110E-1	
-.62614921E-1	-.18980559E-1	-.52953556E-1	-.13952286E-1	.34700110E+0	.383173	
-.66284733E-1						

Table 7. Optical parameters (Marshall-Palmer 4mm/hr)

Freq(Ghz)	ω_0	ω_1	ω_2	ω_3	ω_4	ω_5
	ω_6	ω_7	ω_8	ω_9	ω_{10}	ω_{11}
	ω_{12}	ω_{13}	ω_{14}	ω_{15}	θ_{ext}	ω_{17}
50.50GHz						
.10000000E+1	.27936264E+0	.47868582E+0	.88828239E-1	-.24241288E-1	-.10081960E-1	
-.6224714E-1	-.16744915E-1	-.70998671E-1	-.17965453E-1	-.71809772E-1	-.17256226E-1	
-.65251498E-1	-.14797347E-1	-.52120194E-1	-.10878014E-1	.36732478E+0	.369816	
53.20GHz						
.10000000E+1	.31439899E+0	.48345105E+0	.96808990E-1	-.19747665E-1	-.10603425E-1	
-.62324329E-1	-.18722555E-1	-.7143327E-1	-.20126367E-1	-.7259238E-1	-.19332913E-1	
-.6566219E-1	-.16578150E-1	-.52461921E-1	-.12107055E-1	.39625288E+0	.378498	
54.35GHz						
.10000000E+1	.32612371E+0	.48514269E+0	.10050889E+0	-.17703004E-1	-.10647098E-1	
-.62398036E-1	-.19418578E-1	-.71607836E-1	-.20897355E-1	-.72441265E-1	-.20074386E-1	
-.65328970E-1	-.17214275E-1	-.52586506E-1	-.12655095E-1	.40832036E+0	.382578	
56.90GHz						
.10000000E+1	.33341119E+0	.48635588E+0	.10236397E+0	-.16685712E-1	-.10717014E-1	
-.62422105E-1	-.19831740E-1	-.71712340E-1	-.21352967E-1	-.72549975E-1	-.20512442E-1	
-.65926373E-1	-.17569948E-1	-.52666753E-1	-.12931337E-1	.41400230E+0	.384100	
58.40GHz						
.10000000E+1	.379526117E+0	.49514276E+0	.11479302E+0	-.97308619E-2	-.10933021E-1	
-.62549152E-1	-.22462198E-1	-.72448498E-1	-.24279620E-1	-.73319788E-1	-.23327733E-1	
-.66632457E-1	-.20004632E-1	-.5324964E-1	-.14707537E-1	.44906141E+0	.392979	
59.82GHz						
.10000000E+1	.38281677E+0	.49579889E+0	.11625385E+0	-.88608076E-2	-.10849801E-1	
-.62538125E-1	-.22671747E-1	-.72588961E-1	-.24320767E-1	-.73394912E-1	-.23560197E-1	
-.66701285E-1	-.20204111E-1	-.53290565E-1	-.14854617E-1	.45319756E+0	.394443	
59.40GHz						
.10000000E+1	.39061003E+0	.49751566E+0	.11843982E+0	-.76143673E-2	-.10845311E-1	
-.62554641E-1	-.23116588E-1	-.72657073E-1	-.25021294E-1	-.7350332E-1	-.24041975E-1	
-.668834305E-1	-.20617730E-1	-.53397930E-1	-.15158714E-1	.45875429E+0	.395710	

Table 8. Optical parameters (Marshall-Palmer 5mm/hr)

Freq(Ghz)	\bar{w}_0	\bar{w}_1	\bar{w}_2	\bar{w}_3	\bar{w}_4	\bar{w}_5
	\bar{w}_6	\bar{w}_7	\bar{w}_8	\bar{w}_9	\bar{w}_{10}	\bar{w}_{11}
	\bar{w}_{12}	\bar{w}_{13}	\bar{w}_{14}	\bar{w}_{15}	β_{ext}	\bar{w}_{17}
50.50GHz						
.10000000E+1	.29701037E+0	.48021003E+0	.95563178E-1	-.20291266E-1	-.10044780E-1	
-.62249691E-1	-.17870954E-1	-.71252878E-1	-.1921174E-1	-.72075326E-1	-.18454867E-1	
-.65494738E-1	-.15826063E-1	-.52317221E-1	-.17635461E-1	.45922777E+0	.380662	
53.20GHz						
.10000000E+1	.33364779E+0	.48594835E+0	.10490631E+0	-.15141100E-1	-.10397982E-1	
-.62358333E-1	-.19949749E-1	-.71763088E-1	-.21503033E-1	-.72606676E-1	-.20657868E-1	
-.65980102E-1	-.17715456E-1	-.52709030E-1	-.13024734E-1	.49359412E+0	.300007	
54.35GHz						
.10000000E+1	.34602374E+0	.488003910E+0	.10896940E+0	-.12807568E-1	-.10356365E-1	
-.62367490E-1	-.20686403E-1	-.71969109E-1	-.22328454E-1	-.72822629E-1	-.21452143E-1	
-.66178294E-1	-.18396925E-1	-.52869161E-1	-.13520324E-1	.50785787E+0	.392676	
54.90GHz						
.10000000E+1	.35362231E+0	.49848256E+0	.1110105205E+0	-.11646018E-1	-.10382346E-1	
-.62384982E-1	-.21119020E-1	-.72090750E-1	-.22811007E-1	-.72950132E-1	-.21916366E-1	
-.66294909E-1	-.18795166E-1	-.52963325E-1	-.13819264E-1	.51456302E+0	.394098	
58.40GHz						
.10000000E+1	.40164200E+0	.49986409E+0	.12472816E+0	-.37268698E-2	-.10271454E-1	
-.62451675E-1	-.23865646E-1	-.72942268E-1	-.25910449E-1	-.73848994E-1	-.24900478E-1	
-.67117426E-1	-.21355418E-1	-.53627074E-1	-.15702963E-1	.55574798E+0	.402370	
58.82GHz						
.10000000E+1	.40514901E+0	.50068025E+0	.12632884E+0	-.27413713E-2	-.10144615E-1	
-.62430076E-1	-.24087027E-1	-.73024837E-1	-.26171168E-1	-.73938141E-1	-.25152175E-1	
-.67199188E-1	-.21571546E-1	-.53693186E-1	-.15662288E-1	.56068187E+0	.403769	
59.40GHz						
.10000000E+1	.41324201E+0	.50268880E+0	.12874159E+0	-.13263080E-2	-.10076593E-1	
-.62432216E-1	-.24549362E-1	-.73183344E-1	-.26700501E-1	-.74106899E-1	-.25662317E-1	
-.67353649E-1	-.22009285E-1	-.53817836E-1	-.16184493E-1	.56707465E+0	.404943	

Table 9. Optical parameters (Marshall-Palmer 10nm/hr)

Freq(Ghz)	\bar{w}_0	\bar{w}_1	\bar{w}_2	\bar{w}_3	\bar{w}_4	\bar{w}_5
	\bar{w}_6	\bar{w}_7	\bar{w}_8	\bar{w}_9	\bar{w}_{10}	\bar{w}_{11}
	\bar{w}_{12}	\bar{w}_{13}	\bar{w}_{14}	\bar{w}_{15}	θ_{ext}	\bar{w}_{16}
50.50GHz						
.10000000E+1	.36093848E+0	.48951757E+0	.12262584E+0	-.41402253E-2	-.87863093E-2	
-.62023475E-1	-.21908425E-1	-.72427155E-1	-.23817222E-1	-.73326414E-1	-.22891432E-1	
-.66011428E-1	-.19634845E-1	-.53245206E-1	-.14441571E-1	.89594238E+0	.411507	
53.20GHz						
.10000000E+1	.40258453E+0	.49938498E+0	.13527074E+0	.35405875E-2	-.82581204E-2	
-.61953397E-1	-.24281849E-1	-.7234870E-1	-.26559573E-1	-.74193661E-1	-.25536095E-1	
-.67435929E-1	-.21904511E-1	-.53086577E-1	-.16112319E-1	.95218622E+0	.418062	
54.35GHz						
.10000000E+1	.41701050E+0	.50317153E+0	.14071610E+0	.69763924E-2	-.77908956E-2	
-.61854523E-1	-.25128965E-1	-.73562758E-1	-.27573228E-1	-.74552777E-1	-.26515943E-1	
-.67765408E-1	-.22746010E-1	-.54152811E-1	-.16732326E-1	.97515409E+0	.421319	
54.90GHz						
.10000000E+1	.42556904E+0	.50556084E+0	.14349197E+0	.86890517E-2	-.75975237E-2	
-.61818749E-1	-.25613949E-1	-.73749411E-1	-.28148646E-1	-.74756449E-1	-.27072021E-1	
-.67952174E-1	-.23223385E-1	-.54303589E-1	-.17083881E-1	.98590129E+0	.422445	
58.40GHz						
.10000000E+1	.47941101E+0	.52235422E+0	.16208856E+0	.20282942E-1	-.59096163E-2	
-.61453676E-1	-.28648382E-1	-.75027062E-1	-.31840407E-1	-.76170676E-1	-.3067488E-1	
-.69250019E-1	-.26293969E-1	-.55352102E-1	-.19346159E-1	.10510474E+1	.429964	
58.92GHz						
.10000000E+1	.48359282E+0	.52382556E+0	.16421848E+0	.21703873E-1	-.55778436E-2	
-.61362985E-1	-.28895100E-1	-.75153129E-1	-.32168380E-1	-.76316263E-1	-.30967215E-1	
-.69385021E-1	-.26568938E-1	-.55460665E-1	-.19549150E-1	.10585614E+1	.430178	
59.40GHz						
.10000000E+1	.49258928E+0	.52697968E+0	.16749501E+0	.23761808E-1	-.52130210E-2	
-.61273778E-1	-.29394957E-1	-.75384309E-1	-.32796124E-1	-.76576783E-1	-.31576998E-1	
-.69624639E-1	-.27092870E-1	-.55654148E-1	-.19935314E-1	.10686604E+1	.431085	

Table 10. Optical parameters (Marshall-Palmer 15mm/hr)

Freq(Ghz)	\bar{w}_0	\bar{w}_1	\bar{w}_2	\bar{w}_3	\bar{w}_4	\bar{w}_5
	\bar{w}_6	\bar{w}_7	\bar{w}_8	\bar{w}_9	\bar{w}_{10}	\bar{w}_{11}
	\bar{w}_{12}	\bar{w}_{13}	\bar{w}_{14}	\bar{w}_{15}	β_{ext}	\bar{w}_{17}
50.50GHz						
.10000000E+1	.40489974E+0	.49945961E+0	.14234551E+0	.86064041E-2	.67925486E-2	
-.61550264E-1	-.24612721E-1	-.73452160E-1	-.27083956E-1	-.74456659E-1	-.26050576E-1	
-.67679281E-1	-.22340869E-1	-.54084738E-1	-.16446766E-1	-.13016306E+1	.427672	
53.20GHz						
.10000000E+1	.44941841E+0	.51260638E+0	.15744676E+0	.18158680E-1	.54152315E-2	
-.61228033E-1	-.27113496E-1	-.74472936E-1	-.30122669E-1	-.75588129E-1	-.28993056E-1	
-.69718405E-1	-.24875565E-1	-.54923891E-1	-.18304254E-1	.13745169E+1	.433375	
54.35GHz						
.10000000E+1	.46502350E+0	.51773404E+0	.16391647E+0	.22405226E-1	.45496123E-2	
-.60992755E-1	-.27999760E-1	-.74885064E-1	-.31259461E-1	-.76058520E-1	-.30098638E-1	
-.69151511E-1	-.25825809E-1	-.55273948E-1	-.19005093E-1	.14039892E+1	.436308	
54.90GHz						
.10000000E+1	.474121169E+0	.52084973E+0	.16723198E+0	.24525361E-1	.41537489E-2	
-.60888758E-1	-.28501636E-1	-.75115838E-1	-.31895147E-1	-.76320671E-1	-.30716643E-1	
-.69392801E-1	-.26356845E-1	-.55468810E-1	-.19396531E-1	.14177649E+1	.437277	
58.40GHz						
.10000000E+1	.53119208E+0	.54246361E+0	.18944828E+0	.38836538E-1	.10219920E-2	
-.59998916E-1	-.31595389E-1	-.76670204E-1	-.35969580E-1	-.78124808E-1	-.34693194E-1	
-.71057164E-1	-.29775847E-1	-.56813578E-1	-.21918156E-1	.15005644E+1	.442872	
58.82GHz						
.10000000E+1	.53575518E+0	.54443285E+0	.19196726E+0	.40574308E-1	.50714008E-3	
-.59832359E-1	-.31841726E-1	-.76822736E-1	-.36340519E-1	-.78312949E-1	-.35059194E-1	
-.71231725E-1	-.30091143E-1	-.56954898E-1	-.22151202E-1	.15100086E+1	.443992	
59.40GHz						
.10000000E+1	.54524228E+0	.54842635E+0	.19588108E+0	.43107757E-1	.12957861E-3	
-.59637668E-1	-.32340639E-1	-.77098336E-1	-.37031008E-1	-.78641636E-1	-.357366896E-1	
-.71535870E-1	-.3067404E-1	-.57200689E-1	-.22581343E-1	.15227365E+1	.444759	

Table 11. Optical parameters (Marshall-Palmer 20nm/hr)

Freq(Ghz)	$\bar{\omega}_0$	$\bar{\omega}_1$	$\bar{\omega}_2$	$\bar{\omega}_3$	$\bar{\omega}_4$	$\bar{\omega}_5$
	$\bar{\omega}_6$	$\bar{\omega}_7$	$\bar{\omega}_8$	$\bar{\omega}_9$	$\bar{\omega}_{10}$	$\bar{\omega}_{11}$
	$\bar{\omega}_{12}$	$\bar{\omega}_{13}$	$\bar{\omega}_{14}$	$\bar{\omega}_{15}$	θ_{ext}	$\bar{\omega}_v$
50.50GHz						
.10000000E+1	.43903765E+0	.50919796E+0	.15845329E+0	.19427627E-1	-.45405659E-2	
-.6092917E-1	-.26642226E-1	-.74357782E-1	-.29684166E-1	-.75489565E-1	-.28577161E-1	
-.68630225E-1	-.24520497E-1	-.54054059E-1	-.18045204E-1	-.16838562E+1	.438371	
53.20GHz						
.10000000E+1	.48552493E+0	.52507979E+0	.17558237E+0	.30517876E-1	-.23651432E-2	
-.60324405E-1	-.29190570E-1	-.75339413E-1	-.32946217E-1	-.76842013E-1	-.31751468E-1	
-.69075963E-1	-.2248487E-1	-.59060447E-1	-.20056421E-1	-.17703700E+1	.443509	
54.35GHz						
.10000000E+1	.50193737E+0	.53132037E+0	.18289610E+0	.35426753E-1	-.112863337E-2	
-.59943299E-1	-.30983094E-1	-.76012826E-1	-.34175223E-1	-.77404730E-1	-.32955103E-1	
-.70396209E-1	-.28284035E-1	-.56281167E-1	-.20820792E-1	-.18051030E+1	.446229	
54.90GHz						
.10000000E+1	.51139987E+0	.53503014E+0	.18665708E+0	.37881713E-1	-.54439316E-3	
-.59765431E-1	-.30395711E-1	-.76275507E-1	-.34856000E-1	-.77715034E-1	-.33621469E-1	
-.70683002E-1	-.28857205E-1	-.56532977E-1	-.21243618E-1	-.18213244E+1	.447094	
58.40GHz						
.10000000E+1	.57062622E+0	.56053480E+0	.21184221E+0	.54429277E-1	-.39097171E-2	
-.58321935E-1	-.33632881E-1	-.78019590E-1	-.39212432E-1	-.79836925E-1	-.37910917E-1	
-.72650849E-1	-.32550020E-1	-.58104159E-1	-.23969665E-1	-.19182941E+1	.452083	
58.82GHz						
.10000000E+1	.57544649E+0	.56280685E+0	.21467965E+0	.56426206E-1	-.45898001E-2	
-.58077910E-1	-.33866531E-1	-.78188716E-1	-.39614499E-1	-.80059641E-1	-.38313001E-1	
-.72859018E-1	-.32897094E-1	-.58272864E-1	-.24226486E-1	-.19292605E+1	.453141	
59.40GHz						
.10000000E+1	.58525632E+0	.56756765E+0	.21911441E+0	.59351559E-1	-.54706432E-2	
-.57774342E-1	-.30347081E-1	-.78492791E-1	-.40350446E-1	-.80443102E-1	-.39043284E-1	
-.73216236E-1	-.33326580E-1	-.56561881E-1	-.24691468E-1	-.19440731E+1	.453817	

Table 12. Optical parameters (Marshall-Palmer 25nm/hr)

Freq(Ghz)	\bar{w}_0	\bar{w}_1	\bar{w}_2	\bar{w}_3	\bar{w}_4	\bar{w}_5
	\bar{w}_6	\bar{w}_7	\bar{w}_8	\bar{w}_9	\bar{w}_{10}	\bar{w}_{11}
	\bar{w}_{12}	\bar{w}_{13}	\bar{w}_{14}	\bar{w}_{15}	β_{ext}	\bar{w}_{17}
50.50GHz						
.10000000E+1	.46717341E+0	.51855401E+0	.17232806E+0	.28967801E-1	.21834488E-2	
-.60213211E-1	-.28249334E-1	-.75167057E-1	-.31870951E-1	-.76444522E-1	-.30713691E-1	
-.69512096E-1	-.263358383E-1	-.55567630E-1	-.19402249E-1	.20475379E+1	.446257	
53.20GHz						
.10000000E+1	.51512995E+0	.53678951E+0	.19121456E+0	.413866600E-1	.74454173E-3	
-.59310646E-1	-.30790992E-1	-.76473803E-1	-.35312376E-1	-.77987951E-1	-.34080889E-1	
-.70938188E-1	-.29254492E-1	-.56720548E-1	-.21538707E-1	.21456660E+1	.450900	
54.35GHz						
.10000000E+1	.53214134E+0	.54398351E+0	.19925572E+0	.468867901E-1	.23248313E-2	
-.587779234E-1	-.31677175E-1	-.76992487E-1	-.36614429E-1	-.78630161E-1	-.35365866E-1	
-.71534838E-1	-.30361208E-1	-.57203110E-1	-.22356254E-1	.218484900E+1	.453545	
54.90GHz						
.10000000E+1	.54187524E+0	.54819744E+0	.20340130E+0	.49612777E-1	.30848575E-2	
-.58525542E-1	-.32170743E-1	-.77278504E-1	-.37330886E-1	-.78981650E-1	-.36072509E-1	
-.71861179E-1	-.30969705E-1	-.57467045E-1	-.22805463E-1	.22031299E+1	.454335	
58.40GHz						
.10000000E+1	.60267618E+0	.57697304E+0	.23114114E+0	.68094563E-1	.87655644E-2	
-.56522240E-1	-.35111644E-1	-.79154474E-1	-.41907684E-1	-.81372392E-1	-.40624032E-1	
-.74090999E-1	-.31892315E-1	-.59271781E-1	-.25703557E-1	.23119910E+1	.458881	
58.82GHz						
.10000000E+1	.60768566E+0	.57968392E+0	.23425180E+0	.70314457E-1	.95974271E-2	
-.56201517E-1	-.3525828E-1	-.79333503E-1	-.42333479E-1	-.81624045E-1	-.41059889E-1	
-.74328186E-1	-.35266001E-1	-.59464233E-1	-.25980347E-1	.234242168E+1	.459885	
59.40GHz						
.10000000E+1	.61772795E+0	.584899953E+0	.23913298E+0	.73579252E-1	.10703176E-1	
-.55789220E-1	-.35778189E-1	-.79655550E-1	-.43104248E-1	-.82053374E-1	-.41828149E-1	
-.74730993E-1	-.35934602E-1	-.59790541E-1	-.26474721E-1	.23407661E+1	.460503	

Table 13. Optical parameters (Marshall-Palmer 30mm/hr)

Freq(Ghz)	\bar{w}_0	\bar{w}_1	\bar{w}_2	\bar{w}_3	\bar{w}_4	\bar{w}_5
	\bar{w}_6	\bar{w}_7	\bar{w}_8	\bar{w}_9	\bar{w}_{10}	\bar{w}_{11}
	\bar{w}_{12}	\bar{w}_{13}	\bar{w}_{14}	\bar{w}_{15}	β_{ext}	\bar{w}_{16}
50.50GHz						
.10000000E+1	.49121131E+0	.52749945E+0	.18465455E+0	.37577904E-1	.21290313E-3	
-.59429845E-1	-.29563076E-1	-.75897299E-1	-.33771160E-1	-.77335382E-1	-.3258128E-1	
-.70337569E-1	-.27966255E-1	-.56235893E-1	-.20590112E-1	-.23960056E+1	.452447	
53.20GHz						
.10000000E+1	.54032236E+0	.54780426E+0	.20510323E+0	.51180242E-1	.38509139E-2	
-.58223647E-1	-.32082087E-1	-.77302182E-1	-.37361464E-1	-.79047595E-1	-.3614894E-1	
-.71925555AE-1	-.31008134E-1	-.57520069E-1	-.22035439E-1	.25042903E+1	.4568047	
54.35GHz						
.10000000E+1	.55780879E+0	.555833315E+0	.21379108E+0	.57168584E-1	.57554127E-2	
-.57341798E-1	-.32934138E-1	-.77654825E-1	-.38723578E-1	-.79759449E-1	-.37470051E-1	
-.72289742E-1	-.32176766E-1	-.58057924E-1	-.23699273E-1	.25473123E+1	.459291	
54.90GHz						
.10000000E+1	.56774825E+0	.56048550E+0	.21827777E+0	.60172031E-1	.66808367E-2	
-.57212071E-1	-.33412287E-1	-.78157829E-1	-.39469207E-1	-.80146923E-1	-.38211398E-1	
-.72951209E-1	-.32815977E-1	-.50350499E-1	-.24171486E-1	.25673943E+1	.460022	
58.40GHz						
.10000000E+1	.62976264E+0	.5920A608E+0	.24827964E+0	.80379454E-1	.13569334E-1	
-.54649607E-1	-.36207737E-1	-.80123911E-1	-.44223746E-1	-.82770825E-1	-.42985301E-1	
-.75413257E-1	-.36938696E-1	-.60345256E-1	-.27219927E-1	.268665309E+1	.464224	
58.82GHz						
.10000000E+1	.63491862E+0	.59508925E+0	.25163174E+0	.82797327E-1	.14482012E-1	
-.54253648E-1	-.36399237E-1	-.80308177E-1	-.44668250E-1	-.83047480E-1	-.43442921E-1	
-.75676103E-1	-.37335561E-1	-.60558841E-1	-.27514176E-1	.2699830E+1	.465204	
59.40GHz						
.10000000E+1	.64513795E+0	.60078004E+0	.25690628E+0	.86364644E-1	.15797053E-1	
-.53734037E-1	-.36816316E-1	-.80640734E-1	-.45466419E-1	-.83516071E-1	-.4425464E-1	
-.76119073E-1	-.38038221E-1	-.60918238E-1	-.28034263E-1	.27178708E+1	.465761	

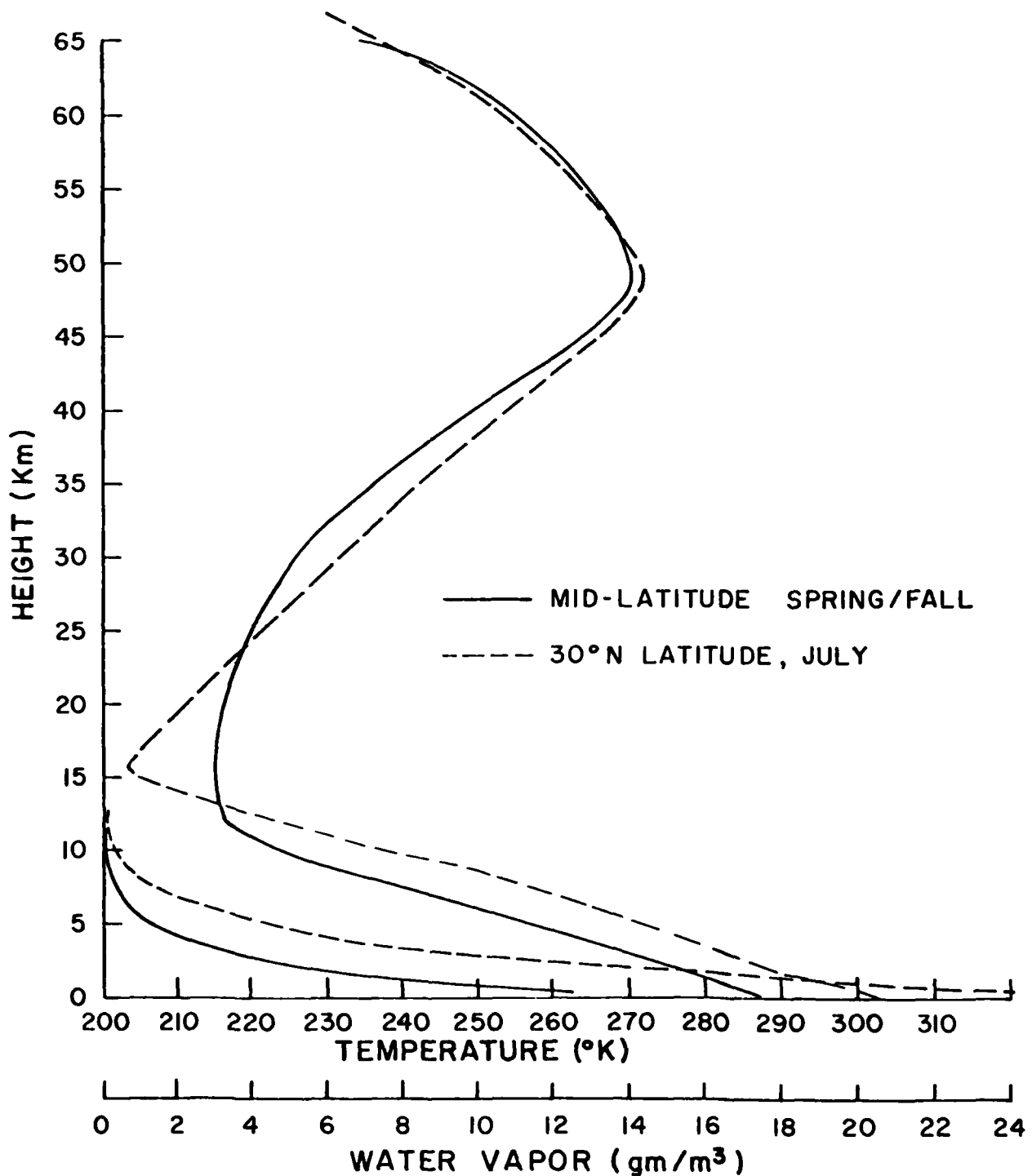


Figure 5. Climatological temperature and water vapor profiles for the northern hemispheric mid-latitude Spring/Fall and 30° north latitude, July.

$$V = \frac{4}{3} \pi \int_0^{\infty} r^3 N(r) dr . \quad (5.1)$$

Therefore the total liquid water content per unit volume of atmosphere is

$$W = \frac{4}{3} \pi \rho \int_0^{\infty} r^3 N(r) dr \text{ (gm cm}^{-3}\text{)} , \quad (5.2)$$

where r is in units of cm, $N(r)$ is in terms of cm^{-4} , and the density of liquid water ρ is 1 gm cm^{-3} . For the Deirmendjian L-Model we have

$$W = 1.16678(10^{-2}) \text{ (gm cm}^{-2} \text{ km}^{-1}\text{)} , \quad (5.3)$$

while for the Marshall-Palmer size distribution we find

$$W = 1.77883(10^{-2}) R^{.84} \text{ (gm cm}^{-2} \text{ km}^{-1}\text{)} . \quad (5.4)$$

Table 14 contains the total mass of liquid water within a column of 1 cm^2 cross section for the cloud models used.

Table 14. Total liquid water content ($10^{-2} \text{ gm cm}^{-2}$).

Thickness (km)	1	2	3	4	5
Deirmendjian	1.16678	2.33356	3.50034	4.66712	5.83390
Marshall-Palmer R(mm/hr)					
1	0.88941	1.77882	2.66823	3.55764	4.44705
2	1.59209	3.18418	4.77627	6.36835	7.96044
3	2.23812	4.47625	6.71437	8.95249	11.1906
4	2.84992	5.69984	8.54975	11.3997	14.2496
5	3.43745	6.87491	10.3124	13.7498	17.1873
10	6.15321	12.3064	18.4596	24.6129	30.7661
15	8.65005	17.3001	25.9502	34.0020	43.2503
20	11.0146	22.0291	33.0437	44.0583	55.0728
25	13.2853	26.5706	39.8559	53.1412	66.4266
30	15.4840	30.9681	46.5421	61.9361	77.4201

SECTION 4

SENSITIVITY ANALYSES ON THE EFFECTS OF CLOUD AND PRECIPITATION ON THE DMSP SSM/T CHANNELS

In this section, we present the results computed from the microwave radiative transfer program for cloudy atmospheres described in Section 2. The computations utilize the single-scattering parameters presented in Section 3 for input to the transfer program. In view of the weighting function diagram depicted in Figure 2, it is anticipated that only 50.50, 53.20 and 54.35 GHz (channels 1-3) whose peaks of the weighting function are below the tropopause will be affected by clouds and precipitation. However, in the following analyses, 54.90 GHz (channel 4) is also included in the computations. Effects of the rainfall rate and cloud layer thickness on the up-welling ($\mu=1$) brightness temperature over land and ocean surfaces are first discussed. Computational results due to variations of the cloud location and atmospheric profile are then reported. Physical interpretation of the results are given in the last Subsection.

4.1 Dependence on Layer Thickness and Rainfall Rate

To determine the effect of varying cloud thicknesses on the brightness temperatures reaching the top of the atmosphere, cloud models were inserted into the atmosphere with a constant cloud base of 1 km.

Thickness cases of 1, 2, 3, 4 and 5 km were examined. Variations of the brightness temperature over land with respect to cloud thickness and rainfall rate for channels 1 through 4 are displayed in Figures 6 through 10. The surface emissivity over land is taken to be 0.97 for all channels in this sensitivity study. The energy sensed by channels 5, 6 and 7 originates sufficiently high in the atmosphere that the brightness temperatures are insignificantly affected by the cloud models as pointed out previously.

The differences due to thickness for channels 3 and 4 may be misleading. It is more likely that a positional dependence for the cloud is being exhibited. Since the cloud base was fixed at 1 km, only the thicker clouds reached into the energy peak source regions for channels 3 and 4 (weighting functions peak at about 7 and 10.5 km, respectively). For example, a 5 km thick cloud with a 1 km base at a 2 mm/hr rainfall rate results in brightness temperatures for channels 3 and 4 of 237.3° K and 228.9° K. The Deirmendjian L-Model cloud used in the position study has liquid water content approximately equal to that of the 2 mm/hr rain model and yet a 2 km thick L-Model cloud with base at 4 km results in nearly the same brightness temperatures for channels 3 and 4 as the 5 km thick cloud discussed above (237.2° K and 228.7° K, respectively).

Channels 1 and 2 (peaking near the surface and 2 km) show decreasing brightness temperatures for increasing cloud thicknesses. The decrease is greater for clouds modeling higher rainfall rates. For channel 1 at a rainfall rate of 1 mm/hr the decrease ranges from 2° K for a 1 km thick cloud to 16° K for a 5 km thick cloud. For a

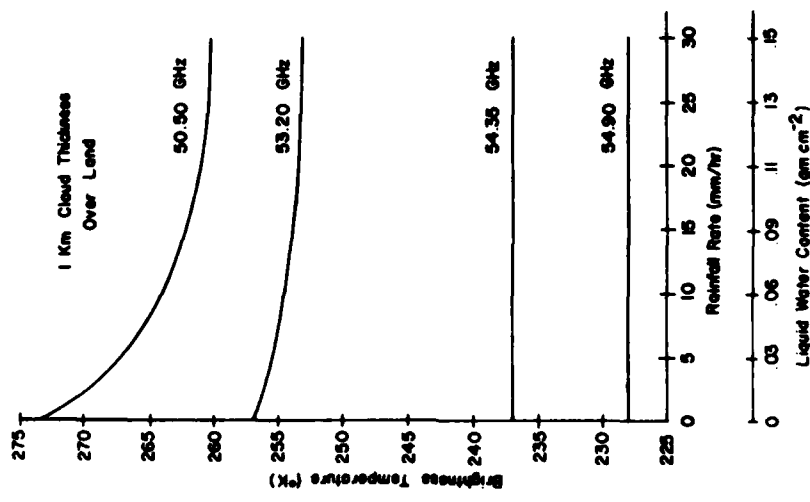


Figure 6. Brightness temperature versus rainfall rate (or liquid water content) for 1 km thick cloud over land (mid-latitude Spring/Fall profile).

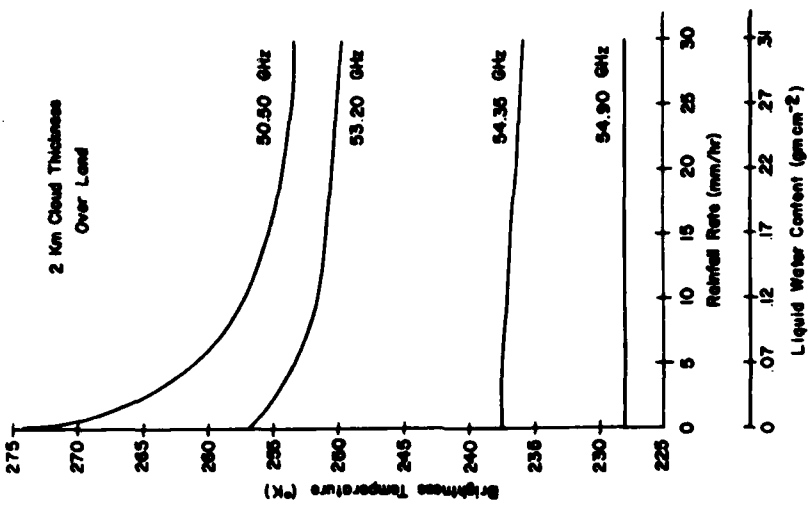


Figure 7. Brightness temperature versus rainfall rate (or liquid water content) for 2 km thick cloud over land (mid-latitude Spring/Fall profile).

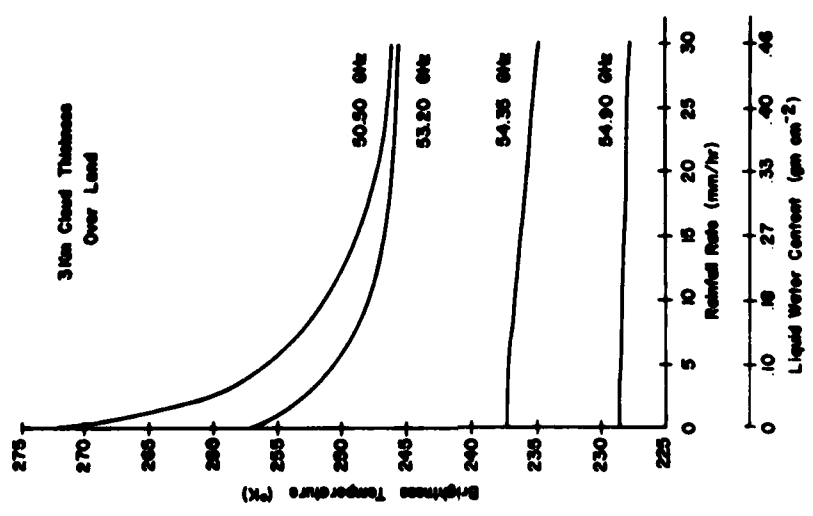


Figure 8. Brightness temperature versus rainfall rate (or liquid water content) for 3 km thick cloud over land (mid-latitude Spring/Fall profile).

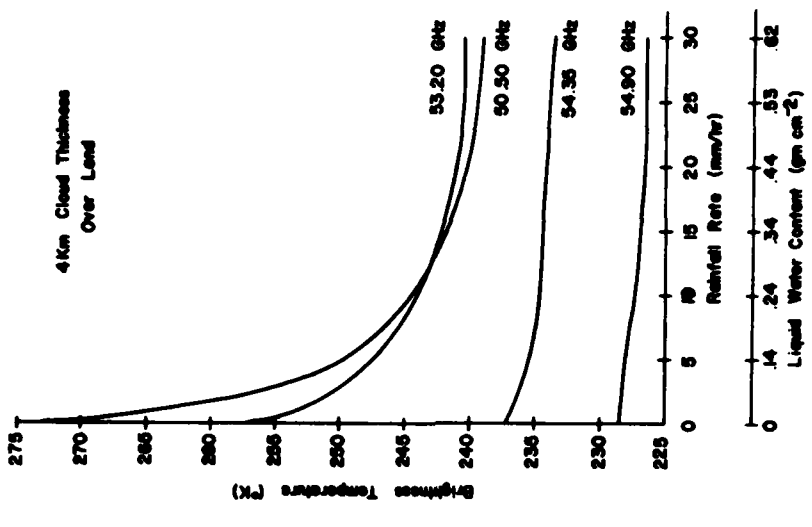


Figure 9. Brightness temperature versus rainfall rate (or liquid water content) for 3 km thick cloud over land (mid-latitude Spring/Fall profile).

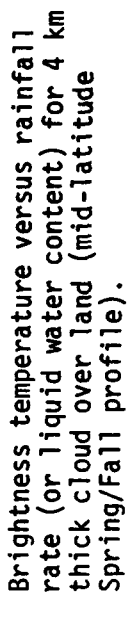


Figure 9. Brightness temperature versus rainfall rate (or liquid water content) for 4 km thick cloud over land (mid-latitude Spring/Fall profile).

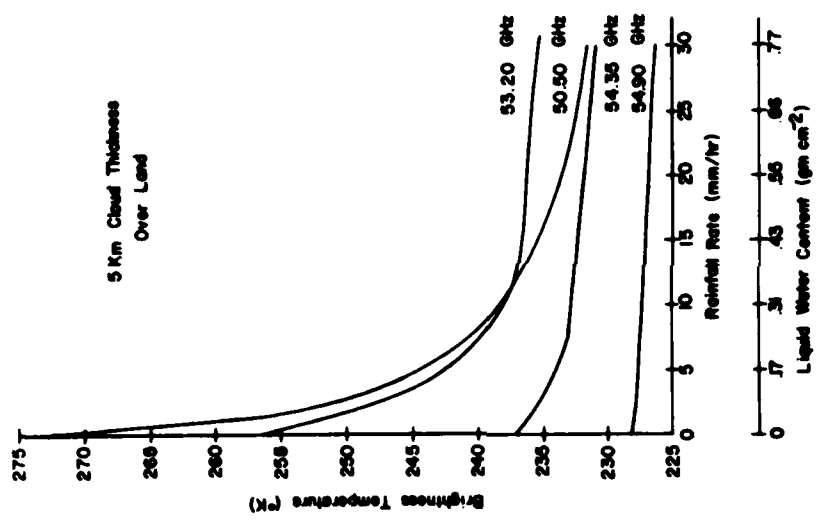


Figure 10. Brightness temperature versus rainfall rate (or liquid water content) for 5 km thick cloud over land (mid-latitude Spring/Fall profile).

rainfall rate of 30 mm/hr the channel 1 brightness temperature decreases 14° K for a 1 km thick cloud and 43° K for a 5 km thick cloud. Channel 2 displays the same trends as channel 1 but to a lesser degree. For a rainfall rate of 1 mm/hr the decrease in channel 2 brightness temperature as a function of cloud thickness ranges from less than 0.5° K to 5° K. For a rainfall rate of 30 mm/hr the range is 4° K to 22° K.

The results for channels 3 and 4 show relatively constant brightness temperatures unaffected by rainfall rates less than about 3 mm/hr. For rainfall rates greater than 3 mm/hr the brightness temperature decreases with increasing cloud thickness. The maximum decreases are 7° K for channel 3 and 2° K for channel 4; both at rainfall rates of 30 mm/hr and cloud thicknesses of 5 km.

Figures 11 through 14 depict the variation of brightness temperatures over ocean having an emissivity of 0.51 with respect to cloud thickness and liquid water content for channels 1-4. The results over the ocean are quite different from the results over land. Note that the only physical difference between these two cases is that the surface emissivity for all channels is taken to be 0.97 for a land surface and 0.51 for an ocean surface. The difference in the surface emissivity reveals that the surface contribution over ocean is approximately one half of the surface contribution over land, and that the atmospheric contribution reflected from the earth's surface is approximately 16 times greater over ocean.

Figures 11 and 12 show that channels 1 and 2 follow similar trends over the ocean but to different degrees. For all cloud thicknesses, an initial reduction in the brightness temperature is observed for clouds with low liquid water content. For channel 1 the maximum

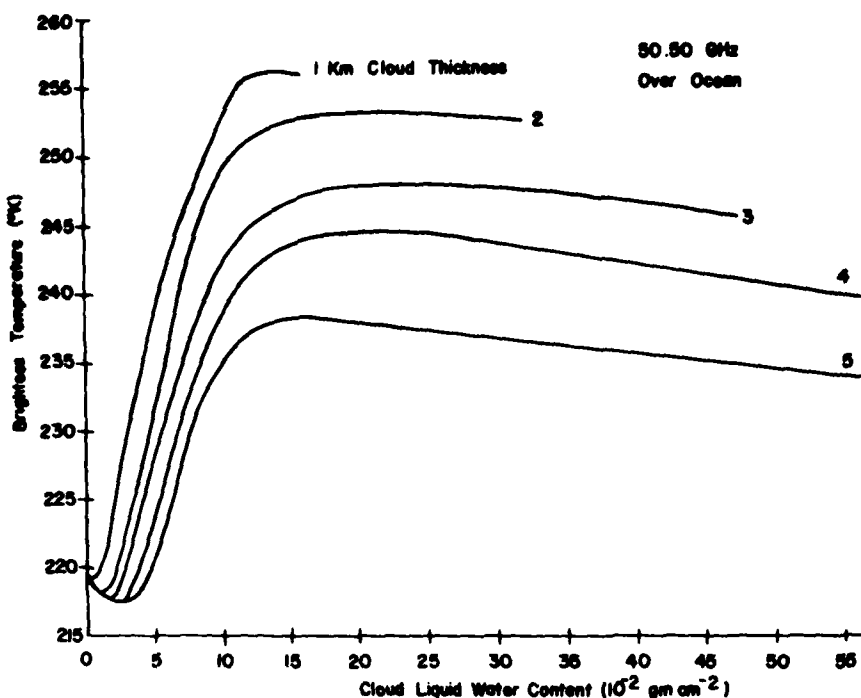


Figure 11. 50.50 GHz brightness temperature as a function of cloud thickness and liquid water content (mid-latitude Spring/Fall profile over ocean).

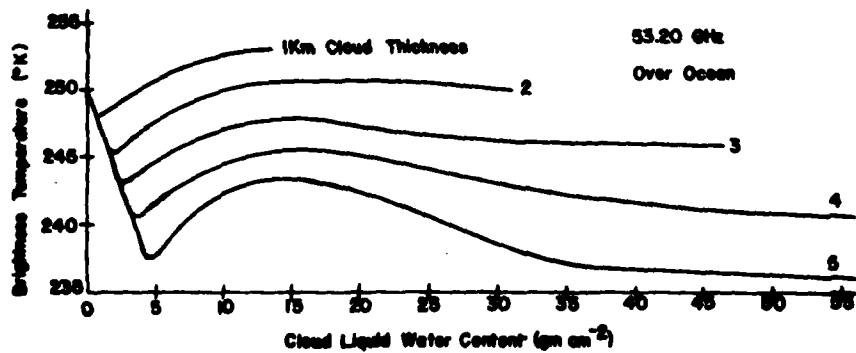


Figure 12. 53.20 GHz brightness temperature as a function of cloud thickness and liquid water content (mid-latitude Spring/Fall profile over ocean). Values of the cloud liquid water content in this figure should be multiplied by 10^{-2} .

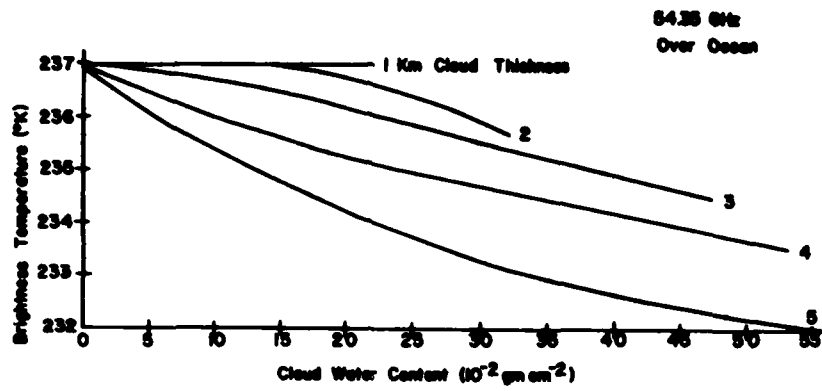


Figure 13. 54.35 GHz brightness temperature as a function of cloud thickness and liquid water content (mid-latitude Spring/Fall profile over ocean).

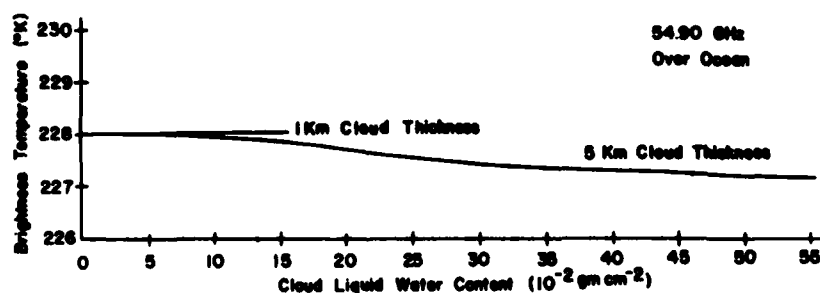


Figure 14. 54.90 GHz brightness temperature as a function of cloud thickness and liquid water content (mid-latitude Spring/Fall profile over ocean).

reduction is 2° K, while for channel 2 the maximum reduction is nearly 13° K. At some liquid water content less than $5 \times 10^{-2} \text{ gm cm}^{-2}$ the brightness temperature begins to increase. The turning point occurs at lower liquid water content for thinner clouds. The brightness temperature then increases until the liquid water content reaches about $15 \times 10^{-2} \text{ gm cm}^{-2}$. For channel 1 this increase results in a maximum brightness temperature more than 35° K higher than the clear column value. For channel 2 the maximum brightness temperature is about 3° K greater than the clear column value. For liquid water contents greater than $15 \times 10^{-2} \text{ gm cm}^{-2}$, the brightness temperature decreases for both channels and all cloud thicknesses. Note that the maximum brightness temperature observed over ocean is very nearly the same as the minimum brightness temperature observed over land (within about 4 - 7° K).

Figures 13 and 14 indicate that channels 3 and 4 are relatively unaffected by a 1 km thick cloud with a cloud base at 1 km. Increasing the cloud thickness above 1 km causes steadily decreasing brightness temperatures. For a constant cloud thickness, increasing the liquid water content causes a decrease in the brightness temperature. Note that channel 4 is affected by less than 1° K for all of the cases studied.

4.2 Dependence on Layer Location and Atmospheric Profile

In this subsection, we first investigate the effect of the position of the cloud layer in the atmosphere on the upwelling brightness temperature. Figures 15 through 20 display the importance of cloud position relative to the peak of the weighting function for each channel over the land surface.

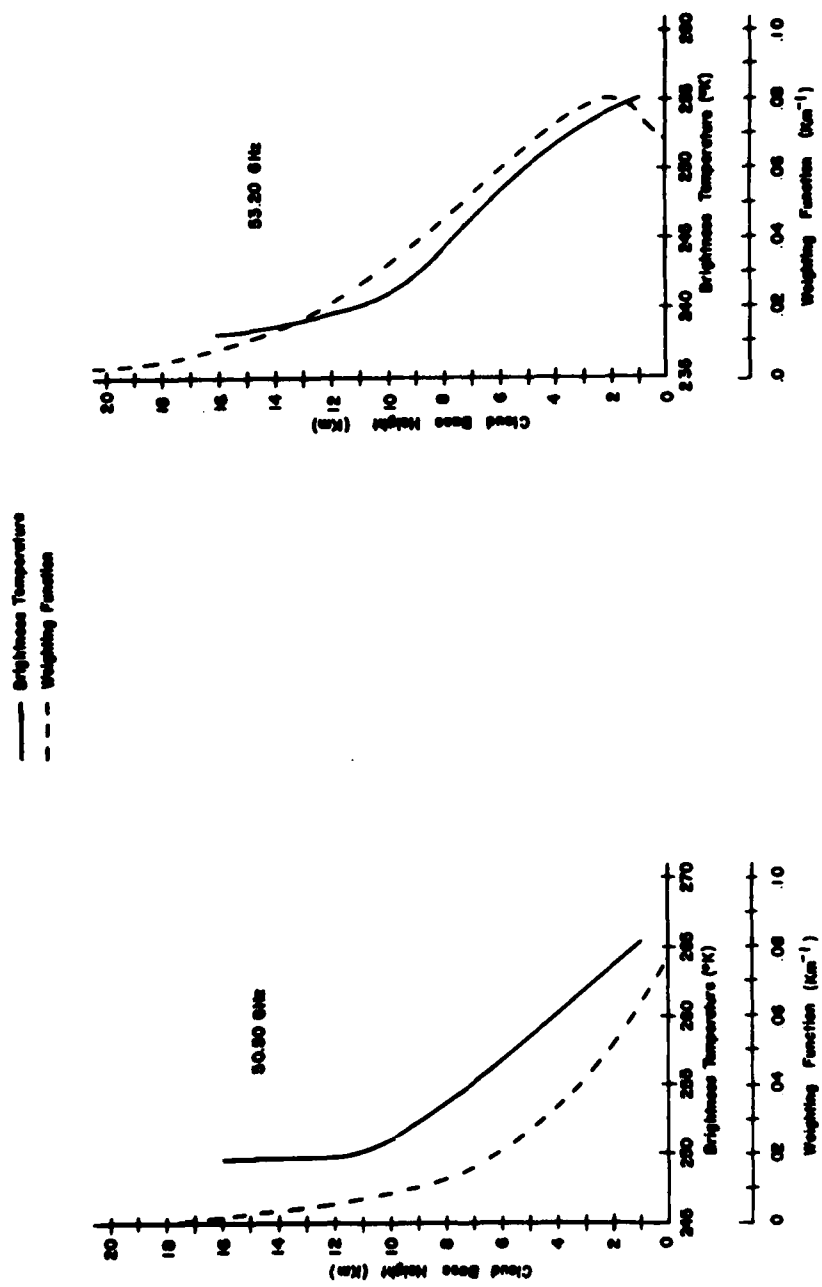


Figure 15. 50.50 GHz brightness temperature dependence on cloud base height for a 2 km thick Deirmendjian L-Model cloud (mid-latitude Spring/Fall profile over land).

Figure 16. 53.20 GHz brightness temperature dependence on cloud base height for a 2 km thick Deirmendjian L-Model cloud (mid-latitude Spring/Fall profile over land).

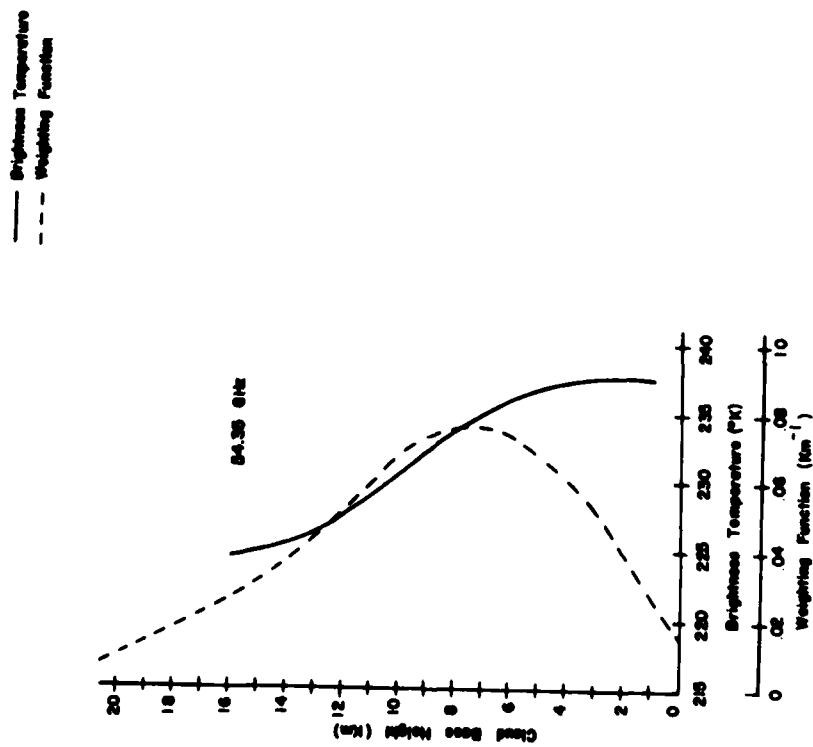


Figure 17. 54.35 GHz brightness temperature dependence on cloud base height for a 2 km thick Deirmendjian L-Model cloud (mid-latitude Spring/Fall profile over land).

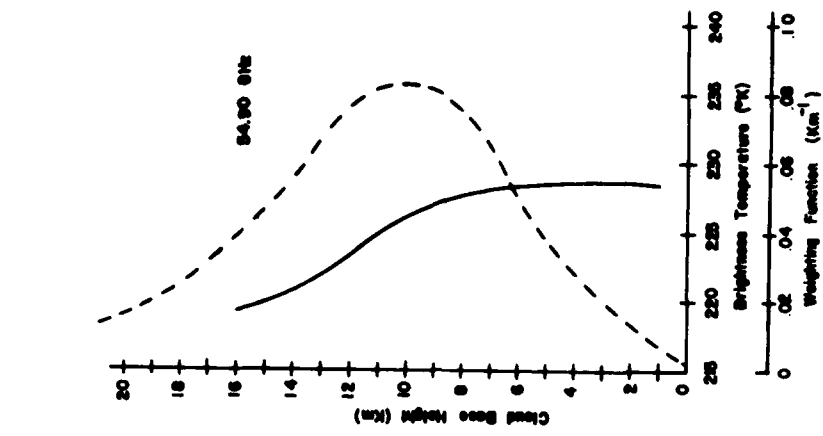


Figure 18. 54.90 GHz brightness temperature dependence on cloud base height for a 2 km thick Deirmendjian L-Model cloud (mid-latitude Spring/Fall profile over land).

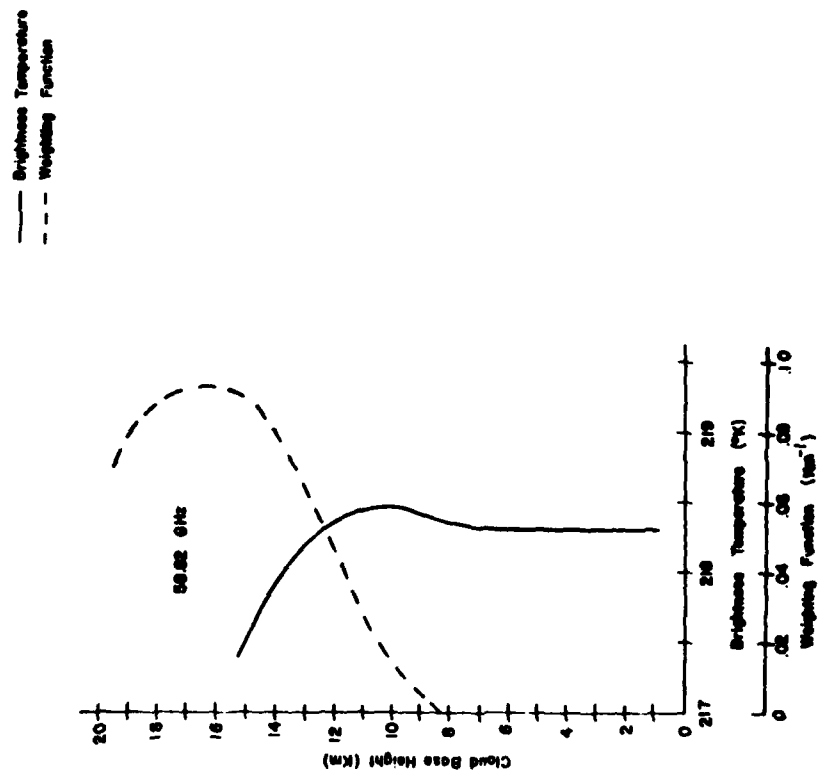


Figure 19. 58.82 GHz brightness temperature dependence on cloud base height for a 2 km thick Deirmendjian L-Model cloud (mid-latitude Spring/Fall profile over land).

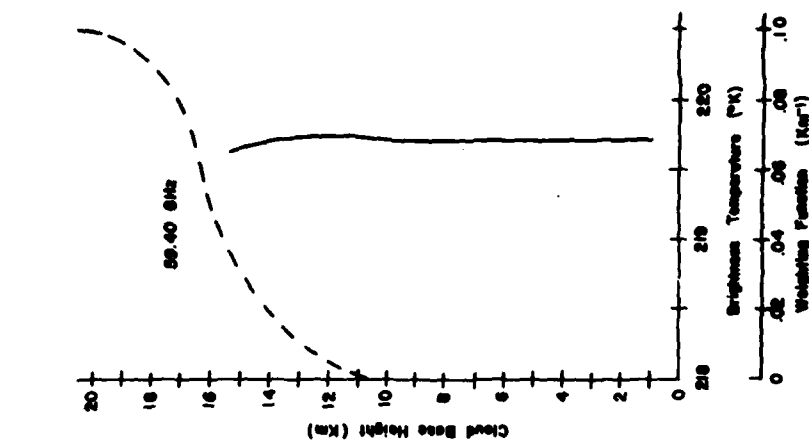


Figure 20. 59.40 GHz brightness temperature dependence on cloud base height for a 2 km thick Deirmendjian L-Model cloud (mid-latitude Spring/Fall profile over land).

Channels 1 and 2 show the effects on a channel when the cloud is at or above the peak of the weighting function, i.e., the prime energy source region for the channel. The brightness temperature decreases rapidly as the cloud is moved higher putting more and more of the energy source for the channel beneath it. Eventually, the brightness temperature becomes near constant as all of the significant source region for channel energy is below the cloud and therefore raising the cloud higher has only slight effects.

Channels 3 and 4 show the results of moving a cloud from below the prime energy source region up through the source region. Far below the energy source the brightness temperature remains nearly constant. Then, as the cloud moves into the source region, the brightness temperature decreases significantly, becoming near constant above the source region as for channels 1 and 2.

Channels 6 and 7 indicate that for channels peaking high enough in the atmosphere to be free of surface effects, brightness temperatures increase slightly as the cloud approaches the energy source region from below.

Sensitivity analyses on the positional dependence were also carried out over the ocean surface. It was found that the same positional dependence exists over the ocean as over the land with no change in trends for any of the channels.

Figures 21 through 28 display the results when the sensitivity analysis is duplicated for the 30° N latitude, July, profile. Although the different profile naturally results in different brightness temperatures, the trends noted for the northern hemispheric mid-latitude Spring/Fall profile for liquid water content greater than about 3×10^{-2} gm cm^{-2} are observed to persist.

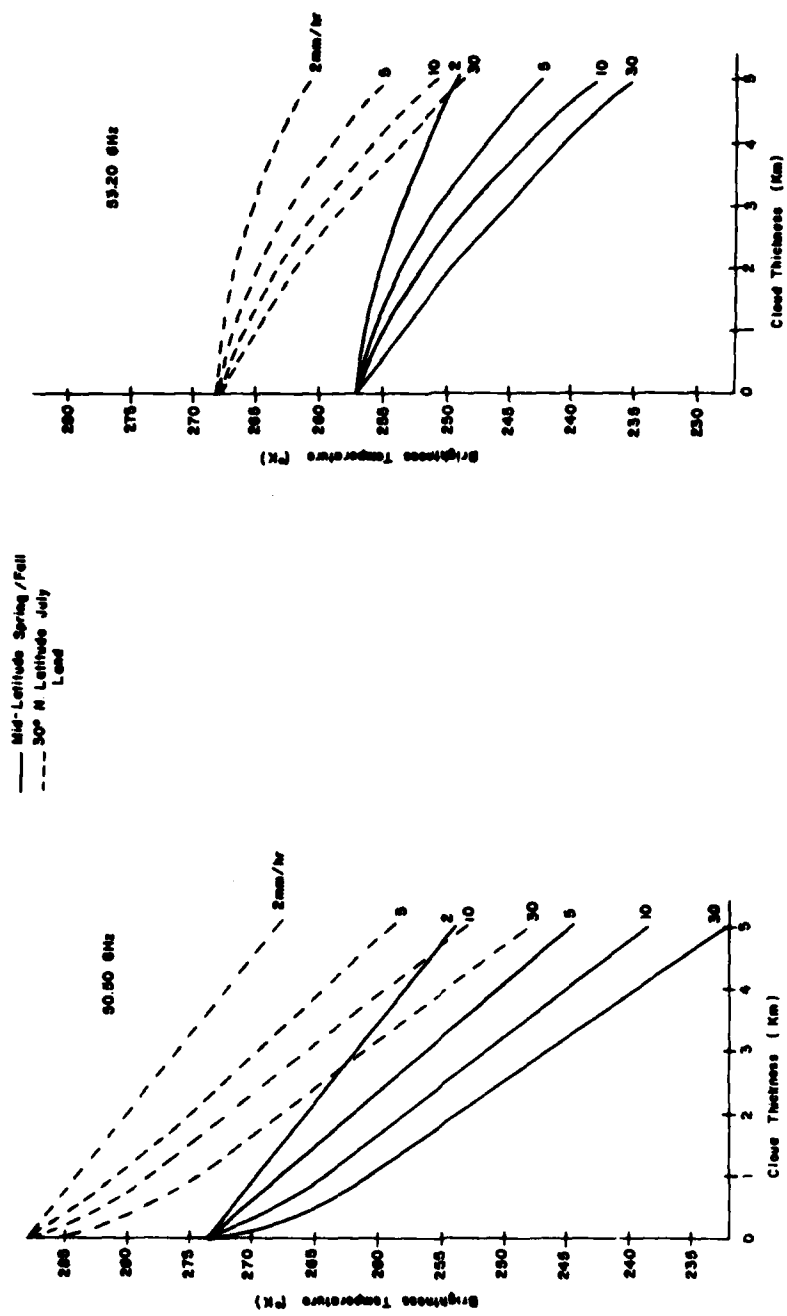
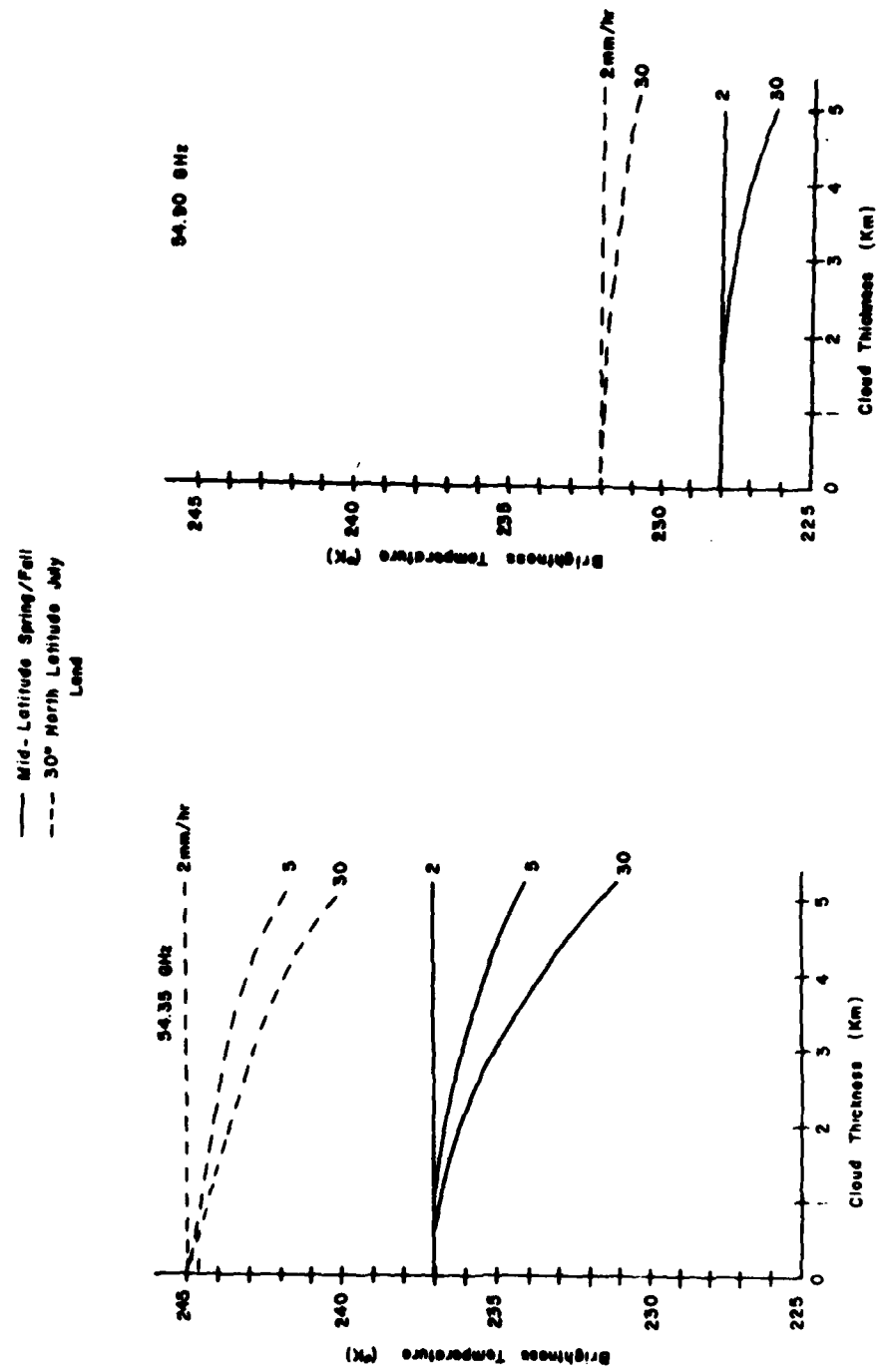


Figure 21. 50.50 GHz channel profile dependence over land.

Figure 22. 53.20 GHz channel profile dependence over land.



50

Figure 23. 54.35 GHz channel profile dependence over land.

Figure 24. 54.90 GHz channel profile dependence over land.

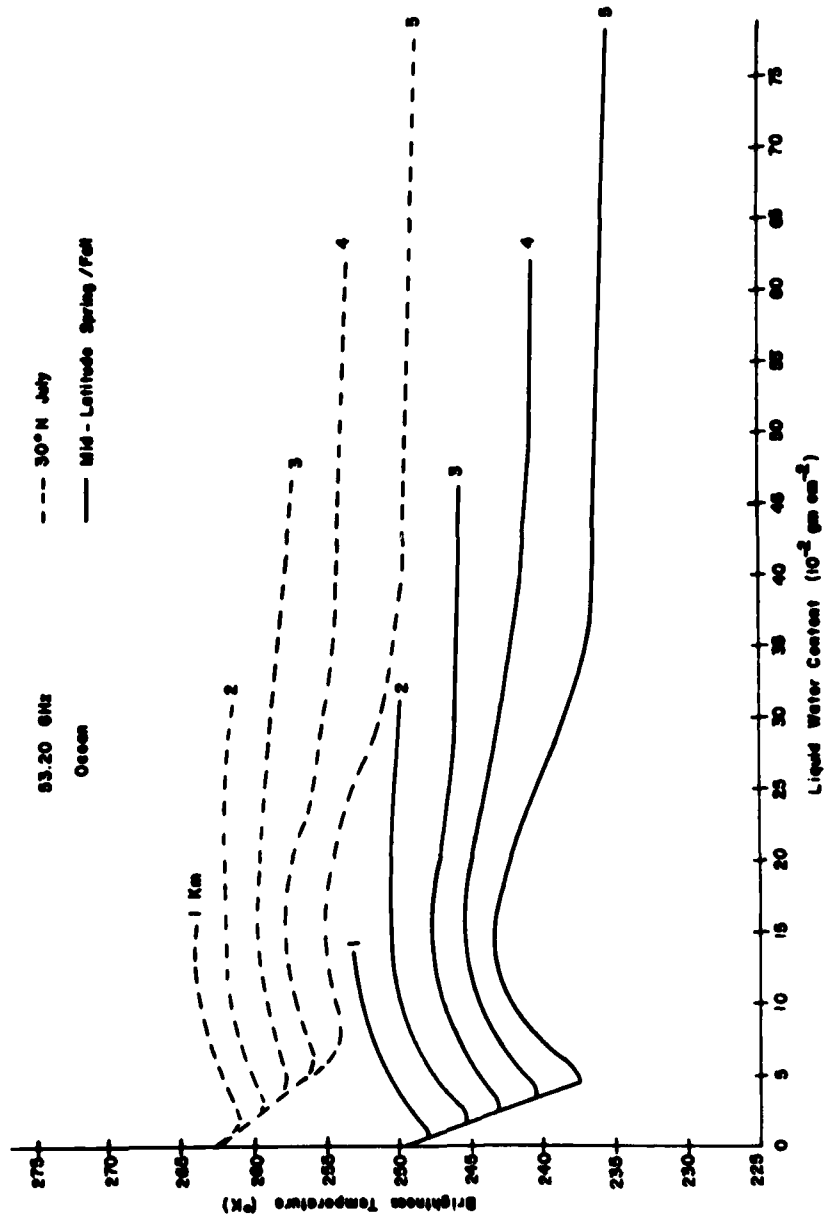


Figure 25. 53.20 GHz channel profile dependence over ocean.

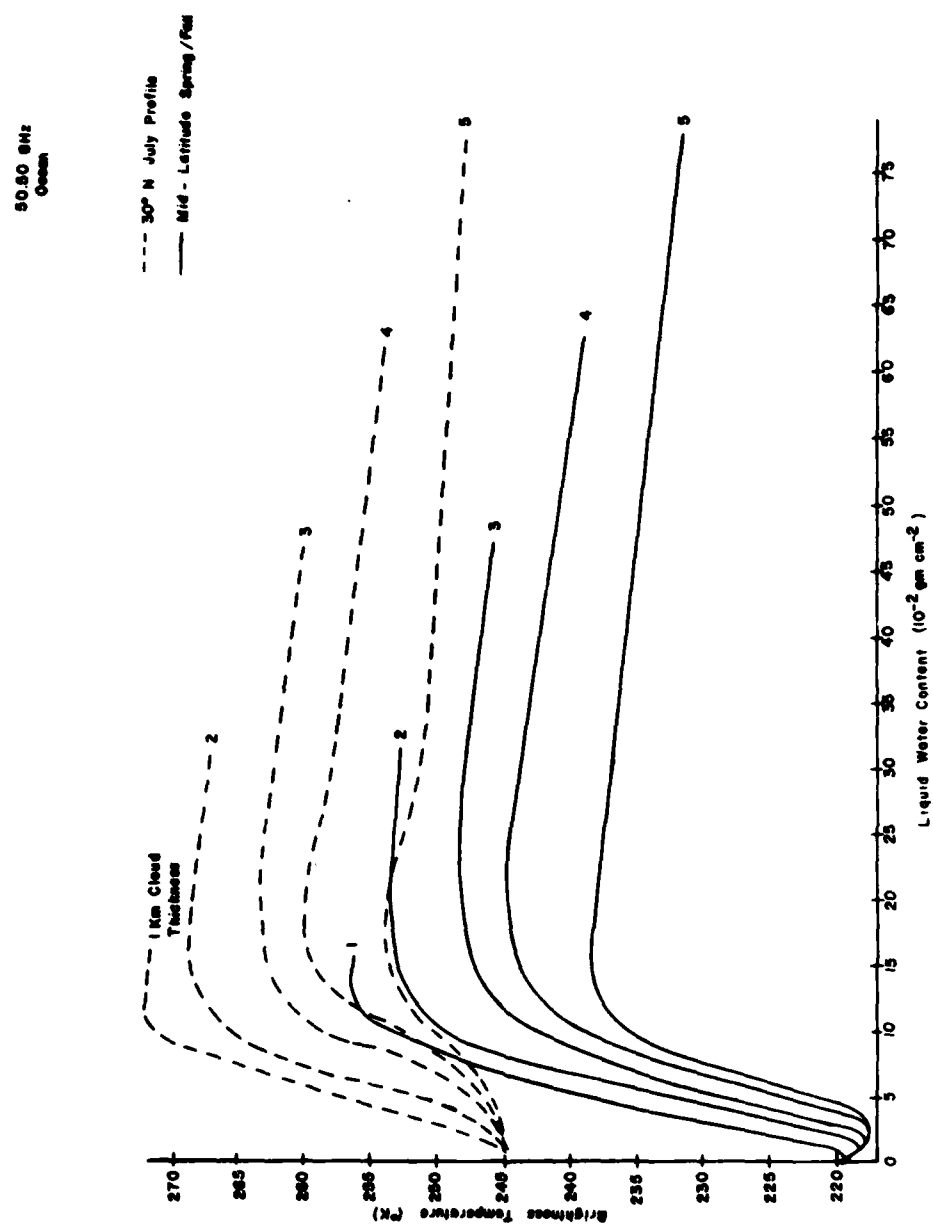


Figure 26. 50.50 GHz channel profile dependence over ocean.

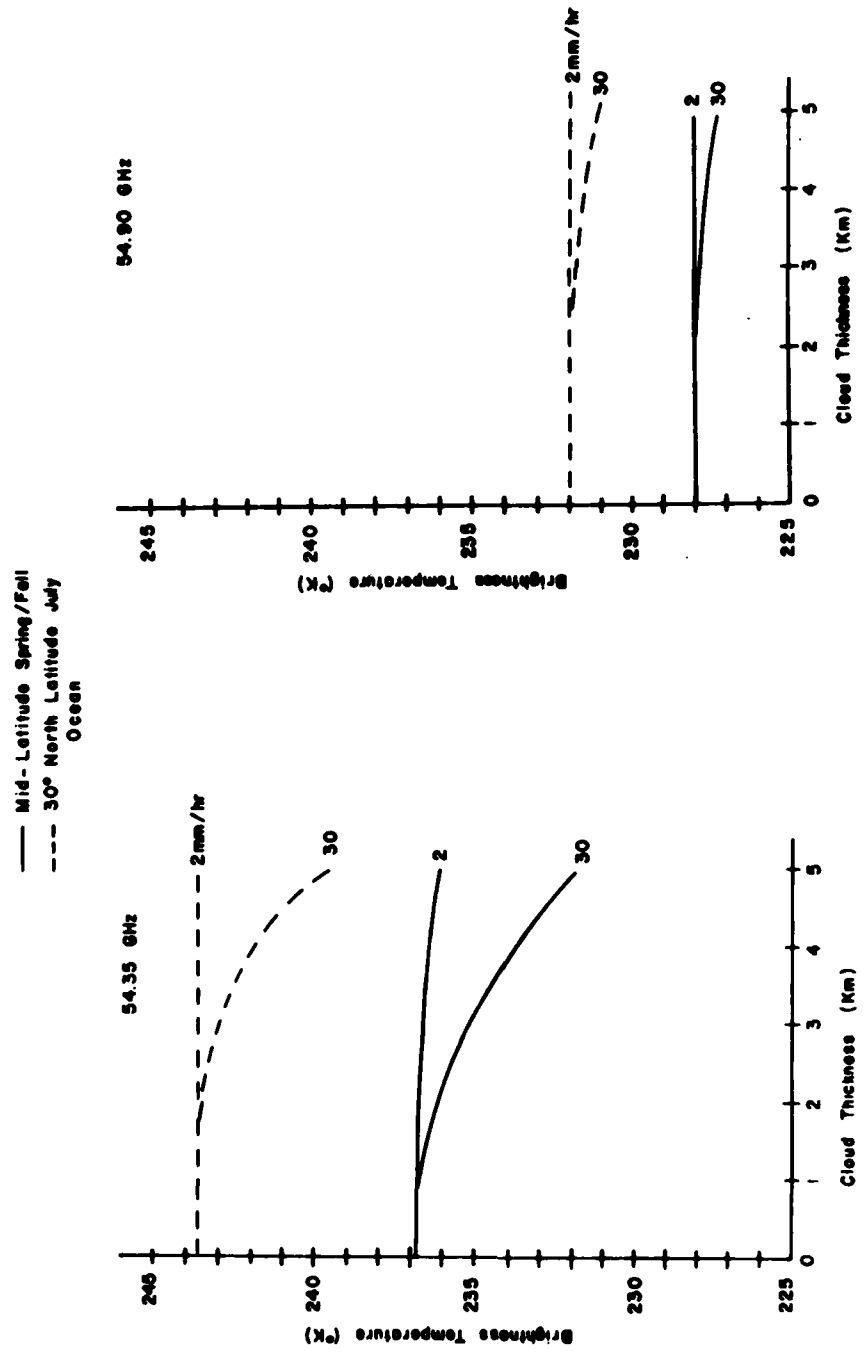


Figure 27. 54.35 GHz channel profile dependence over ocean.

Figure 28. 54.90 GHz channel profile dependence over ocean.

4.3 Interpretation of Results

In order to aid in the interpretation of results Figure 29 is included which graphically depicts the terms contributing to the cloud boundary conditions and the mechanisms for energy loss and gain within the cloud. There are three mechanisms for energy gain within the cloud caused by gaseous emission, droplet emission, and multiple scattering. On the other hand, there are three mechanisms for energy loss due to gaseous absorption, droplet absorption, and single scattering. The balance of these mechanisms determines whether the emergent energy at the cloud top and bottom is greater or less than the respective boundary condition at the cloud bottom and top. Of course, the boundary conditions themselves are an important contribution to the emergent energy at the opposite side of the cloud. The upper boundary condition is totally unaffected by the earth's surface. For the lower boundary condition, quite the opposite is true. When the emissivity (and hence the reflectivity) of the earth's surface varies, three of the four contributing terms for the lower boundary condition are influenced. These include (1) the surface emission term, (2) the atmospheric contribution reflected from the surface of the earth, and (3) the emergent energy from the cloud bottom reflected from the earth's surface. Finally, it is important to note that the emission terms are generally stronger near the cloud bottom due to the temperature gradient within the cloud; and throughout the cloud, emission by water droplets is greater than emission by atmospheric molecules.

Introducing a cloud into the atmosphere will then result in increased emission within the cloud layer and decreased transmission through the cloud layer. The three contributions to the cloud top

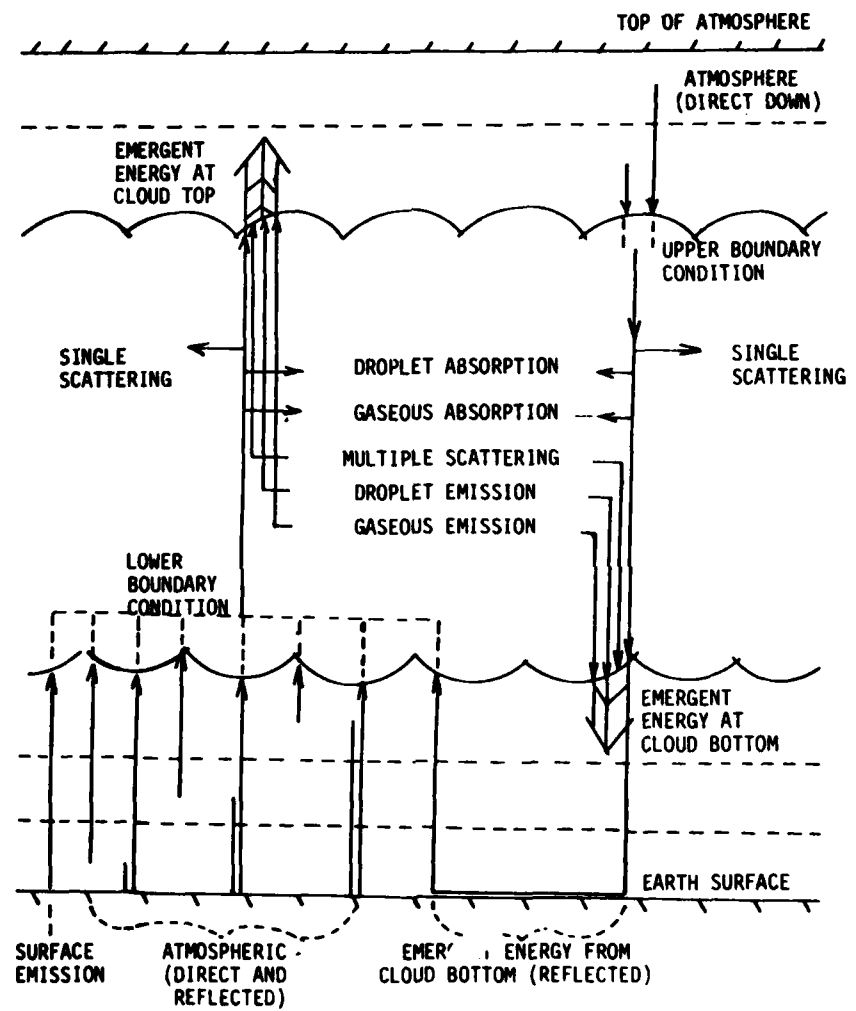


Figure 29. Radiative transfer through a cloud layer.

brightness temperature are emission by the earth's surface, atmospheric emission and emission from within the cloud layer.

To remove the surface term, atmospheric contribution, or cloud emission, we simply set the surface temperature, boundary conditions, or cloud temperature equal to zero, respectively. Each contribution can be analyzed separately by removing the other two.

In Figures 30 through 33 the effects of cloud thickness and liquid water content on the three contributions to the cloud top brightness temperature over the ocean are displayed. The solid line is the graphical sum of these components and the X's are computed cloud top temperatures directly from the microwave transfer program for randomly selected cases. Clearly, for channel 1 the addition of energy by droplet emission is greater than the energy loss due to droplet absorption and single scattering for liquid water contents greater than 0.01 gm cm^{-2} . This explains the region of increasing brightness temperature for channel 1 observed in Figure 11. For liquid water content greater than 0.20 gm cm^{-2} the droplet emission reaching the cloud top is nearly constant and represents almost all of the energy reaching the cloud top. Although the surface emission and atmospheric contributions to cloud top brightness temperature are small in this region, they are decreasing with increasing liquid water content so the cloud top brightness temperature decreases slightly also. This explains the slight decrease in the brightness temperature for channel 1 in this region. The fact that cloud emission accounts for almost all of the cloud top brightness temperature for water content greater than 0.20 gm cm^{-2} explains why the brightness temperatures over ocean and over land are nearly the same in this region. The cloud emission must be less than the reduction

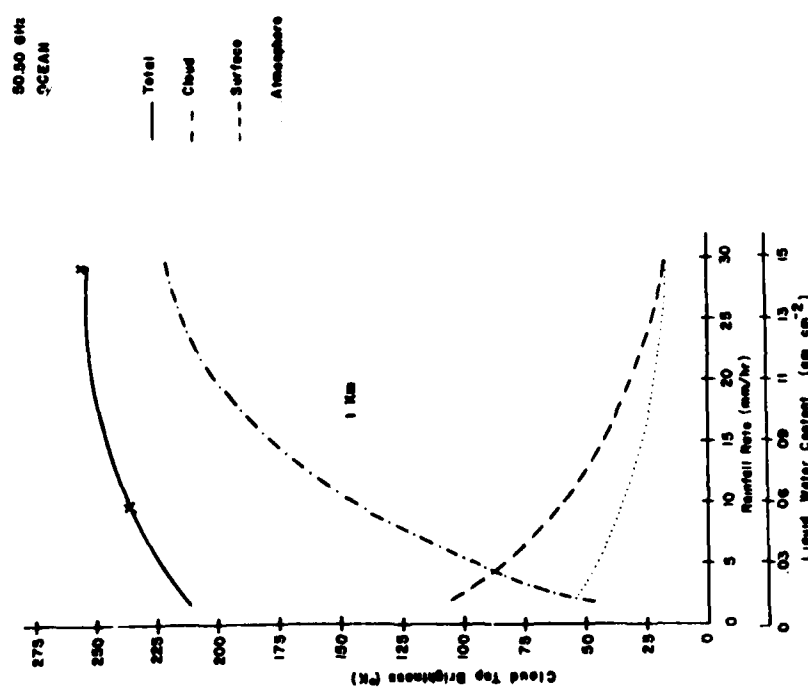


Figure 30. Component contributions to 50.50 GHz cloud top brightness for a 1 km thick cloud over ocean (mid-latitude Spring/Fall profile).

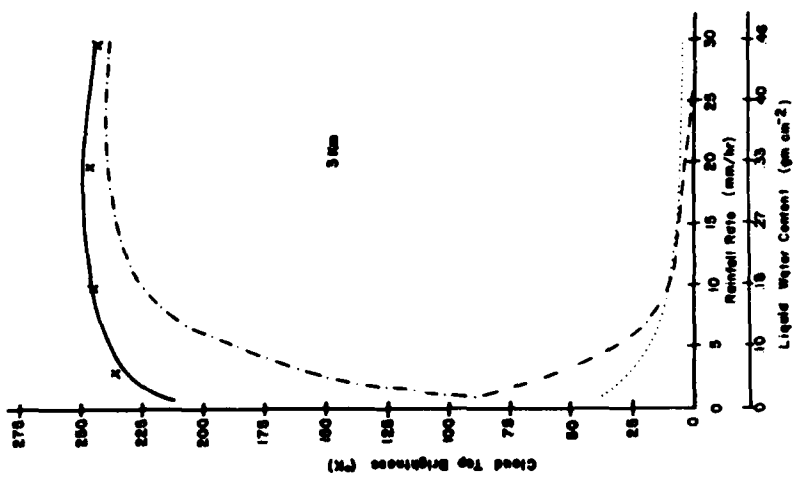


Figure 31. Component contributions to 50.50 GHz cloud top brightness for a 3 km thick cloud over ocean (mid-latitude Spring/Fall profile).

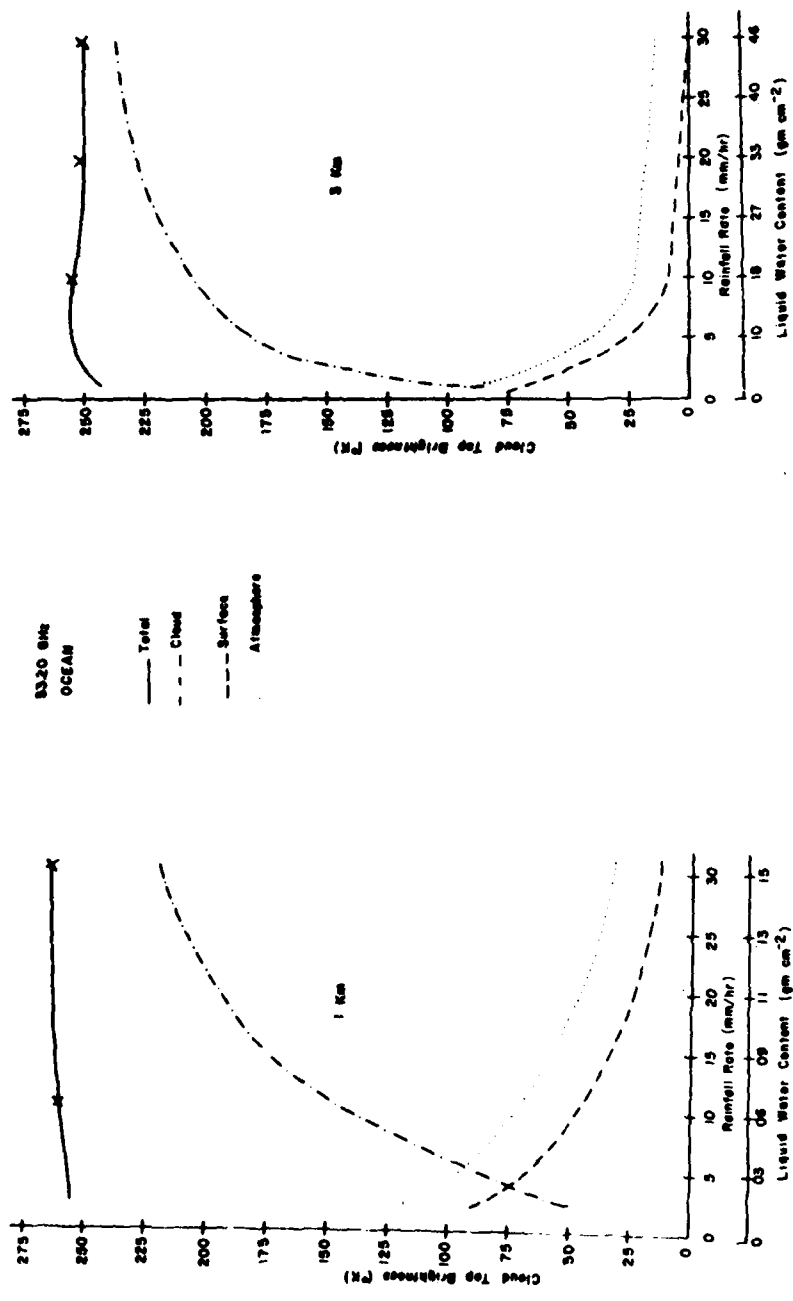


Figure 32. Component contributions to 53.20 GHz cloud top brightness for a 1 km thick cloud over ocean (mid-latitude Spring/Fall profile).

Figure 33. Component contributions to 53.20 GHz cloud top brightness for a 3 km thick cloud over ocean (mid-latitude Spring/Fall profile).

Figure 33. Component contributions to 53.20 GHz cloud top brightness for a 3 km thick cloud over ocean (mid-latitude Spring/Fall profile).

in the surface and atmospheric terms for liquid water content less than 0.01 gm cm^{-2} in order to explain the slight decrease in brightness temperatures in this region.

The cloud emission curves remain the same over land. As previously noted, the surface term is nearly twice as large over land while the reflected terms are only one sixteenth as large. The direct atmospheric contribution remains the same. The net result is that the upwelling brightness temperature at the cloud bottom over land is significantly larger than that over ocean. For example, our numerical experiments show that the lower boundary condition over land for a 1 km thick cloud ranges from 280° K to 285° K for rainfall rates of 1 to 30 mm/hr. Over ocean the range is 200° K to 240° K for the same cloud thickness and rainfall rates. Since the loss of energy within the cloud layer is proportional to the energy incident at the cloud base, a greater reduction takes place over land. This increased reduction is associated with the continuously decrease of brightness temperatures with increasing liquid water content over land for channel 1 as shown in Figures 6 through 10. In these cases, effects of the cloud transmittance is larger than the cloud emission.

For channel 2 the surface contribution to the cloud top brightness temperature over ocean is less than that for channel 1 due to the differences in transmittance as illustrated in Figures 30 and 32 and Figures 31 and 33 for 1 km and 3 km cases, respectively. The atmospheric terms are increased, however, due to the shape of the weighting function for this channel and the high reflectivity of the ocean surface. Although the cloud emission contribution for the 3 km case is slightly greater for channel 1 over channel 2, the net result is a higher cloud top brightness temperature for channel 2. The lower boundary condition is also higher for the same reasons, resulting in a greater reduction in the surface and atmospheric terms as they traverse

the cloud. Thus, for liquid water contents less than about 0.05 gm cm^{-2} (see Figure 12) at which the cloud emission is small, we observe the deepening of the reduction in the brightness temperature. The greater reduction in the surface and atmospheric terms also explains why the increase in brightness temperature for liquid water content of 0.05 through 0.15 gm cm^{-2} is not as large as the corresponding increases for channel 1. Note that the cloud emission is only slightly larger for channel 1 than channel 2 in the 3 km case and for the 1 km case it is approximately the same for both channels.

Based on the numerical experiments carried out for the study of the effects of the liquid water content on the surface, atmospheric, and cloud emission contributions to the cloud top brightness temperature over land, we find that nearly the same discussion applies for channel 2 over land as for channel 1. Thus, no plots similar to Figures 30 - 33 will be presented but rather some general discussions are made here. The surface terms increases due to the change in emissivity of the earth's surface. The increase is smaller than for channel 1, however, due to transmittance differences. The atmospheric terms decrease due to the change in reflectivity of the earth's surface. The decrease is larger than for channel 1 due to the shape of the weighting functions. The net result is that the lower boundary condition increases for channel 2 over land, but the increase is much reduced for channel 1. For example, for a 1 km thick cloud and rainfall rates of 1 and 30 mm/hr the lower boundary condition for channel 2 is nearly constant at 285° K over land but ranges from 250° K to 265° K over ocean. Once again, this increase in the lower boundary condition results in increased reduction through the cloud. Thus, we find that the brightness temperatures are continuously decreasing with increasing rainfall rates.

Channels 3 and 4 are relatively unaffected by the emissivity of the earth's surface. This is due to the fact that the transmittance from the earth's surface to the top of the atmosphere is only 0.023 for channel 3 and 0.003 for

channel 4 based on the results from the transmittance program. This fact explains why the brightness temperatures for channels 3 and 4 do not vary much between land and ocean surfaces. In this study the highest cloud top modeled was set at 6 km. This is just below the peak of the weighting function for channel 3 (7 km), but still well below the peak for channel 4 (10.5 km). As the cloud top moves into the energy source regions for these channels, emission by the cloud is lower since the temperatures are lower at higher altitudes. Furthermore, the transmittance from 6 km to the top of the atmosphere is less than 0.3 for both channels. Therefore, within the energy source region occupied by the upper portion of the cloud, the extinction mechanisms dominate over the mechanisms for the addition of energy, leading to slight decreases in the brightness temperature.

The interpretation of the cloud position dependence illustrated by Figures 15 through 20 is quite straightforward. Note that the lowest cloud base examined is at 1 km where the brightness temperatures over land for channels 1 and 2 are 265.5° K and 255.2° K, respectively. These values are higher than clear column values due to the fact that cloud emission exceeds extinction for a 2 km thick cloud with a base at 1 km for liquid water contents greater than 0.01 gm cm^{-2} (see Figures 30 through 33). The liquid water content for the 2 km thick L-Model cloud is 0.23 gm cm^{-2} . Thus, as the cloud is moved higher in the atmosphere, two changes take place. The emission by the cloud reduces due to the decrease in the cloud temperature. Meanwhile, the lower boundary condition increases because a greater portion of the energy source region for channels 1 and 2 is below the cloud base. This results in the increased energy reduction within the cloud layer. The net result is that brightness temperatures for channels 1 and 2 decrease as the cloud is moved higher up in the atmosphere. Eventually, the cloud is raised high enough that nearly all of the energy source regions for channels 1 and 2 are already below the cloud and cloud

temperatures are sufficiently low that emission by the cloud is very small. Then moving the cloud still higher reveals very little effect so that brightness temperatures are nearly constant. The same discussion applies over ocean except that over ocean even the 1 km cloud base shows a reduction in brightness temperatures as compared with the clear column values.

Channels 3, 4, 6 and 7 have weighting functions which peak higher in the atmosphere, reducing the effects of surface emissivity. Therefore, the effects of a 2 km thick cloud are basically the same over ocean and land surfaces. For clouds well below the peak of the weighting functions they show no effect on the brightness temperature. This is because there is no significant energy source below the cloud to be reduced by the cloud extinction. Also, the transmittance from the cloud top to the top of the atmosphere is sufficiently small that emission by the cloud may be negligible. As the cloud moves into the energy source region, an intricate trade-off of cloud emission and extinction takes place. For channels 3 and 4 this trade off holds the brightness temperatures very nearly constant until the cloud is well into the energy source region. For channels 6 and 7 a very slight increase in the brightness temperatures is noted. This increase is less than 0.2° K, however, which is below the noise level of the SSM/T. Finally, as the cloud is moved above the peaks of the weighting functions, brightness temperatures decrease, eventually becoming near constant as for channels 1 and 2.

SECTION 5

TEMPERATURE PROFILE RETRIEVAL EXERCISES

The main objective of the DMSP SSM/T microwave sounders has been to derive accurate temperature profiles in all weather conditions for operational use. The prime advantage of microwave temperature sounders over infrared sounders is that the longer microwaves are much less affected by clouds and precipitation. It seems therefore important to investigate the effects of clouds and precipitation on the temperature retrieval program. In this section, we first present the hypothetical temperature inversion in precipitating atmospheres using the brightness temperatures calculated from the microwave radiative transfer program. The retrieval program adopted in this study is the statistical method developed for the Air Force Global Weather Central intended for operational use. We also report a number of case studies using the real DMSP SSM/T data that we recently secured for clear, cloudy and precipitating cases.

5.1 Temperature Profile Retrieval Using Simulated Brightness Temperatures

The program that we use for temperature retrieval exercises is based on the statistical method described by Rigone and Stogryn (1977). The computer package for the statistical method was kindly provided to us by the Air Force Global Weather Central.

In the statistical method, the surface emissivity effect is

first removed so that the retrieval method could be applied to all surface conditions. For the purpose of outlining the method, we define

$$T_u(v) = \int_0^{\infty} T(z) \frac{\partial T_v(z, \infty)}{\partial z} dz , \quad (5.1)$$

and

$$T_d(v) = \int_{\infty}^0 T(z) \frac{\partial T_v(0, z)}{\partial z} dz , \quad (5.2)$$

so that Eq. (2.9) can be rewritten as follows:

$$T_B(v) = \epsilon_v T_s T_v(0) [1 - T_d(v)/T_s] + T_a(v) , \quad (5.3)$$

where

$$T_a(v) = T_u(v) + T_d(v) T_v(0) . \quad (5.4)$$

In Eq. (5.3), the second term in the right-hand side denotes the contribution to the upwelling brightness temperature caused by the atmosphere only, and the surface effects are contained in the first term. Since channel 1 centered at 50.5 GHz has a weighting function peak at the surface, it is utilized in the context of removing the surface contribution for other channels. Based on Eq. (5.3), we may define the contribution to the brightness temperature caused by the atmosphere only for channels 2-7 in the form

$$T_a(v_j) = T_B(v_j) - [T_B(v_1) - T_a(v_1)] a(v_j) , \quad j=2,3,\dots,7 , \quad (5.5)$$

where

$$a(v_i) = \frac{\epsilon_{v_i} T_s T_{v_i} (p_s) [1 - T_d(v_i)/T_s]}{\epsilon_{v_1} T_s T_{v_1} (p_s) [1 - T_d(v_1)/T_s]}, \text{ and } a(v_1) = 1.$$

In the statistical approach, it is generally assumed that the derivation of the predicted parameter T_i from the climatological mean \bar{T}_i may be expressed as a linear combination of the deviation of the measured data. Upon finding a linear operator D which will yield a minimum mean square deviation of the predicted temperature profile \hat{T}_i from the true temperature profile T_i in a statistical sense, the predicted temperature profile may be obtained. The linear operator, called the predictor matrix, may be expressed in terms of a covariance matrix, which can be constructed experimentally by collecting coincidences of radiances derived from remote sounders with temperature values obtained from direct soundings. The measured data, in the present case is \hat{T}_a given by Eq. (5.5). Thus, we write

$$\begin{aligned} (\hat{T}_i - \bar{T}_i) &= \sum_j D_{ij} (\hat{T}_{aj} - \bar{T}_{aj}) \\ &= \sum_j D_{ij} [\hat{T}_{Bj} - (\hat{T}_{B1} - \hat{T}_{a1}) a_j - \bar{T}_{aj}] \\ &= \sum_{j=1}^7 D_{ij} \hat{T}_{Bj} - \hat{T}_{B1} \sum_j D_{ij} a_j + \sum_j D_{ij} (\hat{T}_{a1} a_j - \bar{T}_{aj}). \end{aligned} \quad (5.6)$$

where T_a denotes the mean measured value and we note that T_{B1} is not defined in Eq. (5.5), and so the first terms contain $j=2, \dots, 7$. In matrix notations, we find

$$\hat{T} = D' \hat{T}_B + R, \quad (5.7)$$

where

$$\vec{R} = \vec{T} + \hat{T}_{a1} \vec{D}' \vec{a} - \vec{D} \vec{T}_a,$$

and the linear operator \vec{D}' is a matrix whose first column is $-\vec{D} \vec{a}$ and whose remaining columns are the columns of \vec{D} . It is clear that the retrieval technique contains elements depending mainly on the atmosphere but not on the surface, and so it should be valid over land, water, or mixed surface conditions. As pointed out previously, the \vec{D} and \vec{R} may be determined from a large number of upper air soundings for a wide range of meteorological conditions which have been achieved over the years and the brightness temperatures calculated for a given atmosphere.

Shown in Figure 34 is an exercise of temperature retrieval using the statistical covariance method. The mid-latitude Spring/Fall profile of a standard atmosphere (solid curve) is used and the observed brightness temperatures used for the seven SSM/T channels are values theoretically calculated. The exercise has been carried out for cases over ocean and land. It is apparent that the procedure outlined above has very successfully removed surface effects from the temperature retrieval. Also shown are the temperature retrievals when a 2 km thick precipitation layer with a base height set at 1 km, having various rainfall rates, have been added to the atmosphere. It is seen that the surface temperature suffers increased degradation as the rainfall rate increases. Based on these analyses, it seems that large errors in the recovered temperature profile may be anticipated, even with microwave sounders, when the atmosphere within the satellite field-of-view contains precipitation and heavy clouds.

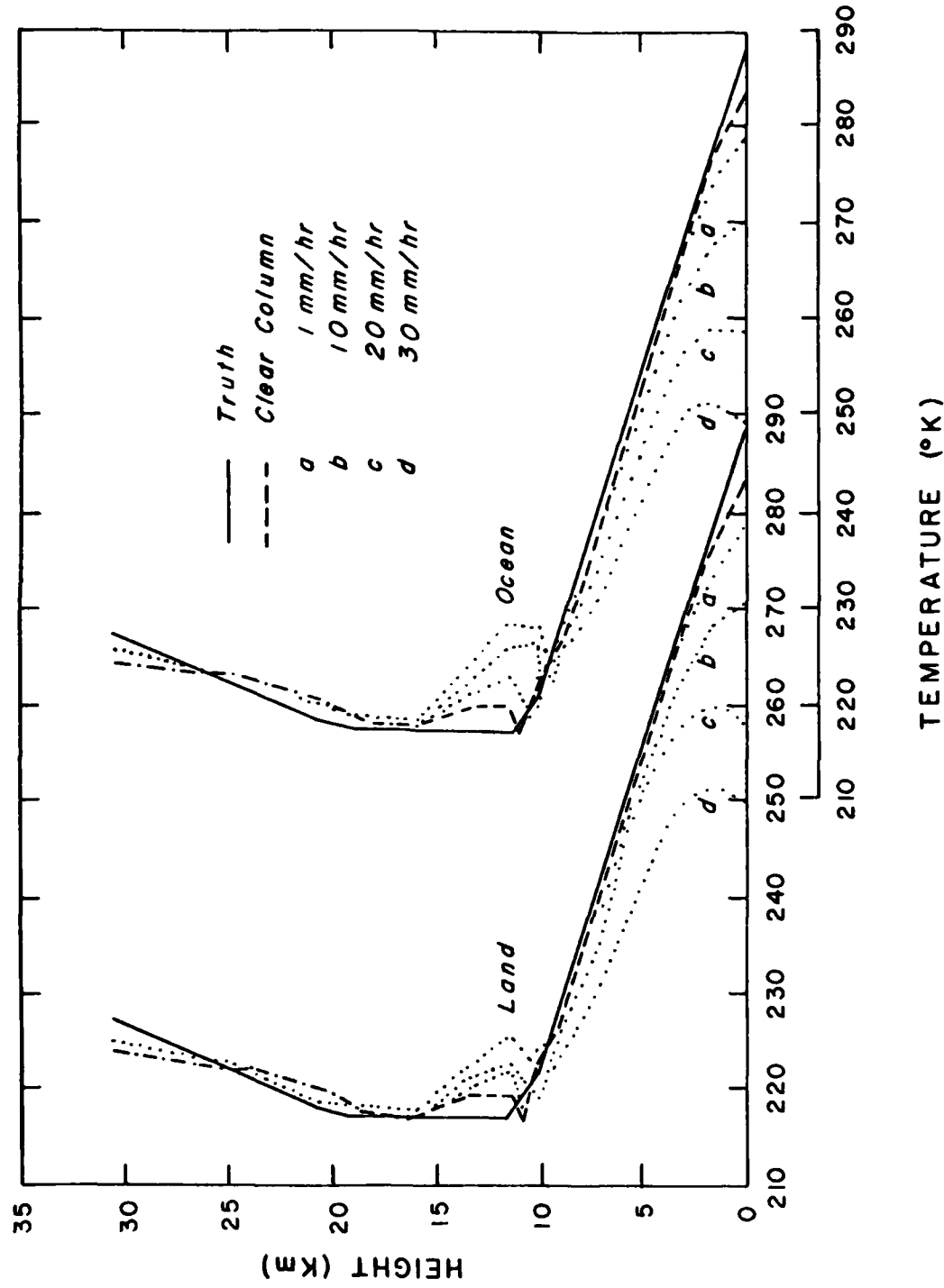


Figure 34. Hypothetical temperature retrieval exercise over land and ocean using the statistical covariance method.

5.2 Temperature Profile Retrieval Using DMSP SSM/T Data

The statistical method for temperature retrieval described in Section 5.1 was applied to a number of cases where SSM/T and radiosonde data were both available. Two days, 30 October 1979 and 23 November 1979, were chosen during which significant cloud and precipitation events were present over the continental United States. The cases selected are presented in Table 15 where the satellite pass times are the actual observation times of the SSM/T instrument. We find that the scan times are generally between 0000 Zulu and 0600 Zulu on these two days. Thus, the 0000 Zulu radiosonde observations were deemed most representative and were used in the comparisons.

Figure 35 shows the retrieved temperature profiles for the four clear cases; two on 30 October 1979 and two on 23 November 1979. Except for the Greensboro case, the retrieved temperature profiles when they are compared with nearby radiosonde data appear to be reasonably good in view of the statistical method used. The failure in the retrieval for the Greensboro case seems largely due to the fluctuated temperature profile that occurred in the atmosphere. Generally, we found that the statistical method is working properly when the actual profile is smooth and when no inversion is present.

The retrieved temperature profiles under cloudy conditions are illustrated in Figure 36. Apparently, the temperature profile retrieval program using the microwave frequencies in the 60 GHz oxygen band is affected insignificantly by non-precipitating clouds. Compared with the temperatures obtained from radiosondes, the retrieved patterns involving clouds are similar to those under clear conditions. Note that in each diagram, the percentage of cloud cover is depicted.

Table 15. Selected cases.

Station Name	Satellite Pass Time	Latitude (°N)	Longitude (°W)	Case Type
Centerville Alabama (AL)	0346 Z 30 Oct 79	32.54	87.15	Clear
Little Rock Arkansas (AR)	0346 Z 30 Oct 79	34.44	92.14	Clear
Greensboro North Carolina (NC)	0251 Z 23 Nov 79	36.03	79.57	Clear
Glasgow Montana (MT)	0435 Z 23 Nov 79	48.13	106.37	Clear
Bismark North Dakota (ND)	0350 Z 30 Oct 79	46.46	100.45	Cloudy
Medford Oregon (OR)	0531 Z 30 Oct 79	42.22	122.52	Cloudy
Green Bay Wisconsin (WI)	0253 Z 23 Nov 79	44.29	88.08	Cloudy
Monterrey Mexico (MEX)	0429 Z 23 Nov 79	25.52	100.12	Cloudy
Dodge City Kansas (KS)	0348 Z 30 Oct 79	37.46	99.58	Precipitating
Omaha Nebraska (NE)	0349 Z 30 Oct 79	41.22	96.01	Precipitating
Pittsburgh Pennsylvania (PA)	0252 Z 23 Nov 79	40.32	80.14	Precipitating
Spokane Washington (WA)	0435 Z 23 Nov 79	47.38	117.32	Precipitating

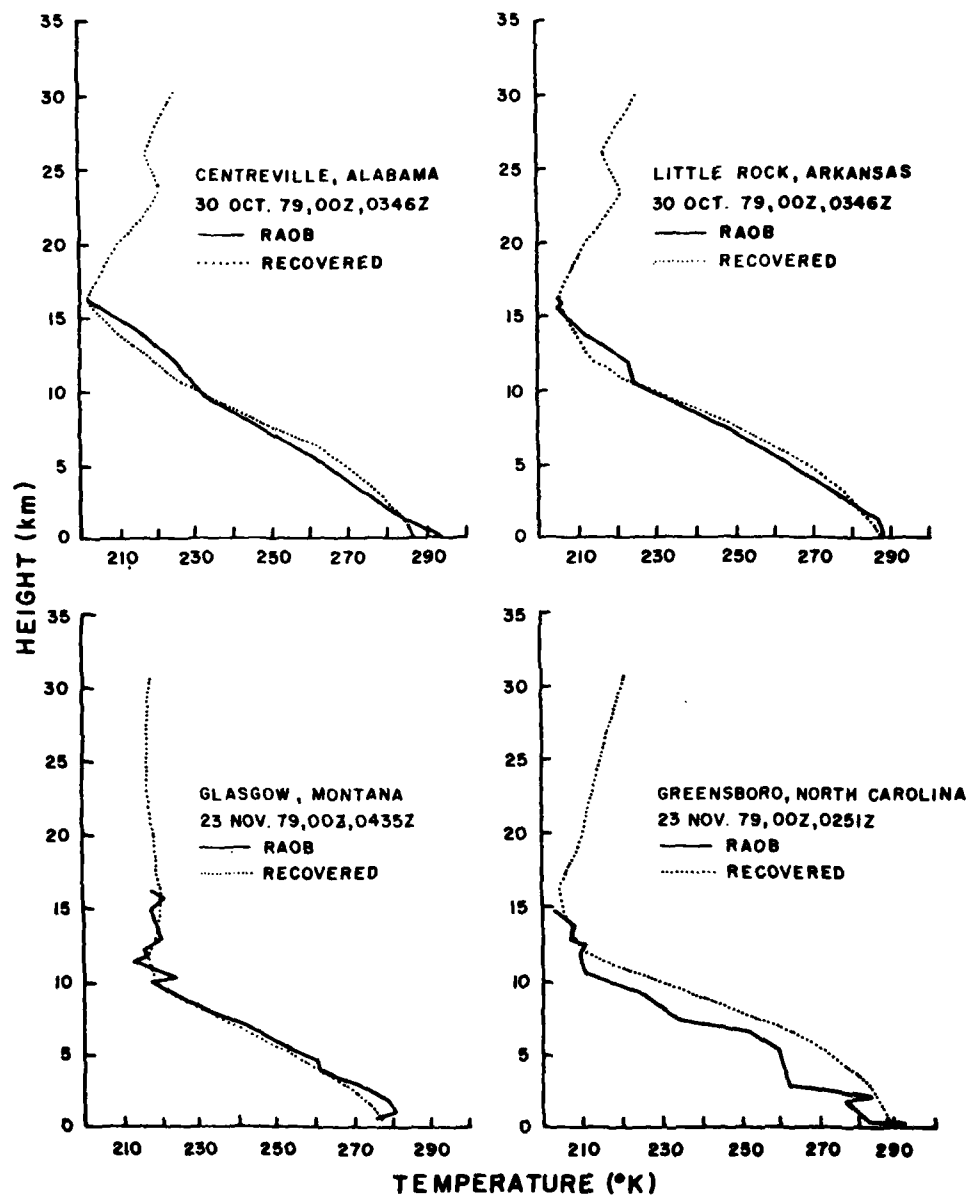


Figure 35. Comparisons of the retrieved temperature profiles (dots) with the radiosonde data (solid lines) for the four clear cases.

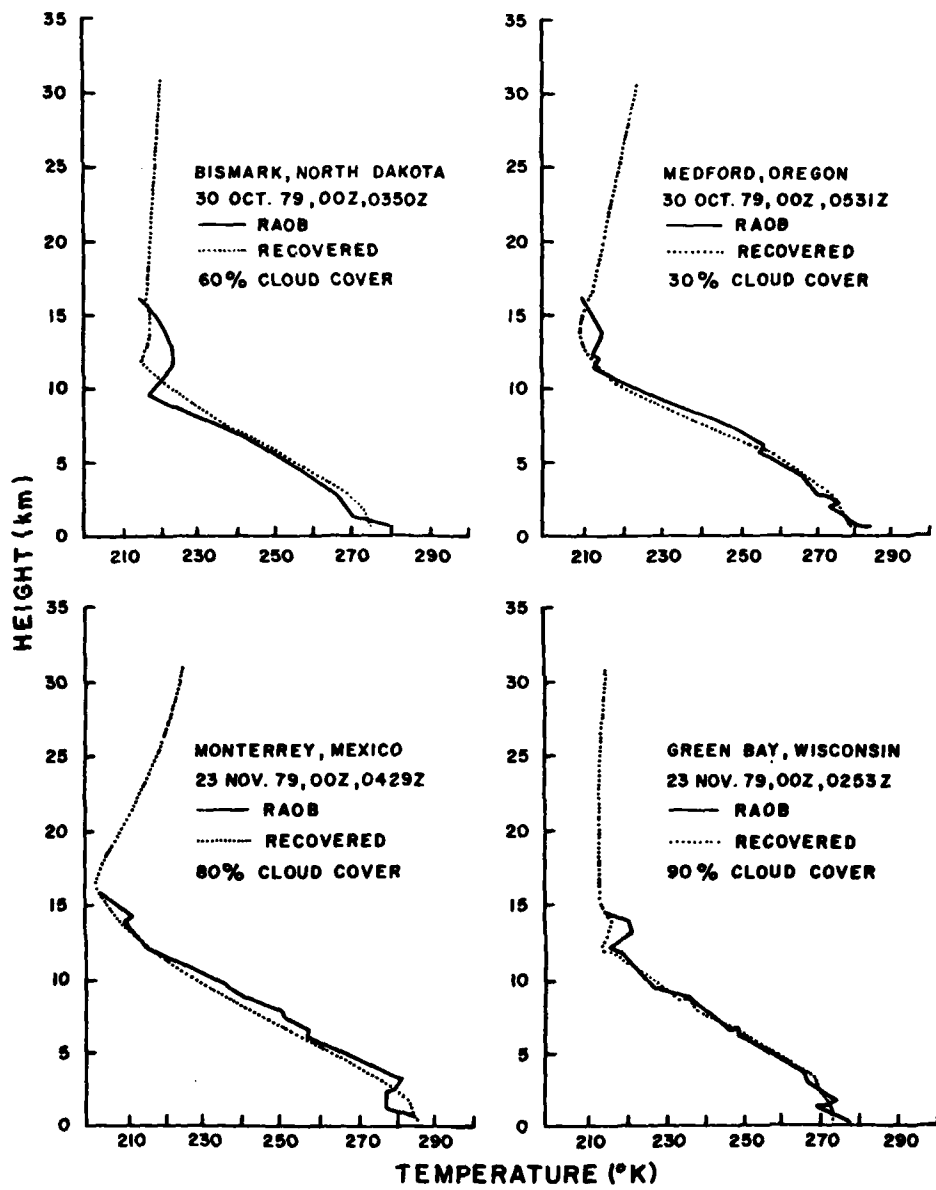


Figure 36. Comparisons of the retrieved temperature profiles (dots) with the radiosonde data (solid lines) for the four cloudy cases.

Generally, the retrieved and observed (radiosonde) temperatures in clear and cloudy conditions are within about 5° K.

In the final figure (Figure 37) we show the retrieved temperature profiles under precipitating conditions. Again, four cases are presented in this study. Two cases are selected from 30 October 1979; both have a 5 mm/hr rainfall rate with 30% cloud cover in the field of view of the SSM/T. In the other two cases, selected from 23 November 1979, both indicate a 1 mm/hr rainfall rate but with cloud covers varying from 50% to 80%. The most distinct feature in the retrieved temperature profiles using the statistical covariance method for precipitating cases is the significant and consistent deviation from the radiosonde data in the lower boundary layer where precipitation takes place. In the moderate 5 mm/hr rainfall rate cases, the differences between the retrieved and radiosonde temperature profiles near the surface are as large as 10 - 15° K. It should be noted that precipitation in these two cases cover only about 30% within the field of view of SSM/T. As for the cases involving 1 mm/hr rainfall rate, about 5 - 10° K differences near the ground are observed. The findings for these precipitation cases using the real SSM/T data are in general agreement with those described previously in the hypothetical temperature retrieval exercises. As shown in Figure 34 the surface temperatures suffer increased degradation from 10° to 20° K as the rainfall rate increases from 1 mm/hr to 20 mm/hr. These hypothetical analyses, of course, assume that the cloud covers the entire field of view.

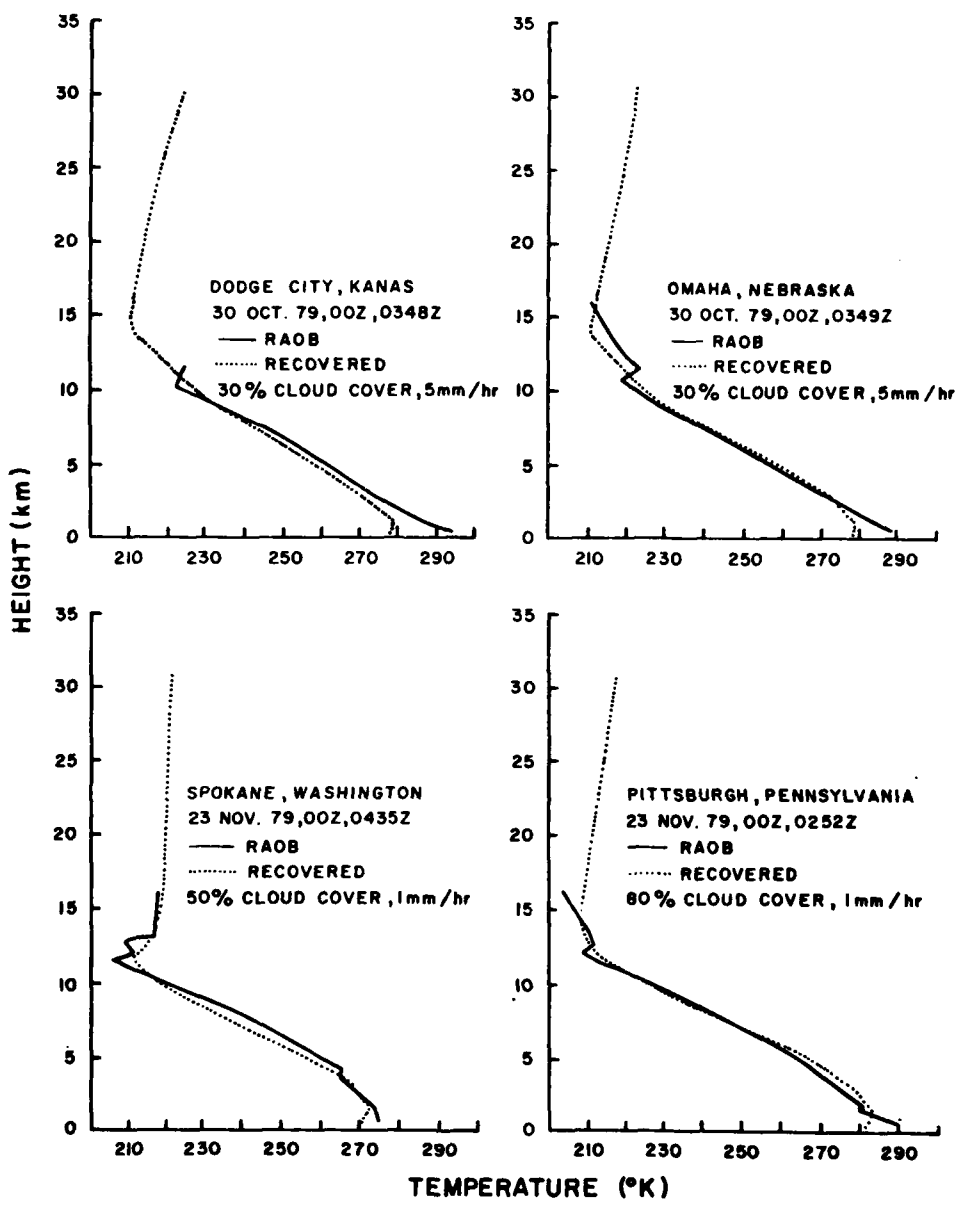


Figure 37. Comparisons of the retrieved temperature profiles (dots) with the radiosonde data (solid lines) for the four precipitation cases.

SECTION 6

CONCLUSION

In this study, we have developed a microwave radiative transfer program for cloudy atmospheres applicable to the DMSP SSM/T channels. The transfer program takes into account the simultaneous effects of multiple scattering and absorption by hydrometeors and absorption due to molecular oxygen and water vapor in the atmosphere.

Sensitivity analyses were carried out to investigate the effects of the rainfall rate, cloud thickness, and cloud location on the upwelling brightness temperature over land and ocean surfaces for two atmospheric profiles. The effects of precipitation on SSM/T channels 1 and 2 are shown to be significant depending on the cloud liquid water content (or rainfall rate), thickness, and surface emissivity. Over the land surface, increasing the cloud liquid water content and thickness reduces the upwelling brightness temperature for channels 1 and 2. For channels 3 and 4, unless high rainfall rates are involved, the reduction in the brightness temperature is normally insignificant. Over the ocean surface, however, the increase of the liquid water content and thickness may increase or decrease the upwelling brightness temperature relative to the clear column value. A significant variation for the brightness temperature is shown for channel 1. This conclusion is in general agreement with that

described by Wilheit et al. (1977) using a simple scattering program for a frequency of 37 GHz. Moreover, sensitivity analyses also reveal the importance of the position of the cloud layer in the atmosphere and the atmospheric temperature profile on the upwelling brightness temperature values.

In addition, investigation of the effects of precipitation on the temperature profile retrieval using both the theoretically simulated values and real data was carried out utilizing the seven SSM/T channels. The retrieval method adopted in this study is the statistical method developed at the Air Force Global Weather Central in which the surface effect is removed in the recovery program. The hypothetical retrieval exercises show that the temperatures close to the surface suffer increased degradation as the rainfall rate increases. This finding is also supported by the analysis employing the real SSM/T data for a number of case studies in which temperature profiles from radiosondes are available for comparison. Furthermore, the latter study indicates that nonprecipitating clouds have an insignificant affect on the microwave temperature retrieval with accuracy generally on the same order as in clear conditions.

Although the current study employs only four precipitating cases in the analysis and may not be conclusive in view of the limited sample used, it appears that the effect of precipitation on the temperature profile retrieval using microwave frequencies is substantial and significant. Of course, the reliability of the statistical method for the temperature profile retrieval in clear atmospheres should be examined comprehensively and completely utilizing the data that are

available in different localities and seasons. In addition, in order to derive the temperature field over the global space, further studies concerning the influence of precipitating clouds on the temperature retrieval in the microwave region seem also warranted.

REFERENCES

- Barrett, A. H. and V. K. Chung, 1962: A method for the determination of high-altitude water vapor abundance from ground-based microwave observations. J. Geophys. Res., 67, 4259-4266.
- Becker, G. and S. Autler, 1946: Water vapor absorption of electromagnetic radiation in the centimeter wavelength range. Phys. Rev., 70, 300.
- Chandrasekhar, S., 1950: Radiative Transfer. Dover, New York.
- Deirmendjian, D., 1969: Electromagnetic Scattering on Spherical Polydispersions. Elsevier, New York.
- Feddes, R. G. and K. N. Liou, 1977: Sensitivity of upwelling radiance in Nimbus 6 HIRS channels to multilayered clouds. J. Geophys. Res., 82, 5977-5989.
- Gunn, K. L. S. and T. W. R. East, 1954: The microwave properties of precipitation particles. Quart. J. Roy. Meteor. Soc., 80, 522-545.
- Hollinger, J. P., 1973: Microwave Properties of a Calm Sea. Naval Research Laboratory Report No. 7110-2, Washington, D.C.
- Liou, K. N. and J. E. Hansen, 1971: Intensity and polarization for single scattering by polydisperse spheres: A comparison of ray optics and Mie theory. J. Atmos. Sci., 28, 995-1004.
- Liou, K. N., T. L. Stoffel, R. G. Feddes and J. T. Bunting, 1978: Radiative properties of cirrus clouds in NOAA 4 VTPR channels: Some explorations of cloud scenes from satellites. Pure Appl. Geophys., 116, 1007-1029.
- King, G. W., R. M. Hainer and P. C. Cross, 1947: Effective microwave absorption coefficients of water and related molecules. Phys. Rev., 71, 433-443.

- Marshall, J. S. and W. M. Palmer, 1948: The distribution of raindrops with size. J. Meteor., 5, 165-166.
- Meeks, M. L. and A. E. Lilley, 1963: The microwave spectrum of oxygen in the earth's atmosphere. J. Geophys. Res., 68, 1683-1703.
- Rigone, J. L. and A. P. Stogryn, 1977: Data processing for the DMSP microwave radiometer system. Eleventh International Symposium on Remote Sensing of the Environment, University of Michigan Press, 1-9.
- Rosenblum, E. S., 1961: Atmospheric absorption of 10-400 kmcps radiation: Summary and bibliography to 1961. Microwave J., 4, 91-96.
- Savage, R. C., 1976: The Transfer of Thermal Microwaves through Hydrometeors. Ph.D. Dissertation, University of Wisconsin-Madison.
- Saxton, J. A. and J. A. Lane, 1952: Electrical properties of sea water: Reflection and attenuation characteristics at v.h.f. Wireless Engineer, 29, 269-275.
- Sekhon, R. S. and R. C. Srivastava, 1970: Snow size spectra and radar reflectivity. J. Atmos. Sci., 27, 299-307.
- U. S. Standard Atmosphere, 1966: Superintendent of Documents, U.S. Government Printing Office, Washington, D.C.
- Van Vleck, J. H., 1947: The absorption of microwave by oxygen. Phys. Rev., 71, 413-424.
- Wilheit, T. T., A. T. C. Chang, M. S. V. Rao, E. B. Rodgers and J. S. Theon, 1977: A satellite technique for quantitatively mapping rainfall rates over the oceans. J. Appl. Meteor., 16, 551-560.

APPENDIX

LISTING OF MICROWAVE TRANSFER PROGRAM

```

*****+
C MAIN PROGRAM
*****
PARAMETER NUMCHN=6,NUMLV=40,NG=16, NMOST=NUMLV+10
DIMENSION T(NMOST),W(NMOST),TAUM(NMOST,NUMCHN),TAUS(NMOST,NUMCHN),
* EMIS(NUMCHN),TANT(NUMCHN)
COMMON /ANGLE/ UM(NG),A(NG),PI
COMMON /SFCEMS/ EMIS
COMMON/FREQ/ FMU(NUMCHN)
COMMON/HANDU/H(NMOST),U(NMOST,NUMCHN)
COMMON /TAUVAL/ TAUM
COMMON/TANDW/T,W
COMMON/PRES/P(NMOST)
COMMON/NEWLEV/ADDHT(10),NUMNEW,LVNUM
REAL*8 SFC(2)
DATA SFC/'LAND','WATER'/
DATA KTAU1,KTAU2/'TAU','GHZ'/
CALL PROFIL
CALL TRANMW(TAUM,TAUS,0.,1,NUMCHN,1,1.)
WRITE(6,900) (KTAU1,FMU(J),KTAU2,J=1,NUMCHN)
DO 20 I=1,LVNUM
WRITE(6,901) P(I),T(I),W(I),(TAUM(I,J),J=1,NUMCHN)
20 CONTINUE
READ(5,903) (EMIS(I),I=1,NUMCHN)
60 CALL ANTEMP(TAUM,TAUS,T,T(LVNUM),EMIS,TANT,LVNUM,1,NUMCHN)
WRITE(6,902) SFC(1),EMIS,TANT
CALL BUFF(P,T,W,H,U)
900 FORMAT('1 P(MB) T(K.) W(G/KGM)',2X,7(2X,A4,F5.2,A4),/)
901 FORMAT(2(2X,F6.1),2X,E8.3,5X,6(E10.5,5X),E10.5)
902 FORMAT(1H0,A6,'... EMISSIVITY',4X,6F15.3,/,1H0,12X,
* 'ANTENNA TEMP.',1X,7F15.3)
903 FORMAT( )
STOP
END

```

SUBROUTINE PROFIL

```

*****+
C THIS SUBROUTINE IS TO READ OBSERVED PROFILES (TEMPERATURE K, MIXING
C RATIO G/KG, PRESSURE MB, AND HEIGHT KM) OF ATMOSPHERE, AND
C INTERPOLATE THE PROFILES TO THE DESIRED PRESSURE LEVELS (40 STANDARD
C LEVELS).
C THE LEVELS CAN BE ADDED UP TO 10 LEVELS OF YOUR CHOICE.
*****

```

```

PARAMETER NUMLV=40, NMOST=NUMLV+10
DIMENSION T(NMOST),W(NMOST),H(NMOST),OBPR(40)
* ,OBM(40),OBTEMP(40),OBW(40)
COMMON/PRES/P(NMOST)
COMMON/HANDU/H,U
COMMON/TANDW/T,W
COMMON/NEWLEV/ADDHT(10),NUMNEW,LVNUM
200 FORMAT( )
201 FORMAT(1X,'LEVELS TO HIGH. MAX VALUE EQUALS 40. ')

```

```

      REAL(5,200) NLVOBS
      IF(4U-NLVB5)202,203,203
202 PRINT 201
      RETURN 0
203 IF(NLVOBS)105,105,204
204 N=NLVOBS
      READ(5,200)(OBTEMP(I),I=N,1,-1)
      READ(5,200)(OBW(I),I=N,1,-1)
      READ(5,200)(OBPR(I),I=N,1,-1)
      READ(5,200)(OBH(I),I=N,1,-1)
      WRITE(6,301) OBTEMP
      WRITE(6,301) OBW
      WRITE(6,301) OBPR
      WRITE(6,301) OBH
301 FORMAT(10FB,3)
302 FORMAT(1A,'PROFIL USED CLIMO DATA (MID LAT SPRING/FALL) ABOVE ',
* F7.2,' MB')
      K=1
      DO 100 I=1,NUMLV
      IF (OBPR(K).EQ.0.0) GO TO 100
10     IF (OBPR(K).EQ.P(I)) GO TO 90
      IF (OBPR(N).LT.P(I)) GO TO 101
      IF (OBPR(K).LT.P(I)) GO TO 89
      IF (K.EQ.1) GO TO 100
      DELT=OBTEMP(K)-OBTEMP(K-1)
      DELW=OBW(K)-OBW(K-1)
      DLNP=ALOG(OBPR(K)/OBPR(K-1))
      T(I)=DELT/DLNP+ALOG(P(I)/OBPR(K-1))+OBTEMP(K-1)
      W(I)=DELW/DLNP+ALOG(P(I)/OBPR(K-1))+OBW(K-1)
      CALL MINTRP(OBPR(K),OBPR(K-1),P(I),OBH(K),OBH(K-1),H(I))
      GO TO 100
89     K=K+1
      IF (K.EQ.2) PRINT 302,P(I)
      GO TO 10
90     T(I)=OBTEMP(K)
      W(I)=OBW(K)
      H(I)=OBH(K)
99     K=K+1
100    CONTINUE
101    CONTINUE
105    READ(5,200) NUMNEW
      NEW=NUMNEW
      LVNUM=NUMLV+NUMNEW
      IF (NUMNEW.EQ.0) GO TO 210
      READ(5,200)(ADDHT(I),I=1,NEW)
      NTOP=NUMLV
      K=1
      DO 206 I=NUMLV,1,-1
110    IF(M(I).LE.ADDHT(K)) GO TO 206
      J=I+1
      DO 175 L=NTOP,J,-1
      P(L+1)=P(L)
      T(L+1)=T(L)
      W(L+1)=W(L)
      H(L+1)=H(L)
175    CONTINUE
      NTOP=NTOP+1
      H(J)=ADDHT(K)
      CALL NEWLVL(J)
      K=K+1
      IF(K.GT.NUMNEW) GO TO 210
      GO TO 110
206    CONTINUE
210    CONTINUE
      RETURN
      END

```

```

SUBROUTINE MINTRP(SPTOP,SPBOT,SPP,SZTOP,SZBOT,SZZ)
C ****
C THIS SUBROUTINE IS TO INTERPOLATE THE OBSERVED HEIGHTS TO THE HEIGHTS
C OF DESIRED PRESSURE LAYERS.
C ****

IMPLICIT DOUBLE PRECISION(A-H,O-Z)
DATA TOL/1.0=4/RADKM/6.37122D3/N/11/
REAL SPTOP,SPBOT,SPP,SZTOP,SZBOT,SZZ
DIMENSION ZMATR(50,50),F(50),ZMAT(2500),COLF(50)
DIMENSION ARRAY(12)/1.00-1,1.25D-1,1.40D-1,1.60D-1,1.55D-1,
* 1.7D-1,1.55D-1,1.47D-1,1.42D-1,1.32D-1,1.21D-1,1.31D-1/
IENTER=1
1 ZHOT=DHLE(SZHOT)
ZTOP=DHLE(SZTOP)
PHOT=DHLE(SPHOT)
PTOP=DHLE(SPTOP)
PP=DHLE(SPP)
ZTST=ZHOT
IF(ZTST.GT.ZTOP) ZTST=ZTOP
IF(1.0D0.LE.ZTST) GO TO 2
CONS=(SZTOP-SZHOT)/ ALOG(SPTOP/SPBOT)
SZZ=ALOG(SPP/SPBOT)+CONS+SZHOT
GO TO 99
2 RK=(PTOP-PBOT)/(1.0D0/(ZTOP+RADKM)-1.0D0/(ZHOT+RADKM))
KNUM=1.0D0-RADKM*(1.0-PBOT)/RK-RADKM/(ZHOT+RADKM)
KDEN=(PP-PBOT)/RK+1.0D0/(ZHOT+RADKM)
IF(IENTER.EQ.1) SZZ=5NGL(KNUM/KDEN)
IF(ZTST-1.0D0)99,5,5
5 LVLA=1
ZTS1=DHLE(SZ2)
IF(ZTST.GT.6.00D1) LVLA=LVLA+1
IF(ZTST.GT.4.75D1) LVLA=LVLA+1
IF(ZTST.GT.4.25D1) LVLA=LVLA+1
IF(ZTST.GT.3.75D1) LVLA=LVLA+1
IF(ZTST.GT.3.25D1) LVLA=LVLA+1
IF(ZTST.GT.2.45D1) LVLA=LVLA+1
IF(ZTST.GT.2.15D1) LVLA=LVLA+1
IF(ZTST.GT.1.65D1) LVLA=LVLA+1
IF(ZTST.GT.1.45D1) LVLA=LVLA+1
IF(ZTST.GT.1.25D1) LVLA=LVLA+1
IF(ZTST.GT.6.5D0) LVLA=LVLA+1
IF(ZTST.GT.0.6D0) LVLA=LVLA+1
A=ARRAY(LVLA)
ZINC=(ZTOP-ZHOT)/FLOAT(N-1)
DO 10 I=1,N
ZMATRX(I,1)=1.
10 CONTINUE
DO 20 I=1,N
ZMATRX(I,2)=1.0/(ZHOT+FLOAT(I-1)*ZINC)
DO 15 J=3,N
ZMATRX(I,J)=ZMATRX(I,J-1)*ZMATRX(I,2)
15 CONTINUE
Z2=1.0/ZMATRX(I,2)
GRAD=Z2+RADKM
F(I)=DEXP(-A*Z2)/(GRAD*GRAD)
COEF(I)=F(I)
20 CONTINUE
K=0
DO 23 I=1,N
DO 21 J=1,N
K=K+1
ZMAT(K)=ZMATRX(J,1)
21 CONTINUE
23 CONTINUE
CALL SIMU(ZMAT,COLF,N,K)
SUMHOT=COEF(1)*ZHOT+COEF(2)*ALOG(ZBOT)
SUMTOP=COEF(1)*ZTOP+COEF(2)*ALOG(ZTOP)
HOT=1./ZHOT
TOP=1./ZTOP

```

```

DO 40 J=3,N
CUEF(J)=COEF(J)/FLUAT(J-2)
SUMHOT=SUMBOT+CUEF(J)*AUT
BLT=BOT/ZHOT
SUMTOP=SUMTOP+CUEF(J)*TOP
TOP=TOP/ZTOP
40 CONTINUE
AINT=SUMTOP-SUMHOT
RK=(PHUT-PTOP)/AINT
GO TO (61,96),IENTRY
61 CONS=(PHUT-PP)/RK+SUMBOT
FH=CONS-SUMHOT
FT=CONS-SUMTOP
ZMEAN=(ZHOT+ZTOP)/2.
IF (4RS(ZTOP-ZBOT)-TUL) 95,95,65
65 SUMEAN=COEF(1)*ZMLAN+COEF(2)*ULOG(ZMEAN)
EAN=1./ZMEAN
DO 66 J=3,N
SUMEAN=SUMEAN+CUEF(J)*EAN
EAN=EAN/ZMEAN
66 CONTINUE
FMEAN=CONS-SUMEAN
IF (FH+FMEAN) 70,95,80
70 ZTOP=ZMEAN
FH=FMEAN
GO TO 62
80 ZBOT=ZMEAN
FH=FMEAN
GO TO 62
95 SZZ=SINGL(ZMEAN)
96 ZZ=DHLE(SZZ)
SUMTOP=CUEF(1)*ZZ+COEF(2)*DLUG(ZZ)
EZZ=1./ZZ
DO 97 J=3,N
SUMTOP=SUMTOP+CUEF(J)*EZZ
EZZ=ZZ/ZZ
97 CONTINUE
AINT=SUMTOP-SUMHOT
PF=-RK*AINT+PHOT
SPP=SINGL(PP)
GO TO 94
ENTRY PINTRP(SP101,SPROT,SPP,SZTOP,SZHOT,SZZ)
IENTRY,H=2
GO TO 1
99 CONTINUE
RETURN
END

```

```

SUBROUTINE SIMQ (A,B,N,KS)
C ****
C   OBTAINS SOLUTION OF A SET OF SIMULTANEOUS LINEAR EQUATIONS ...
C   A - MATRIX OF COEFFICIENTS STORED COLUMNWISE. THESE ARE
C   DESTROYED IN THE COMPUTATIONS. THE SIZE OF MATRIX 'A'
C   IS N X N.
C   B - VECTOR OF ORIGINAL CONSTANTS (LENGTH N) WHICH IS REPLACED
C   BY FINAL SOLUTION VALUES, VECTOR X.
C   N - NO. OF EQUATIONS AND VARIABLES.
C   KS - OUTPUT DIGIT
C       0 FOR NORMAL SOLUTION
C       1 FOR A SINGULAR SET OF EQUATIONS
C ****

DOUBLE PRECISION A,H,BIGA,TOL,SAVE
DIMENSION A(1),H(1)
TOL=0.0001
KS=0
J=1
DO 80 J=1,N
JY=J+1
JJ=JJ+N+1
BIGA=0.0000
IT=JJ-J
DO 20 I=J,N
IJ=IT+1
IF (DAHS(BIGA)=DAHS(A(IJ))) 10,20,20
10 H(IG)=A(IJ)
IMAX=I
20 CONTINUE
IF (DAHS(BIGA)=TOL) 30,30,40
30 KS=1
RETURN
40 I1=J+N*(J-2)
I1=IMAX-J
DO 50 K=J,N
I1=I1+N
I2=I1+IT
SAVE=A(11)
A(11)=A(12)
A(12)=SAVE
50 A(11)=A(11)/BIGA
SAVE=H(IMAX)
H(IMAX)=H(J)
H(J)=SAVE/BIGA
IF (J=N) 60,90,60
60 I=J+N*(J-1)
DO 60 IX=JY,N
IXJ=1QS+IX
IT=J-IX
DO 70 JX=JY,N
IXJX=N*(JX-1)+IX
JJX=IXJX+IT
70 A(IAJX)=A(IAJX)-(A(IXJ)*A(JJX))
80 H(IX)=B(IX)-(H(J)*A(IXJ))
90 NY=N-1
IT=N
DO 100 J=1,NY
IA=IT-J
IB=N-J
IC=N
DO 100 K=1,J
B(IB)=B(IB)-A(IA)*B(IC)
IA=IA-N
100 IC=IC-1
RETURN
END

```

```

SUBROUTINE NEWLVL(K)
PARAMETER LEV=40, INT=6, NMOST=LEV+10
COMMON/PRES/PHE(NMOST)
COMMON/HANDU/ALT(1,NMST) H1(NMOST)
COMMON/TANOW/TEMP(NMOST),H20(NMOST)
SPTOP=PHE(K+1)
SPHOT=PHE(K-1)
SZTOP=ALT(K+1)
SZHOT=ALT(K-1)
SZZ=ALT(K)
TEST=SZHOT
IF(TEST.GT.SZTOP) TEST=SZTOP
IF(TEST.GT.1) GO TO 10
RHUG=(SPTOP-SPHOT)/(SZTOP-SZHOT)
PHE(K)=SPHOT+RHUG*(SZZ-SZHOT)
GO TO 11
10 CALL PINTRP(SPTOP,SPHOT,PHE(K),SZTOP,SZHOT,SZZ)
11 SPHOT=PHE(K)
TEMP(K)=(TEMP(K+1)-TEMP(K-1))*ALOG(SPP/SPBOT)/ALOG(SPTOP/SPBOT)
* +TEMP(K-1)
H20(K)=(H20(K+1)-H20(K-1))*ALOG(SPP/SPBOT)/ALOG(SPTOP/SPBOT)
* +H20(K-1)
RETURN
END

```

```

SUBROUTINE TRANMW(TAW,TAWSQ,Z,NU1,NU2,KOUNT,UMD)
*****C COMPUTE TRANSMISSIVITIES TO THE TOP OF THE ATMOSPHERE FROM EACH LFVEL
*****C OF THE PROFILE FOR EACH CHANNEL (ANTENNA GAIN CHARACTERISTICS INCLUDED)
*****
PARAMETER NUMCHN=6,NUMLV=40,NG=16, NMOST=NUMLV+10
DOUBLE PRECISION TAU,TAX,T0,T1,T2
COMMON/INPUT/ALT(1,NMST),TEMP(NMOST),PHE(NMOST),H20(NMOST),
* THKNS(9),NTHICK,NUASE,TRN(NMOST,NUMCHN),NLEV(10)
COMMON/STOKAL/ ALFA
COMMON/TANOW/ T0,W
COMMON/HANDU/H(NMST),U(NMOST,NUMCHN)
COMMON/NEWLEV/ADFT(10),NUMNEW,LVNUM
DIMENSION T(NMST),W(NMST),ALFA(NMST,NUMCHN),TAW(NMOST,NUMCHN),
* TAWSQ(NMST,NUMCHN),GSUM(NUMCHN)
DIMENSION DLS(126),TUK(127),SA(127),SZ(127),G(127,NUMCHN)
COMMON/GAIN/GANT(127,NUMCHN)
COMMON/PRES/ P(NMST)
LEV1=LVNUM
NP=NUMLV
ZLAST=994.
DIN=.0174533
NANG=127
ISWE1
CRH=1.17268

```

```

1 IF (ISW) 10,10,1
1 I=NINT+ANG/2
MM=NINT
MM=NINT+1
CA=1.
AU=0.
DO 2 I=1,NINT
AA=1.
CH=CAC-CH
DC=DC-DC
ULS(I+MM)=DD
ULS(MM-I)=DD
2 CA=CB
DO 7 KK=NU1,NU2
DO 3 I=1,127
3 G(I,KK)=GANT(I,KK)*GANT(I,KK)
DO 4 I=1,63
4 G(I,KK)=G(128-I,KK)
GS=0.
G1=G(1,KK)
DO 6 I=2,127
G2=G(I,KK)
GS=GS+(G1+G2)*DCS(I-1)
6 G1=G2
GSUM(KK)=GS
7 CONTINUE
SMAX=ASIN(1./CRH)/DTR
ISW=0
10 IF (Z,FQ,ZLAST) GO TO 20
DO 12 K=1,127
DU=FLOAT(K-MM)
SA(K)=AHS(Z+DU)
SZ(K)=1.
IF (SA(K),GT,SMAX) GO TO 12
A=CH=SIN(DTR*SA(K))
OU=ASIN(A)
SZ(K)=1./COS(OU)
12 CONTINUE
ZLAST=Z
20 IF (Z,LE,KOUNT) GO TO 30
CALL RASEU(LVNUM)
30 DU 120 J=NU1,NU2
TAU=0.
DU 110 I=1,LEV1
UI=U(I,J)/UM0
100 IF (UI) 101,101,102
101 TAU=1.
GO TO 103
102 IF (UU.GT.,89E1) GO TO 53
GO TO 54
53 UU=.40E1+TAU
TAU=TAU+.2
54 TAU=EXP(-UU)
103 DU 104 K=1,127
TAX=TAU
IF (SA(K),GT,SMAX) GO TO 104
IF (TAX,LT.,0001) GO TO 104
IF (TAX,GT.,9999) GO TO 104
IF (SZ(K),EQ,1.) GO TO 104
TAX=TAX**SZ(K)
104 TOW(K)=TAX
GS=0.
G1=G(1,J)
T1=TOW(1)

```

```

      GO TO 106 K=2,127
      G2=G(K,J)
      T2=TOW(K)
      IF(SA(K).GT.SMAX) GO TO 105
      GS=GS+(G1*T1+G2*T2)*DCS(K-1)
105  G1=G2
106  T1=T2
      TAW(I,J)=GS/GSUM(J)
      TAU2=TAW(I,J)
      TAWR=.5*(TAU1+TAU2)
      TAWSQ(I,J)=TAWR*TAWR
      TAU1=TAU2
110  CONTINUE
120  CONTINUE
      RETURN
      END

```

```

SUBROUTINE BASEU(LEV1)
PARAMETER NUMCHN=6,NUMLV=40, NMOST=NUMLV+10
DIMENSION KERNEL(NMOST,NUMCHN),GAMT(NMOST),RHOW(NMOST)
REAL KERNEL
COMMON/FREQ/FRGHZ(NUMCHN)
COMMON/HANDU/H(NMOST),U(NMOST,NUMCHN)
COMMON/PRES/F(NMOST)
COMMON/TANOW/T(NMOST),W(NMOST)
COMMON/TRNSMT/TRANS(NMOST,NUMCHN)
COMMON/INPUT/ALT(NMOST),TEMP(NMOST),PRE(NMOST),H2O(NMOST),
* THNS(9),NTHICK,NBASE,TRN(NMOST,NUMCHN),NEWLEV(10)
REAL NBASE
DATA RSURV/4.615E6/RSUBD/2.87E6/
C
C P = PRESSURE (MB)
C T = TEMPERATURE (DEG K.)
C W = MIXING RATIO (GM/KGM)
C H = HEIGHT (KM)
C RHOW = WATER VAPOR DENSITY (GM/M***3)
C KERNEL = WEIGHTING FUNCTION (TRANSMITTANCE/KM)
C GAMT = ATTENUATION IN LAYER I TO I+1 (DB/KM)
C FRGHZ = CHANNEL FREQUENCIES IN GHZ
C
C      PRINT 16,(FRGHZ(I),I=1,NUMCHN)    @ ECHO CHECK
C      PRINT 17,LEV1,P(LEV1),F(1)      @ ECHO CHECK
C
C*****COMPUTE WATER VAPOR DENSITY (RHOW) FROM PRES,TEMP AND MIXING RATIO.
C*****DO 30 I=1,LEV1
      RSUBM=(1./(1.+W(I)*1.E-3))*(W(I)*1.E-3*RSURV+RSUBD)
      PCGS=F(I)*1.E3
      RHOM=PCGS/(RSUBM*T(I))          @ MOIST AIR DENSITY (GM/CM***3)
      RHOW(I)=RHOM*W(I)*1.E-3/(1.+W(I)*1.E-3)  @ H2O VAPOR DENSITY (GM/CM***3)
      RHOW(I)=RHOW(I)*1.E6            @ H2O VAPOR DENSITY (GM/M***3)
30  CONTINUE

```

```

C
C*****COMPUTE ATTENUATION COEFFICIENTS*****
C
C*****PRINT 1B
DO 35 I=LEV1,1,-1
35 PRINT 19,F(I),H(I),T(I),RHOW(I)
NUMLAY=LEV1-1          * NUMBER OF LAYERS IN VERTICAL PROFILE
DO 500 J=1,NUMCHN
B=1.0                  * TRANSMITTANCE AT EARTHS SURFACE.
A=0.0
DO 215 I=2,LEV1
TRANS(I-1,J)=B
U(I-1,J)=A
PTORR=F(I)*760./1013.25  * CONVERT PRESSURE TO TORR (MM HG)
GAM1=GAM02(FRGHZ(J),T(I),PTORR)  * ATTENU. AT PTORR,T(I) BY O2 (DB/KM)
GAM2=GAMH20(FRGHZ(J),T(I),PTORR,RHOW(I))  * ATTENU. AT PTORR,T(I),RHO(I)
GAMT(I)=GAM1+GAM2  * TOTAL ATTENUATION BETWEEN LEVEL I AND I+1 (DB/KM)
C FOR GROUND UP USE  DH=H(I+1)-H(I)
C FOR TOP DOWN USE  DH=H(I)-H(I+1)
DH=H(I-1)-H(I)          * THICKNESS OF LAYER (KM)
IF(H(I-1).EQ.H(I)) DH=H(I-1)-H(I+1)  *FOR FRICIPITATING CASE
C*****LET ADB=GAMT(1)*IH  (FLUX ATTENUATION IN DB)
C BUT DB=10LOG10(I(1)/I(2))  WHERE I(1).GT.I(2)
C THEREFOR ADB=GAMT(1)*DH=10LOG10(I(1)/I(2))
C ADB/10=LOG10(I(1)/I(2)), OR  10***(ADB/10)=I(1)/I(2)
C (ADB/10)*LN(10)=LN(I(1)/I(2)), OR  (LN(10)/10)*ADB=LN(I(1)/I(2))
C SO (.230259)*GAMT(1)*DH=LN(I(1)/I(2))=-LN(I(2)/I(1))=A
C SINCE TRANSMITTANCE, TNU2=I(2)/I(1)
C THEREFOR (.230259)*GAMT(1)*DH=-LN(TNU2)=A, AND EXP(-A)=TNU2
C
C SIMILARLY FOR LEVEL 3, ADB=GAMT(2)*DH
C AND (.230259)*GAMT(2)*DH=-LN(I(3)/I(2))
C AND (.230259)*GAMT(2)*DH+A=A  YIELDS
C -LN(I(3)/I(2))-LN(I(2)/I(1))=-LN(I(3)/I(1))=A
C THEN -A=LN(I(3)/I(1))=LN(TNU3), THUS EXP(-A)=TNU3
C
C SIMILARLY FOR ANY LEVEL N, EXP(-A)=TNUN
C*****FORMAT(1HO,'CHANNEL FREQS(GHZ)  ',(10F7.2,2X))
C*****FORMAT(1HO,'PROFILE CONTAINS ',I3,' LEVELS FROM ',F7.2,'MB TO',
* F7.2,'MB')
C*****FORMAT(1HO,'ECHO CHECK',T15,'PRES(MB)',T35,'HEIGHT(KM)',T55,
* 'TEMP(DEG K)',T75,'H2O VAPOUR DENSITY(GM/M**3)',/)
C*****FORMAT(1X,T15,F8.3,T35,F7.3,T55,F6.2,T75,E9.4)
C*****RETURN
C*****END

```

```

FUNCTION GAMU2(FREQ,T,P)
C*****COMPUTES OXYGEN ATTENUATION USING MEeks AND LILLEY PARAMETERS*****
C
C FREQ = FREQUENCY (GHZ)
C NU = FREQUENCY (HZ)
C T = TEMPERATURE (DEGREES KELVIN)
C P = PRESSURE (TORR)
C
REAL NU
REAL NUPL(45),NUMI(45)
IF(IJ.EQ.10396) GO TO 2
C
C OXYGEN ABSORPTION LINES
C
NUPL(1)=56.2648E9
NUPL(3)=58.4466E9
NUPL(5)=59.5910E9
NUPL(7)=60.4348E9
NUPL(9)=61.1506E9
NUPL(11)=61.6002E9
NUPL(13)=62.4112E9
NUPL(15)=62.9980E9
NUPL(17)=63.5685E9
NUPL(19)=64.1272E9
NUPL(21)=64.6779E9
NUPL(23)=65.2240E9
NUPL(25)=65.7626E9
NUPL(27)=66.2978E9
NUPL(29)=66.8313E9
NUPL(31)=67.3627E9
NUPL(33)=67.8923E9
NUPL(35)=68.4205E9
NUPL(37)=68.9478E9
NUPL(39)=69.4741E9
NUPL(41)=70.0000E9
NUPL(43)=70.5244E9
NUPL(45)=71.0497E9
NUMI(1)=118.7505E9
NUMI(3)=62.4863E9
NUMI(5)=60.3061E9
NUMI(7)=59.1642E9
NUMI(9)=58.3239E9
NUMI(11)=57.6125E9
NUMI(13)=56.9682E9
NUMI(15)=56.3634E9
NUMI(17)=55.7839E9
NUMI(19)=55.2214E9
NUMI(21)=54.6728E9
NUMI(23)=54.1294E9
NUMI(25)=53.5960E9
NUMI(27)=53.0695E9
NUMI(29)=52.5458E9
NUMI(31)=52.0259E9
NUMI(33)=51.5091E9
NUMI(35)=50.9949E9
NUMI(37)=50.4830E9
NUMI(39)=49.9730E9
NUMI(41)=49.4648E9
NUMI(43)=48.9582E9
NUMI(45)=48.4530E9
PM=267.41
IJ=10396
2 CONTINUE
NU=1.E9*FREQ

```

```

C
C COMPUTE LINEWIDTH
C
B=.25
IF(P.LT.PM) B=.25*(1.+(ALOG(PM/P))/1.323)
IF(P.LT.(18.957)) B=.75
DNU1 =1.95E+0*P *(0.21+0.78*B)*(300./T ) **.85
DNU12=DNU1**2
C
C GAM02 = ATTENUATION COEFFICIENT (DB/KM)
C
SUM=0.0
DO 1103 N=1,45,2
FN=N
SUM=SUM
1+((1. /((NUPL(N)-NU)**2+DNU12))
2+1. /((NUPL(N) + NU)**2 + DNU12))
3*(FN*(2.0*FN + 3.0)/(FN + 1.0))
4+(1. /((NUMI(N) - NU)**2 + DNU12))
5+1. /((NUMI(N) + NU)**2 + DNU12))
6*(FN + 1.0)*(2.0*FN - 1.0)/FN
7+1. /((NU*2 + DNU12)
8*2.0*(FN*2 + FN + 1.0) *(2.0*FN + 1.0)/(FN**2 + FN))
9*EXP(-2.0684*FN*(FN+1.0)/T)
1103 CONTINUE
GAM02 =2.6742E-9*P/T**3*NU**2*SUM*DNU1
RETURN
END

```

```

FUNCTION GAMH20(FREQ,T,PTORR,RHO)
C
C NU = FREQUENCY (HZ)
C T = TEMPERATURE (DEGREES KELVIN)
C PTORR = PRESSURE (TORR)
C RHO = WATER VAPOR DENSITY (G/M3)
C GAMH20 = ATTENUATION COEFFICIENT (DB/KM)
C
REAL NU,NUN
DATA NUN/22.235E9/
P=PTORR
IF(FREQ.GT.60.) GO TO 300
***** COMPUTES WATER VAPOR ATTENUATION USING BARRETT AND CHUNG FORMULA. *****
C
C BARRETT AND CHUNG LINELWILTH.
C
DNU2= (2.62E+9*P/760.)/(T/318.)**.625*(1.0+.012 *RHO*T/P)
C
C COMPUTE WATER VAPOR ATTENUATION COEFFICIENT GAMH20.
C
NU=FREQ*1.E9
GAMH20 =4.56E-23+3.35E16*RHO *NU**2/T**1.5
1*(EXP(-644./T)/T*(DNU2/((NU - NUN)**2 + DNU2**2))
2 + DNU2/((NU + NUN)**2 + DNU2**2)) + 7.23E-24*DNU2
RETURN

```

AD-A087 434 UTAH UNIV. SALT LAKE CITY DEPARTMENT OF METEOROLOGY
DEVELOPMENT OF THE MICROWAVE RADIATIVE TRANSFER PROG...ETC.(U)
SEP 79 LIOU, KUO-NAN

F/G 20/13

F19628-78-C-0144

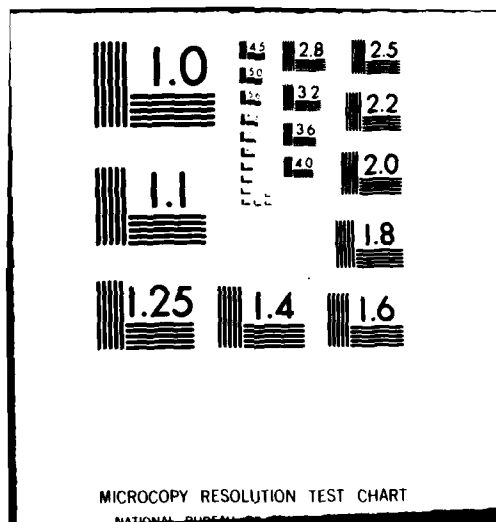
UNCLASSIFIED

PROJ. 7670 TASK 13 AFGL TR-80-0051

N/I

2 or 2
R&B-13

END
DATE FILMED
2-81
DTIC



```

C
300 CONTINUE
C*****COMPUTES WATER VAPOR ABSORPTION FROM GAUT LINE MODEL FOR 183 GHZ
C LINE
C*****
PMH=1013.25/760.*PTURR
CALL ALPHAS(FREQ,PMH,T,RHO,RES,RESNON)
GAMM20=RES+RESNON
RETURN
END

```

```

SUBROUTINE ALPHAS (FREQ,P,T, RHOBAR,RES,RESNON)
C*****COMPUTES ATTENUATION FROM 183 GHZ WATER VAPOR LINE PLUS
C NONRESONANT BACKGROUND
C ORIGINAL PROGRAM BY N. GAUT
C*****
C
C FREQ = FREQUENCY (GHZ)
C P    = PRESSURE (MILLIBARS)
C T    = TEMPERATURE (DEGREES KELVIN)
C
SQRTH(X)=SQRT(X)
EXP(X)=EXP(X)
CONV=1000.
F093=323.758
F164=183.310
DLN164=(3.561*10.**(-7)*FREQ)**2*T /18.0
LN0043=2.79*(P/1013.25)*(300./T)**(0.619)*(1.+0.0066*RHOBAR)
LN0043=SQRTH((DELDSQ+LNU093**2))
LN0WW=1.04*0.200*RHOBAR*(T/300.)**(0.1)
DNU0VV=SQRT((DNUWV**2+DELDSQ))
DNU0WW=0.66*0.019*T*(300./T)**0.62
DNU1WW=SQRTH((DNUWW**2+DELDSQ))
DNU1WW=2.08*(P/1013.25)*(300./T)**(0.70)*(1.+0.0064*RHOBAR)
DNU164=SQRTH((DNU164**2+DELDSA))
S1=1./((F164-FREQ)**2+DNU164**2)+1./((F164+FREQ)**2+DNU164**2)
S2=1./((F093-FREQ)**2+DNU093**2)+1./((F093+FREQ)**2+DNU093**2)
GAM1=0.97*RHOBAR*FREQ**2/T**2.5*EXP(-197.3/T)*DNU164*S1
GAM2=0.0499*RHOBAR*FREQ**2/T**2.5*EXP(-454./T)*DNU093*S2
GAM3=2.55*FREQ**2/F164**3*(DNUWV+DNUWW)*(300./T)**(1.5)/1000.*RHO
RHOBAR=4.165*T+0.760/1013.25
RES=GAM1*CONV
RESNON=(GAM2+GAM3)*CONV
RETURN
END

```

```

SUBROUTINE ANTEMP(TAU,TAUSQ,T,TSFC,EMIS,TA,ISFC,NU1,NU2)
C*****C CALCULATE CLEAR COLUMN BRIGHNESS VALUES FOR EACH CHANNEL (ANTENNA
C TEMPERATURES).
C*****
PARAMETER NUMCHN=6,NUMLV=40, NMOST=NUMLV+10
DIMENSION TAU(NMOST,NUMCHN),TAUSQ(NMOST,NUMCHN),T(NMOST),
* EMIS(NUMCHN),TA(NU1,NU2)
DIMENSION TAU1(NUMCHN),TAU2(NUMCHN),F(NUMCHN)
B1=T(1)
DO 3 J=NU1,NU2
TAUS=TAU(ISFC,J)
REFL=1.-EMIS(J)
F(J)=TAUS*TAUS*REFL
TAU1(J)=TAU(1,J)
3 TA(J)=0.
DO 5 I=2,ISFC
B2=T(I)
DO 4 J=NU1,NU2
TAU2(J)=TAU(I,J)
TA(J)=TA(J)+0.5*(B1+B2)*(TAU1(J)-TAU2(J))*(1.+F(J)/TAUSQ(I,J))
4 TAU1(J)=TAU2(J)
5 RI=H2
DO 6 J=NU1,NU2
RS=TSFC*EMIS(J)
TAUS=TAU(ISFC,J)
6 TA(J)=TA(J)+RS*TAUS
RETURN
END

```

```

SUBROUTINE HUFF(P,T,W,H,U)
C*****C INVERT PROFILES FOR COMPATIBILITY WITH REMAINING ROUTINES.
C MAKE THE OPTION FOR CLEAR, CLOUDY, OR PRECIPITATING ATMOSPHERES.
C*****
PARAMETER LEV=40,NUMCHN=6, NMOST=LEV+10
DIMENSION P(NMOST),T(NMOST),W(NMOST),H(NMOST),TRN(NMOST,NUMCHN)
*,U(NMOST,NUMCHN),TAUABS(NMOST,NUMCHN)
COMMON/INPUT/ALT(NMOST),TEMP(NMOST),PRE(NMOST),H2O(NMOST),
* THKNS(9),NTHICK,NBASE,TRN,NEWLEV(10),TAUABS
COMMON/TAUVAL/TRANS(NMOST,NUMCHN)
COMMON/SFCEMS/EMIS(NUMCHN)
COMMON/NEWLEV/ADDHT(10),NUMNE,LVNUM
J=LVNUM+1
DO 100 I=1,LVNUM
K=J-1
PRE(K)=P(I)
TEMP(K)=T(I)
H2O(K)=W(I)
ALT(K)=H(I)
DO 50 L=1,NUMCHN
TRN(I,L)=TRANS(I,L)
TAUABS(K,L)=U(I,L)
50 CONTINUE
100 CONTINUE

```

```

READ (5,200) ICHOSE
GO TO (125,150,175,225), ICHOSE
125 RETURN
150 CALL DRIVER
RETURN
175 CALL PFILE
RETURN
225 CALL SIMPLR
RETURN
200 FORMAT( )
END

```

SUBROUTINE DRIVER

```

C ****DRIVER SUBROUTINE****
C THIS IS DRIVING ROUTINE FOR CALCULATION OF BRIGHTNESS TEMPERATURES
C WITH INTERVENING CLOUD LAYER.
C EXECUTIVE PROGRAM FOR CLOUD AND PRECIPITATION--A SOLUTION OF THE
C RADIATIVE TRANSFER EQUATION FOR A PLANE-PARALLEL CLOUDY ATMOSPHERE
C USING THE DISCRETE-ORDINATE METHOD. THIS PROGRAM WILL CALCULATE THE
C RADIANCE (INTENSITY) ABOVE AND BELOW NON-ISOTHERMAL CLOUDS AT THE
C WAVENUMBERS OF SCAMS OF NIMBUS 6. CLOUD TEMPERATURE GRADIENTS
C IN THE VERTICAL ARE APPROXIMATED BY DIVIDING THE CLOUD DEPTH INTO
C 'N' LAYERS, EACH LAYER ASSIGNED A RESPECTIVE TEMPERATURE ACCORDING
C TO THE INPUT ATMOSPHERIC PROFILE. A SYSTEM OF EQUATIONS FOR THE
C RADIANCE IS DERIVED FOR THE 16 DISCRETE RAYS.
C ****INPUT PARAMETERS**** (UNITS)
C **ATMOSPHERIC CONDITIONS**
C ALT ALTITUDE OF ATMOSPHERIC LAYER ABOVE THE SURFACE KM
C TEMP TEMPERATURE CORRESPONDING TO 'ALT' DEG K
C PNE PRESSURE CORRESPONDING TO 'ALT' MILLIBARS
C H2O WATER VAPOR CONCENTRATION CORRESPONDING TO 'ALT' GM CM-3
C LEV NUMBER OF ATMOSPHERIC PROFILE LAYERS NONE
C
C **CLOUD PARAMETERS**
C INTICK NUMBER OF CLOUD THICKNESS CASES PER RUN (10 MAX) NONE
C THICKS ARRAY OF CLOUD THICKNESS (MAX OF 9 VALUES) KM
C WBASE ALTITUDE OF CLOUD BASE (REAL NUMBER) KM
C NLYR NUMBER OF LAYERS WITHIN THE CLOUD (DEFAULT=3) NONE
C
C **EXTINCTION PROPERTIES**
C PINI LEGENDRE POLYNOMIAL EXPANSION OF PHASE FUNCTION NONE
C PT SINGLE SCATTERING ALBEDO ACCORDING TO 'NU' NONE
C NU WAVE NUMBER (LIMITED TO 'INT'=7) CM-1
C DEXT EXTINCTION COEFFICIENTS ACCORDING TO 'NU' NONE
C LV LINE CONTRIBUTION TO ABSORPTION COEFFICIENT NONE
C CK1 CONTINUUM CONTRIBUTION TO ABSORPTION COEFF TAKEN NONE
C CK2 FROM PAPER BY K J BIGNELL (1970) NONE

```

```

REAL NU,LV,NBASE
DOUBLE PRECISION PINO,UM,A,Z
PARAMETER LEV=40, INT=6, MZ=25, NG=16, NG2=8, NMOST=LEV+10
COMMON/INPUT/ALT(NMOST),TEMP(NMOST),PRE(NMOST),H2O(NMOST),
* THKNS(9),NTHICK,NBASE,TRN(NMOST,INT),NWLEV(10),
* TAUAB(S(NMOST,INT))
COMMON /ANGLE/ UM(NG),A(NG),PI
COMMON/LBMULT/UBC,ATMD,ATMR,ATMA,SFC,THRUSV(INT),THRUPR(INT),ITER
* ,ECB,IPCHAN(INT),CLDEM
COMMON /POLY/ PINO(NG)
COMMON /WINDOW/ UP(NG2,INT),DW(NG2,INT),THETA(NG),NU(INT),LV(INT),
CK1(INT),CK2(INT),LUVERT(INT),CDVERT(INT)
COMMON /ADATA/ PINI(NG,INT),PT(INT),BEXT(INT)
COMMON/NWLEV/ADDH1(10),NUMNEW,LVNUM
COMMON /FREQ/FGHZ(1INT)
COMMON Z(1300)
COMMON/FLAGS/IFLAG(2)
DIMENSION NE=LV(10)
DATA SPDLGT/2.997929E10/
9 FORMAT( )
10 READ 9, LAST
   IF (LAST,NE,0) GO TO 100
C ***** INPUT CLOUD PARAMETERS *****
READ 9, (IPCHAN(I),I=1,INT)
READ 9, UBC,ATMD,ATMR,ATMA,SFC,ECB,CLDEM,ITER
READ 9,NTHICK,NBASE,NLYR
NTH=NTHICK
READ 9,(THKNS(I),I=1,NTH)
READ 9,(PT(I),I=1,INT)
READ 9,(BEXT(I),I=1,INT)
DO 12 J=1,INT
12 READ (5,1900) (PINI(I,J),I=1,16)
1900 FORMT(5F16.8)
READ(5,9)(IFLAG(J),J=1,2)
C
C IFLAG(1)= 0 DO NOT INCLUDE SFC REFLECTION OF BRIGHTNESS CONTRIBUTION
C FROM ABOVE SCATTERING LAYER WITH LOWER BOUNDARY VALUE.
C
C           1 INCLUDE SFC REFLECTION OF BRIGHTNESS CONTRIBUTION
C FROM ABOVE SCATTERING LAYER WITH LOWER BOUNDARY VALUE.
C ( ASSUME TOP/DOWN THROUGHPUT EQUALS 1.)
C
C IFLAG(2)= 0 DO NOT WRITE SCATTERING PARAMETERS TO FILE 20.
C
C .NE.0 WRITE SCATTERING PARAMETERS TO FILE 20.
C (IFLAG(2)=RAINFALL RATE IN MM/HR 100 YIELDS RFR=0
C
C
DO 15 I=1,INT
15 NU(I)=(FGHZ(I)*1.E9)/SPDLGT      & CHANNEL WAVE NUMBERS.
K=1
KK=1
TEST=NBASE
DO 50 I=1,LVNUM
IF (ABS(ALT(I)-ADDH(K))-1.E-6)35,35,38
35 NEWLV(KK)=I
KK=KK+1
38 IF (ABS(ALT(I)-TEST)-1.E-6)40,40,50
40 NWLEV(K)=I
KK+1
TEST=NBASE+THKNS(K-1)
IF (KK.GT.NUMNEW) GO TO 60
50 CONTINUE
60 PRINT 2000

```

```
2000 FORMAT(1HD,'THE LEVELS ADDED TO THE PROFILE ARE - ',/,'5X,
* 'PRESS(MB)',10X,'HEIGHT(KM)',10X,'TEMP(DEG K)',10X,
* 'MIX RAT(GM/KGM)')
DO 81 I=1,NUMNEW
J=NEWLV(I)
PRINT 2001,PHE(J),ALT(J),TEMP(J),H2O(J)
2001 FORMAT(5X,F9.2,10X,F10.2,10X,F11.2,10X,E15.5)
81 CONTINUE
KSTOP=0
C
C CHECK FOR LAST DATA CASE
C DETERMINE EXTINCTION COEFFICIENTS ONCE PER DATA CASE USING 'KSTOP'
C IN SUBSEQUENT ROUTINE.
C EXECUTE ENTIRE CODE ONCE FOR EACH INPUT CLOUD THICKNESS (THKNS)
C
DO 90 KTHK=1,NTHICK
85 CALL BNDRY (KSTOP,KTHK,NLYR)
CALL RAD (KTHK,NLYR,KSTOP,$85)
90 CONTINUE
100 CONTINUE
RETURN
END
```

```

SUBROUTINE BNORY(KSTOP,KTHK,NLYR)
C*****CALCULATE UPWARD AND DOWNWARD BRIGHTNESS TEMPERATURES AT THE CLOUD
C BOTTOM AND TOP (BOUNDARY CONDITIONS)
C*****C
C
      REAL LV,NU
      PARAMETER LEV=40, INT=6, NZ=25, NG=16, NG2=8, NMOST=LEV+10
      DOUBLE PRECISION UM,A,CCRAD
      REAL NBASE
      COMMON/LBMULT/UBC,ATMO,ATHR,ATMA,SFC,THRUSV(INT),THRUPT(INT),INTER
      * ,ECB,IPCHAN(INT),CLOEM
      COMMON/INPUT/ALT(NMOST),TEMP(NMOST),PRE(NMOST),H2O(NMOST),
      * ,THKNS(9),NTHICK,NBASE,TRN(NMOST,INT),NWLEV(10)
      * ,TAUABS(NMOST,INT)
      COMMON /ANGLE/ UM(NG),A(NG),PI
      COMMON /INDOW/ UP(NG2,INT),DW(NG2,INT),THETA(NG),NU(INT),LV(INT),
      * ,CK1(INT),CK2(INT),CUVERT(INT),CDVERT(INT)
      COMMON/NWLEV/ADUHT(10),NUMNEW,LVNUM
      COMMON /SFCEMS/ EMIS,NB
      COMMON /HADATA/ PINI(NG,INT),PT(INT),BEXT(INT)
      COMMON/FLAGS/IFLAG(2)
      DIMENSION TAUSQ(NMUST,INT)
      DIMENSION TAUM(NMOST,INT),TAU(NMOST,INT)
      DIMENSION TAUMOD(NMOST,INT),EMIS(INT),EUP(INT),EDW(INT)
      DIMENSION CUHORZ(INT),CDHORZ(INT),CCRAD(INT,NG)
      PI=3.1415926536
      KSTOP=KSTOP+1
      IF (KSTOP.GT.1) GO TO 40
      WRITE (6,160) NBASE,THKNS(KTHK)
      WRITE (6,180)
      DO 30 I=1,INT
      IF (IPCHAN(I).EQ.0) GO TO 30
      WRITE (6,190) (NU(I),PT(I),BEXT(I),(PINI(J,I),J=1,NG))
      30 CONTINUE
      40 CONTINUE
C
C DETERMINE GAUSSIAN QUADRATURE WEIGHTS FOR DISCRETE ORDINATE METHOD
C NG=NUMBER OF GAUSS POINTS (16)
C UM=COSINE(THETA)
C AZQUADRATURE WEIGHT VALUES
C
      CALL GAUSS (NG,-1.000,1.000)
C
C LOOP FOR ANGLES
C
      KOUNT=2
      DO 102 J=1,NG2
      JJ=J+NG2
      UMO=SNGL(UM(J))
      UM(JJ)=UM(J)
      A(JJ)=A(J)
      UML=SNGL(UM(J))
      UM2=SNGL(UM(JJ))
      THETA1(J)=ACOS(UM1)*180./PI
      THETA1(JJ)=ACOS(UM2)*180./PI
      CALL TRANMW(TAUM,TAUSQ,0.,1,INT,KOUNT,UM0)
      JJ=LVNUM+1
      DO 70 K=1,LVNUM
      L=JJ-J
      DO 60 M=1,INT
      60 TAU(L,M)=TAUM(K,M)
      70 CONTINUE
      NB=NWLEV(1)
      NTOP=NWLEV(KTHK+1)

```

```

C
C LOOP FOR CHANNELS
C
    DO 80 I=1,INT
    THRUPT(I)=1.0
    IF(IPCHAN(I),EQ,0) GO TO 80
    DO 75 M=NTOP,LVNUM
    IF(TAU(M,I),NE,0.) GO TO 74
    TAUMOD(M,I)=0.
    GO TO 75
74   TAUMOD(M,I)=TAU(NTOP+I)/TAU(M,I)
75   CONTINUE
80   CONTINUE
    DO 101 I=1,INT
    IF(IPCHAN(I),EQ,0) GO TO 101
C
C COMPUTE DOWNWARD INTENSITY AT THE CLOUD TOP
C
    EDW(I)=0.
    NTOP=NTOP+1
    DO 95 M=NTOP,LVNUM
    TBAR=(TEMP(M-1)+TEMP(M))*5
    EDW(I)=EDW(I)+TBAR*(TAUMOD(M-1,I)-TAUMOD(M,I))
95   CONTINUE
    DW(J,I)=EDW(I)*UBC
    CCRAD(I,J)=DBLE(DW(J,I))
    DO 97 K=1,LVNUM
    TAUMOD(K,I)=TAU(1,I)/TAU(K,I)
97   CONTINUE
C
C COMPUTE UPWARD INTENSITY AT BOTTOM OF CLOUD
C
    BSFC=0.
    DATM=0.
    RATMB=0.
    RATMU=0.
    REFL=1.-EMIS(I)
    IF(NB,EQ,1) GO TO 98
    DO 100 K=2,NB
    TBAR=(TEMP(K)+TEMP(K-1))*5
    IF(TAU(NB,I),NE,0.) GO TO 98
    DATM=DATH
    GO TO 96
90   DATM=DATM+TBAR*(TAU(K,I)-TAU(K-1,I))/TAU(NB,I)*ATMO
96   RATMB=RATMB+TBAR*(TAUMOD(K-1,I)-TAUMOD(K,I))*REFL+TAUMOD(NB,I)
*     *ATMN
100  CONTINUE
98   BSFC=TEMP(I)*EMIS(I)*TAUMOD(NB,I)*SFC
    RATMU=EDW(I)*TAUMOD(NB,I)*REFL+TAUMOD(NB,I)*ATMA*THRUPT(I)
    IF(ATMA,EQ,0)
*     RATMU=CDVENT(I)*TAUMOD(NB,I)*REFL+TAUMOD(NB,I)*ECB
    IF(IFLAG(I),EQ,0) RATMU=0.
    EUP(I)=DATM+HATMU+RATMU
    UP(J,I)=EUP(I)+BSFC
    CCRAD(I,J)=DBLE(UP(J,I))
101  CONTINUE
102  CONTINUE
C
C EXTRAPOLATE INTENSITIES TO THETA=0, AND 90 DEG.
C
    ICCHAN=1
    IEMIS=0
    DO 110 JAY=1,INT
    IF(IPCHAN(JAY),EQ,0) GO TO 110
    JNUM=INT
    IUPLEN=0

```

```

CALL EXTRP0(THETA,CCRAD,TVERT,JAY,JDUM,IUPDN)
CALL EXTRP9(THETA,CCRAD,THORIZ,JAY,JDUM,IUPDN)
CUVERT(JAY)=TVERT
CUMORZ(JAY)=THORIZ
IUPDN=1
CALL EXTRP0(THETA,CCRAD,RVERT,JAY,JDUM,IUPDN)
CALL EXTRP9(THETA,CCRAD,RHORIZ,JAY,JDUM,IUPDN)
CUVERT(JAY)=RVERT
CUMORZ(JAY)=RHORIZ
110 CONTINUE
WRITE (6,200) (THKNS(KTHK), (THETA(J),J=1,NG2))
DO 120 I=1,INT
IF (IPCHAN(I).EQ.0) GO TO 120
WRITE (6,210) (NU(I),CUVERT(I),(UP(J,I),J=1,NG2),CUMORZ(I))
120 CONTINUE
NG21=NG2+1
WRITE (6,220) (THETA(J),J=NG21,NG)
DO 130 I=1,INT
IF (IPCHAN(I).EQ.0) GO TO 130
WRITE (6,210) (NU(I),CDVERT(I),(DW(J,I),J=1,NG2),CDHORIZ(I))
130 CONTINUE
RETURN
160 FORMAT (//,54X,'CLOUD STRUCTURE',//,22X,'CLOUD TEMPERATURES = (DENI
IVED FROM THE ATMOS. TEMP. PROFILE + CLOUD THICKNESS)',//22X,'CLOUD
2 BASE HEIGHT =',F5.2,'KM',//,28X,'CLD THKNS =',F4.1,'KM (MAXIMU
3M OF 10 VALUES)',//,35X,'INPUT ABSORPTION COEFF ',
4//44X,'NU',9X,'LV',8X,'CK1',6X,'CK2')
180 FORMAT (/,37X,'SINGLE SCATTERING PROPERTIES OF WATER DROPLETS',//,
111X,'NU',9X,'PT',7X,'BEXT',5X'.....',P
2IN1,.....)
190 FORMAT (9X,F6.4,2(4X,F6.3),9X,B(F8.5,1X),/,39X,B(F8.5,1X))
200 FORMAT (1M1,37X,' BRIGHTNESS TEMPERATURE AT THE CLOUD TOP AND ',
* 'BASE',//,48X,'CLOUD THICKNESS ',F5.3,' KM',//49X,'THE UPWARD ',
* 'BRIGHTNESS',//4X,'(THETA) (0,0000)',3X,B('(',F7.4,')',3X),
* '(90,0000)',//,5X,'WAVE NO')
210 FORMAT (5X,F6.4,F10.3,1X,B(F10.3,2X),F10.3)
220 FORMAT (/,48X,'THE DOWNWARD BRIGHTNESS',//,4X,'(THETA) (180.000)',
*3X,B('(',F7.3,')',3X),'( 90.000)',//,5X,'WAVE NO')
END

```

```

SUBROUTINE GAUSS(N,XL,XU)
C **** SUBROUTINE 'GAUSS' DETERMINES THE GAUSSIAN QUADRATURE VARIABLES
C ('R'='UM'= COSINE(THETA), 'W'='A'= WEIGHTING FACTOR) FOR THE
C DISCRETE ORDINATE METHOD.
C ****
C
      IMPLICIT DOUBLE PRECISION (A=H,O=Z)
      COMMON /ANGLE/ R(16),W(16),PI
      DIMENSION Z(50),PA(50)
      TOL=1.0D-16
      PI1=3.141592653589793D+00
      AA2Z=0.0D+00/PI1**2
      AB=-6.2_00/00/(3.0_00+00*PI1**4)
      AC=15.116_00/00/(15.0_00+00*PI1**6)
      AL=-12554474.0_00/00/(105.0_00+00*PI1**8)
      PA(1)=1.0D+00
      EN=N
      NP1=N+1
      U=1.0D+00-(2.0D+00/PI1)**2
      U=1.0D+00/DSQRT((LN+0.5D+00)**2+U/4.0D+00)
      DO 10 I=1,N
      SM=1
      AZ=4.0D+00*SM-1.0D+00
      AT=AA/AZ
      AF=AB/AZ**3
      AG=AC/AZ**5
      AH=AD/AZ**7
10    Z(I)=0.25U+00*PI1*(AZ+AE+AF+AG+AH)
      DO 60 K=1,N
      X=DCOS(Z(K)*I)
      PA(2)=X
      DO 30 NN=3,NP1
      ENN=NN-1
      30  PA(NN)=((2.0D+00*ENN-1.0D+00)*X*PA(NN-1)-(ENN-1.0D+00)*PA(NN-2))/ENN
      PNP=ENN*(PA(N)-X*PA(NP1))/(1.0D+00-X*X)
      XI=X-PA(NP1)/PNP
      XU=DAB5(XI-X)
      XDD=XD-TOL
      IF (XDD) 50,50,40
40    X=XI
      GO TO 20
50    R(K)=X
50    W(K)=2.0D+00*(1.0D+00-X*X)/(EN*PA(N))**2
      RETURN
      END

```

```

SUBROUTINE EXTRPO(THETA,INTENS,TVERT,JAY,JDUM,IUPDN)
C*****+
C THIS SUBROUTINE IS TO EXTRAPOLATE THE INTENSITIES TO THETA=0, AND 90
C BY APPLYING LEAST-SQUARE POLYNOMIAL.
C*****+
C
      IMPLICIT DOUBLE PRECISION (A-H,O-Z)
      REAL THETA,TVERT
      DOUBLE PRECISION INTENS
      DIMENSION THETA(16),INTENS(JDUM,16)
      K1=1+A*IUPDN
      XX=FLOAT(IUPDN*180)
      S
      K2=K1+1
      K3=K1+2
      T1=THETA(K1)
      T2=THETA(K2)
      T3=THETA(K3)
      R1=INTENS(JAY,K1)
      R2=INTENS(JAY,K2)
      R3=INTENS(JAY,K3)
      C3=(R2-R1)/((T2-T1)*(T2-T3))+(R1-R3)/((T3-T1)*(T2-T3))
      C2=(R3-R1)-C3*(T3-T1)*(T3+T1)/(T3-T1)
      C1=R1-C2*T1-C3*T1*T1
      TVEN=C1+C2*XX+C3*XAXX
      GO TO 50
C
C THE FOLLOWING ENTRY IS FOR THETA=90.
C
      ENTRY EXTRP9(THETA,INTENS,TVERT,JAY,JDUM,IUPDN)
      XX=90.
      K1=6+A*IUPDN
      GO TO S
      50 CONTINUE
      RETURN
      END

```

```

SUBROUTINE RAD (KTHK,NLYR,KSTOP,S)
C *****
C FOR A GIVEN CLOUD DEPTH ('KTHK') THIS ROUTINE APPLIES THE DISCRETE
C ORDINATE METHOD TO THE RADIATIVE TRANSFER EQUATION FOR EACH OF THE
C SPECIFIED WAVE NUMBERS ('NU').
C *****
C
PARAMETER LEV=40, INT=6, MZ=25, NG=16, NG2=8, NMOST=LEV+10
DOUBLE PRECISION PINO,UM,A
COMMON /ANGLE/ UM(NG),A(NG),PI
COMMON/LBMULT/UBC,ATMD,ATHR,ATMA,SFC,THRUSV(INT),THRUPT(INT),ITER
* ,ECB,IPCHAN(INT)
COMMON /POLY/ PINO(NG)
COMMON /RADATA/ PINI(NG,INT),PT(INT),BEXT(INT)
C
C LOOP THRU MAIN CALCULATIONS FOR EACH WAVE NUMBER (INDEX='JAY')
C
DO 30 JAY=1,INT
IF(IPCHAN(JAY).EQ.0) GO TO 30
DO 10 L=1,NG
PINO(L)=UBLE((PINI(L,JAY))+PT(JAY))
10 CONTINUE
IF (KSTOP.GT.1) GO TO 20
CALL IGEN (JAY)
20 CALL TGRAD (JAY,KTHK,NLYR)
30 CONTINUE
DO 40 I=1,INT
IF(IPCHAN(I).EQ.0) GO TO 40
IF(ABS(THRUSV(I)-THRUPT(I)).GT.0.1) RETURN 4
40 CONTINUE
RETURN
END

```

```

SUBROUTINE IGEN (JAY)
C **** SUBROUTINES 'IGEN', 'START', 'FILLH', 'FILLC', 'FILLD', 'FILLS', 'GMPRD'
C 'LEP', 'IPRHM', AND 'LPOFB' DETERMINE THE EIGENVALUES RT(I)
C ACCORDING TO THE WAVE NUMBER (LIOU, 1973, APPENDIX)
C ****
C
PARAMETER NG=16, NG2=8, INT=6
DOUBLE PRECISION P1NO,Z,VALUES
COMMON Z(1300)
COMMON /EIGEN/ VALUES(INT,NG2)
COMMON /POLY/ P1NO(NG)
NDIM=1300
N=NG
MDIM=3*N*(N+1)
IF (MDIM.GT.NDIM) GO TO 10
ND2=(NDIM-N)/2
N=N*2
NS=3*NN+1
CALL START (Z(1),Z(NN+1),Z(2*NN+1),P1NO,Z(1),Z(NS+2*N),N,Z(2*N+1),
Z(3*N+1),JAY)
GO TO 20
10 WRITE (6,30) N,NDIM,MDIM
PRINT 40
20 CONTINUE
RETURN
C
30 FORMAT (5I5)
40 FORMAT ('PROGRAM MUST BE REDIMENSIONED AT NDIM')
END

```

```

SUBROUTINE START (B,C,P,T,D,S,N,COMPLE,POL,JAY)
C*****SUBROUTINE 'START' IS TO COMPUTE EIGENVALUES 'VALUES(JAY,I)' AND
C RETURNS THE EIGENVALUES THROUGH 'IGEN' TO 'TGRAG' WHERE THE
C RADIANCE CALCULATIONS ARE MADE.
C*****
C
PARAMETER NG2=8, NG=16, INT=6
DOUBLE PRECISION UM,A,P,C,B,S,D,T,DMU,COMPLE,POL,G,SQRT,PROOT,
  VALUE,VALUES
COMMON /ANGLE/ UM(NG),A(NG),PI
COMMON /EIGEN/ VALUES(INT,NG2)
DIMENSION B(N,N),C(N,N),P(N,N),T(N),D(N),S(N)
DIMENSION COMPLE(I,),POL(N),G(NG),DMU(30),VALUE(NG2)
C
NL1=N-1
DO 10 I=1,N
10 CALL LEP (P(1,I),UM(I),NL1)
DO 20 J=1,N
  CALL FILLC (T,P(1,I),P(1,J),A(J),C(1,J),N)
20 CONTINUE
  CALL FILLH (A,C,UM,N,NL1)
  CALL FILLS (S,A,C,P,N)
  CALL FILLD (D,S,N)
  IF (ABS(T(1))-1.0).LE.1.E-10 D(N)=0.
  DO 30 I=1,N
    DMU(I)=1.0/UM(I)
30 CONTINUE
N2=N/2+1
IM=N+2
G(N2)=1.00
DO 40 I=2,N/2
  J=(IM-1)/2
  G(J)=D(I)
40 CONTINUE
  CALL DPRHM (G,N2,VALUE,COMPLE,POL,IR,IER)
  DO 50 I=1,IR
    SQRT=DSQRT(DAHS(VALUE(I)))
    PROOT=SQRT
    DO 50 J=1,NL1
      PROOT=(PROOT+I)(J)*SQRT
      PROOT=PROOT+I(N)
      VALUE(I)=SQRT
      IF (PROOT.GT.1.0D-02) WRITE (6,80) PROOT
60 CONTINUE
  DO 70 I=1,NG2
    VALUES(JAY,I)=VALUE(I)
70 CONTINUE
  RETURN
C
80 FORMAT ('0////// EIGENVALUE ERROR =',D18.8)
END

```

```

SUBROUTINE LEP (Y,X,N)
C ***** LEGENDRE POLYNOMIAL EXPANSION *****
C
      DOUBLE PRECISION Y,X,G
      DIMENSION Y(1)
      Y(1)=1.
      IF (N) 10,10,20
10  RETURN
20 Y(2)=X
      IF (N-1) 10,10,30
30 DO 40 I=2,N
      G=X*Y(I)
40 Y(I+1)=G-Y(I-1)+G-(G-Y(I-1))/FLOAT(I+1)
      RETURN
END

```

```

SUBROUTINE FILLC (T,PI,PJ,AJ,C,N)
C COMPUTE COEFFICIENT C(I,J)
C SEE LIOU, 1973 (APPENDIX)
C
      DOUBLE PRECISION T,PI,PJ,AJ,C
      DIMENSION T(1),PI(1),PJ(1)
      C=0.
      DO 10 L=1,N
10  C=C+T(L)*PI(L)*PJ(L)
      C=C/AJ/2.
      RETURN
END

```

```

SUBROUTINE FILLH (B,C,UM,N,NL1)
C SEE LIOU, 1973 (APPENDIX)
C
      DOUBLE PRECISION B,C,UM
      DIMENSION B(N,N),C(N,N),UM(N)
      DO 20 I=1,NL1
      IP1=I+1
      DO 10 J=IP1,N
      H(I,J)=C(I,J)/UM(I)
  10  H(J,I)=C(J,I)/UM(J)
  20 H(I,I)=(C(I,I)-1.0)/UM(I)
      H(N,N)=(C(N,N)-1.0)/UM(N)
      RETURN
      END

```

```

SUBROUTINE FILLS (S,B,C,P,N)
C S(N) IS TRACE OF A(N,N)
C SEE LIOU, 1973 (APPENDIX)
C
      DOUBLE PRECISION S,B,P,C
      DIMENSION S(1),H(N,N),P(N,N),C(N,N)
      DO 10 I=1,N
      S(I)=0.
      S(1)=S(1)+B(I,I)
      DO 10 J=1,N
  10  C(I,J)=B(I,J)
      NH=N
      IF (MOD(N,2).EQ.0) NH=N-1
      IF (N.LE.2) GO TO 50
      DO 40 I=2,NH,2
      CALL GMPRD (H,C,P,N,N,N)
      DO 20 J=1,N
  20  S(I)=S(I)+P(I,J)
      CALL GMPRD (A,P,C,N,N,N)
      IP1=I+1
      DO 30 J=1,N
  30  S(IP1)=S(IP1)+C(J,J)
  40  CONTINUE
  50  IF (NH.EQ.N) RETURN
      CALL GMPRD (A,C,P,N,N,N)
      DO 60 J=1,N
  60  S(N)=S(N)+P(J,J)
      RETURN
      END

```

```

SUBROUTINE GMPROD (A,B,R,N,M,L)
C THE SUBROUTINE IS TO COMPUTE GENERAL MATRIX PRODUCT.
C
DOUBLE PRECISION K,A,B
DIMENSION A(1),B(1),R(1)
IR=0
IK=N
DO 10 K=1,L
IK=IK+M
DO 10 J=1,N
IR=IR+1
JI=J-N
IH=IK
R(IK)=0
DO 10 I=1,M
JI=JI+N
IR=IR+1
10 R(IK)=R(IR)+A(JI)*B(IR)
RETURN
END

```

```

SUBROUTINE FILLD (D,S,N)
C D(I) ARE COEFFICIENTS OF THE EXPANDED POLYNOMIAL OF EIGENVALUES.
C SEE LIOU, 1973 (APPENDIX)
C
DOUBLE PRECISION D,S,X
DIMENSION S(1),D(1)
D(1)=-S(1)
DO 20 I=2,N
IL1=I-1
X=0.
DO 10 J=1,IL1
10 X=X+D(1-J)*S(J)
20 D(I)=-(X+S(I))/FLOAT(I)
RETURN
END

```

```

SUBROUTINE DPHRM (C,IC,RH,RC,POL,IR,IER)
C SUBROUTINES 'DPHRM' AND 'DPOFB' ARE FOR THE CALCULATION OF ROOTS
C (EIGENVALUES) ACCORDING TO POLYNOMIAL EXPANSIONS
DIMENSION C(1),RR(1),RC(1),POL(1),Q(4)
DOUBLE PRECISION C,RH,RC,POL,Q,EPS,A,H,H,Q1,Q2

C TEST ON LEADING ZERO COEFFICIENTS
C
EPS=1.0E-6
LIM=100
IR=1,L+1
10 IR=IR-1
IF (IR=1) 420,420,20
20 IF (C(IR)) 30,10,30

C WORK UP ZERO ROOTS AND NORMALIZE REMAINING POLYNOMIAL
C
30 IER=0
J=IR
L=0
A=C(IR)
DO 40 I=1,IR
IF (L) 40,40,70
40 IF (C(I)) 60,50,60
50 RR(1)=0.0D0
RC(I)=0.0D0
POL(J)=0.0D0
J=J-1
GO TO 80
60 L=1
IST=I
J=0
70 J=J+1
C(I)=C(I)/A
POL(J)=C(I)
CALL OVERFL (N)
IF (N=2) 420,80,80
80 CONTINUE

C START HAIRSTOW ITERATION
C
Q1=0.0D0
Q2=0.0D0
90 IF (J=2) 330,100,140
C DEGREE OF POLYNOMIAL IS EQUAL TO ONE
100 A=POL(1)
RH(IST)=-A
RC(IST)=0.0D0
IR=IR-1
G2=0.0D0
IF (IR=1) 130,130,110
110 DO 120 I=2,IR
Q1=Q2
Q2=POL(I+1)
120 POL(I)=A*Q2+Q1
130 POL(IR+1)=A*Q2
GO TO 340

C DEGREE OF POLYNOMIAL IS GREATER THAN ONE
140 DO 220 L=1,10
NC1
150 Q(1)=Q1
Q(2)=Q2
CALL DPWFR (POL,J,Q,LIM,I)
IF (I) 160,240,230
160 IF (Q1) 160,170,160
170 IF (Q2) 180,210,180
180 GO TO (190,200,190,210), N
190 Q1=-Q1
N=N+1
GO TO 150

```

```

200 Q2=-Q2
N=N+1
GO TO 150
210 Q1=1.00+Q1
220 Q2=1.00-Q2
IER=3
IK=IK-J
RETURN
230 IER=1
240 Q1=6(1)
Q2=Q1(2)
B=0.00
A=0.00
I=J
250 H=-Q1+B-Q2+A+POL(I)
POL(I)=H
B=A
A=H
I=I-1
IF (I-2) 260,260,250
260 POL(2)=H
POL(1)=A
L=IK-1
IF (J-L) 270,270,290
270 DO 280 L=J,L
280 POL(I-1)=POL(I-1)+POL(I)*Q2+POL(I+1)*Q1
290 POL(L)=POL(L)+POL(L+1)*Q2+Q1
POL(IR)=POL(IR)+Q2
H=-.5D0*Q2
A=H+H-Q1
H=D$GRT(DABS(A))
IF (A) 300,300,310
300 RR(IST)=H
RC(IST)=B
IST=IST+1
RR(IST)=H
RC(IST)=B
GO TO 320
310 B=M+DSIGN(B,H)
RR(IST)=Q1/B
RC(IST)=0.00
IST=IST+1
RR(IST)=H
RC(IST)=0.00
320 IST=IST+1
J=J-2
GO TO 90
330 IR=IR-1
340 A=0.00
DO 340 I=1,IR
Q1=C(I)
Q2=POL(I+1)
POL(I)=Q2
IF (Q1) 350,360,350
350 Q2=(Q1-Q2)/Q1
360 Q2=DARS(Q2)
IF (Q2-A) 380,380,370
370 A=Q2
380 CONTINUE
I=IK+1
POL(I)=1.00
RR(I)=A
RC(I)=0.00
IF (IER) 390,390,410
390 IF (A-EPS) 410,410,400
400 IER=-1
410 RETURN
420 IER=2
IR=0
RETURN
END

```

```

SUBROUTINE DPWFB (C,IC,G,LIM,IER)
DIMENSION C(1),G(1)
DOUBLE PRECISION A,H,AA,RR,CA,CB,CC,CD,A1,B1,C1,H,HH,Q1,Q2,Q3,
1Q42,WQ1,WQ2,DQ1,DQ2,EPS,EPS1,C,Q
IER=0
JC=IC+1
10 JC=J-1
IF (J-1) 400,400,20
20 IF (C(J)) 30,10,30
30 A=C(J)
IF (A-1.00) 40,60,40
40 DO 50 I=1,J
C(I)=C(I)/A
CALL OVEHFL (N)
IF (N-2) 400,50,50
50 CONTINUE
60 IF (J-3) 410,380,70
70 EPS=1.0-14
EPS1=1.0-6
EPS=0
LL=0
Q1=G(1)
Q2=G(2)
Q3=0.00
Q4=0.00
AA=C(1)
BB=C(2)
CH=DARS(AA)
CA=DARS(BB)
IF (LH=CA) 80,90,100
80 CC=CH+CA
CH=CH/CA
CA=1.00
GO TO 110
90 CC=CA+CB
CA=1.00
CB=1.00
GO TO 110
100 CC=CA+CB
CA=CA/CA
CB=1.00
110 CD=CC*.100
120 A=0.00
Q=A
A1ZA
R1ZA
IZJ
Q001=Q1
QWQ2=Q2
DQ1=MH
DQ2=MH
130 HZ=Q1*B-Q2*A+C(1)
CALL OVERFL (N)
IF (N-2) 420,140,140
140 BZA
AZH
IZI=1
IF (I-1) 180,150,160
150 HZ=0.00
160 HZ=Q1*B1-Q2*A1+H
CALL OVERFL (N)
IF (N-2) 420,170,170
170 C1ZB1
B1ZA1
A1ZH
GO TO 130
180 HZ=CA*DABS(A)+CB*DABS(B)
IF (LL) 190,190,390
190 LSL+}

```

```

      IF (DABS(A)-EPS>DABS(C(1))) 200,200,210
200  IF (DABS(B)-EPS>DABS(C(2))) 390,390,210
210  IF (H-C1) 220,220,230
220  AAZA
     BBZH
     CCZH
     GG1=U1
     GG2=U2
230  IF (L-LIM) 280,280,240
240  IF (H-C0) 430,430,250
250  IF (G(1)) 270,260,270
260  IF (G(2)) 270,420,270
270  G(1)=0.00
     G(2)=0.00
     GO TO 70
280  HH=UMAX1(DARS(A1)+DABS(B1)+DABS(C1))
     IF (HH) 420,420,290
290  A1=A1/HH
     H1=U1/HH
     C1=L1/HH
     H=A1+C1-H1*B1
     IF (H) 300,420,300
300  A=AA/MM
     B=BB/MM
     HH=(H-A-B)/H
     H=(A+C1-B)/H
     G1=U1+HH
     G2=U2+H
     IF (DABS(HH)-EPS>LAHS(Q1)) 310,310,330
310  IF (DARS(H)-EPS>DABS(Q2)) 320,320,330
320  LL=1
     GO TO 120
330  IF (L=1) 120,120,340
340  IF (DABS(HH)-EPS1>DABS(Q1)) 350,350,120
350  IF (DABS(H)-EPS1>UAHS(Q2)) 360,360,120
360  IF (DABS(UU61+HH)-DABS(Q1+DU1)) 370,440,440
370  IF (DABS(UU62+H)-UAHS(Q2+DQ2)) 120,440,440
380  Q(1)=C(1)
     Q(2)=C(2)
     Q(3)=0.00
     Q(4)=0.00
     RETURN
390  Q(1)=Q1
     Q(2)=Q2
     Q(3)=A
     Q(4)=B
     RETURN
400  IER=-1
     RETURN
410  IER=-2
     RETURN
420  IER=-3
     GO TO 440
430  IER=1
440  U(1)=UU1
     U(2)=UU2
     U(3)=AA
     U(4)=BB
     RETURN
END

```

```

SUBROUTINE TGHAD (JAY,KTHK,NLYR)
C ****=  

C SUBROUTINE 'TGHAU' FORMS THE MATRIX OF LINEAR EQUATIONS RESULTING  

C FROM THE LAYERED CLOUD STRUCTURE AND BOUNDARY CONDITIONS IMPOSED  

C BY THE SURROUNDING NON-SCATTERING MOLECULAR ATMOSPHERE IN LOCAL  

C THERMODYNAMIC EQUILIBRIUM. THE PRINCIPLE CALCULATIONS ARE  

C PERFORMED IN THIS ROUTINE WITH THE RESULTANT OUTPUT OF THE SPATIAL  

C DISTRIBUTION OF RADIANT INTENSITY ACCORDING TO THE DISCRETE RAYS  

C ('NG2') ABOVE AND BELOW THE CLOUD. VALUES FOR THE ZENITH ANGLES  

C 0 AND 90 DEG FOR THE TRANSMITTED AND REFLECTED RADIANCE ARE  

C EXTRAPOLATED FROM A LEAST-SQUARES POLY. FIT TO THE CALCULATIONS.  

C ****=  

C
PARAMETER LEV=40, INT=6, MZ=25, NG=16, NG2=8, NGLM=48
* ,NMUST=LEV+10 ,INT2=2*INT
REAL NU,LV,NBASE
DOUBLE PRECISION AX,DIFF,DIFNB,ENTENS,FNOR, FUNC,INTENS,LE,L1,ORT,
OSADA,PINO,PULI,KT,SADA,TAU,W,W1,W2,XPL,XXR,YPL,YYR,UM,A,
VALUES
COMMON /INPUT/ ALT(NMOST),TEMP(NMOST),PRE(NMOST),H2O(NMOST),
* THKNS(9),NTHICK,NBASE,TRN(NMOST,INT),NEWLEV(10)
* ,TAUABS(NMOST,INT),
COMMON /ANGLE/ UM(NG),A(NG),PI
COMMON /LBMULT/ UBC,ATMD,ATMR,ATMA,SFC,THRUSV(INT),THRUPR(INT),ITER
* ,ECB,IPCHAN(INT),CLUEM
COMMON /POLY/ PINO(NG)
COMMON /INDOU/ UP(NG2,INT),DW(NG2,INT),THETA(NG),NU(INT),LV(INT),
CK1(INT),CK2(INT),CUVERT(INT),CDVERT(INT)
COMMON /CLOUD/ TEMPC(10)
COMMON /EIGEN/ VALUES(INT,NG2)
COMMON /SFCEMS/ EMIS(INT),NB
COMMON /NEWLEV/ ADJM(10),NUMNEW,LVNUM
COMMON /FLAGS/ IFLAG(2)
COMMON /RADATA/ PINI(NG,INT),PT(INT),BEXT(INT)
DIMENSION YPL(NG),YYR(NG),INTENS(3,NG),POLI(NG,NG)
DIMENSION LE(NGLM),W1(NGLM,NGLM),W2(NGLM,NGLM),ACOSUM(NG)
DIMENSION SADA(NG,NG),OSADA(NG,NG),OPTH(9),W(NG,NG),L1(NGLM)
DIMENSION BINTC(3),TAU(3),ENTENS(3,NG),RT(NG),SAVE(INT2)
C
C DETERMINE EXTINCTION COEFFICIENTS
C
DO 10 I=1,NG2
  II=I+NG2
  RT(I)=VALUES(JAY,I)
  KT(II)=-KT(I)
  10 CONTINUE
C
C COMPUTE LEGENDRE POLYNOMIAL
C
DO 30 I=1,NG
  DO 20 L=1,NG
    L1=L-1
    XPL=UM(I)
    CALL LEP (YPL,XPL,L1)
    POLI(I,L)=YPL(L)
  20 CONTINUE
  30 CONTINUE

```

```

      DO 40 I=1,NG
      UMI=SNGL(UM(I))
      ACOSUM(I)=ACOS(UMI)
40 CONTINUE
C
C COMPUTE SADA
C
      DO 60 K=1,NG
      DO 50 L=1,NG
      L1=L-1
      XXR=RT(K)
      CALL DSAWA (YYR,XXR,L1)
      SADA(K,L)=YYR(L)
50 CONTINUE
60 CONTINUE
C
C FIND RIGHT W FOR THE SMALLEST ROOT
C
      IF (NG.LT.10) GO TO 170
      DO 160 NGS=NG2,NG2
      ORT=RT(NGS)
      IS=1
      COUNT=0.0
70 CONTINUE
      COUNT=COUNT+1.0
      RT(NGS)=ORT
      DO 90 L=1,NG
      L1=L-1
      XXR=RT(NGS)
      CALL DSAWA (YYR,XXR,L1)
      SADA(NGS,L)=YYR(L)
      IF (IS.EQ.1) GO TO 80
      SADA(NGS,L)=USADA(NGS,L)
80 CONTINUE
90 CONTINUE
      FUNC=0.0D0
      DO 110 I=1,NG
      W(I,NGS)=0.0D0
      DO 100 L=1,NG
      W(I,NGS)=W(I,NGS)+PINO(L)*POLI(I,L)*SADA(NGS,L)/(1.0D0+UM(I)*
      1RT(NGS))
100 CONTINUE
      FUNC=FUNC+A(I)*W(I,NGS)/2.0D0
110 CONTINUE
      DO 120 L=1,NG
      OSADA(NGS,L)=0.0D0
      DO 120 I=1,NG
120 OSADA(NGS,L)=OSADA(NGS,L)+A(I)*POLI(I,L)*W(I,NGS)/2.0D0
      FNOR=OSADA(NGS,1)
      DO 130 L=1,NG
      OSADA(NGS,L)=OSADA(NGS,L)/FNOR
      SADA(NGS,L)=OSADA(NGS,L)
130 CONTINUE
      IS=2
      ORT=(1.0D0-PINO(1))/OSADA(NGS,2)
      DIFF=1.0D0-FUNC
      DIFF=DABS(1.0D0-FNOR)
      IF (DIFF.LE.1.0E-7) GO TO 150
      IF (COUNT.GE.90.0) GO TO 140
      GO TO 70
140 WRITE (6,410) DIFF
      GO TO 400
150 CONTINUE

```

```

DO 160 L=1,NG
SADA(NGS,L)=0
160 CONTINUE
170 CONTINUE
DO 172 I=1,INT
J=I+INT
SAVE(I)=PT(I)
SAVE(J)=BEXT(I)
172 CONTINUE
BSCA=PT(JAY)+BEXT(JAY)
NBOT=NEWLEV(1)
NTOP=NEWLEV(KTHK+1)
DTAUAB=TAUABS(NBOT,JAY)-TAUABS(NTOP,JAY)
BABS=DTAUAB/THKNS(KTHK)
BEXT(JAY)=BEXT(JAY)+BABS
PT(JAY)=BSCA/BEXT(JAY)
PRINT 175,JAY,PT(JAY),BEXT(JAY)
OPTH(KTHK)=THKNS(KTHK)
GN=FLOAT(NLYR)
OPTHI=OPTH(KTHK)/GN
DO 180 I=1,NLYR
TAU(I)=DBLE(FLOAT(I)*OPTHI*BEXT(JAY))
180 CONTINUE
C VALUES OF W OF CHARACTERISTIC EQ. FOR SEARCHING THE EIGENVALUES.
C
DO 200 I=1,NG
DO 200 K=1,NG
W(I,K)=0.0D0
DO 190 LL=1,NG
W(I,K)=W(I,K)+PINO(LL)*POLI(I,LL)*SADA(K,LL)/(1.0D0+(UM(I))*RT(K))
190 CONTINUE
200 CONTINUE
C MAXIMUM DIMENSIONS OF SOLUTION MATRIX = NGL
NGL=NLYR*NG
DO 210 I=1,NGL
DO 210 K=1,NGL
W(I,K)=0.0D0
210 CONTINUE
C FOR W(-U)---CLOWW TOP BOUNDARY CONDITION, USE W(9,K) TO W(16,K)
DO 220 I=1,NG2
II=I+NG2
DO 220 K=1,NG
W(I,K)=W(II,K)
220 CONTINUE
IF (NLYR.EQ.1) GO TO 240
L1=NLYR-1
DO 230 L=1,L1
DO 230 I=1,NG
II=I+NG2+(L-1)*NG
DO 230 K=1,NG
KK=K+NG*(L-1)
NK=K+NG*L
W(II,KK)=W(I,K)*DEXP(-RT(K)*TAU(L))
W(I,K)=W(II,KK)
230 CONTINUE
240 CONTINUE

```

```

C FOR W(+U)---CLOUD BASE BOUNDARY CONDITION, USE W(1,K) TO W(8,K)
DO 250 I=1,NG2
II=I+NLXR+NG2+(NLXR-1)*NG2
DO 250 K=1,NG
KK=K+(NLXR-1)*NG
W1(I,KK)=W(I,K)*DEXP(-RT(K)*TAU(NLXR))
250 CONTINUE
DO 260 I=1,NGL
DO 260 K=1,NGL
W2(I,K)=W1(I,K)
260 CONTINUE
C EVALUATE THE 'L' COEFFICIENTS OF THE SOLUTIONS FOR INTEGRAL-
C DIFFERENTIAL TRANSFER EQUATION.
C THE CLOUD TEMPERATURE GRADIENT IS DETERMINED FROM ATMOSPHERIC PROFILE
C INPUT DATA.
C
HGT=THKNS(KTHK)
CALL TC (NLXR,OPTH1,HGT,JAY,KTHK)
DO 270 I=1,NLXR
U=NU(JAY)
BINTC(I)=TEMPC(I)
270 CONTINUE
DO 280 I=1,NG2
LI(I)=DBLE(DW(I,JAY)-BINTC(I))
C THE ARRAY 'LE' IS USED FOR EMISSIVITY CALCULATIONS IN WHICH THE
C UPWARD AND DOWNWARD INTENSITIES (UP,DW) OF THE MOLEC ATMOS
C ARE SET TO ZERO
C
LE(I)=DBLE(-BINTC(I))
280 CONTINUE
IF (NLXR,EQ,1) GO TO 300
DO 290 L=1,L1
DO 290 I=1,NG
II=I+NG2+(L-1)*NG
LI(II)=DBLE(BINTC(L+1)-BINTC(L))
LE(II)=LI(II)
290 CONTINUE
300 CONTINUE
DO 330 I=1,NG2
IF (NLXR,GT,1) GO TO 310
II=I+NG2
GO TO 320
310 II=I+NG2+(2*NLXR-1)
320 LI(II)=DBLE(UP(I,JAY)-BINTC(NLXR))
LE(II)=DBLE(-BINTC(NLXR))
330 CONTINUE
C COMPUTE UPWARD + DOWNWARD INTENSITIES
C THE MATRIX INVERSION WILL RETURN THE L - COEFFICIENTS
C
NTOT=NG*NLXR
CALL SIMU (W1,LI,NTOT,KS)
CALL SIMU (W2,LE,NTOT,KS)
C INTENSITY(I,J) IS FOR THE ITH LAYER - JTH ANGLE 'MU'
DO 380 I=1,NLXR
DO 370 J=1,NG2
JJ=J+NG2
INTENS(I,J)=0.0000
INTENS(I,JJ)=0.0000
ENTENS(I,J)=0.0000
ENTENS(I,JJ)=0.0000
370
380

```

```

DO 360 K=1,N6
NKEK
AX=DEXP(-RT(K)*TAU(I))
IF (I,NE.1) NKEK=N6*(I-1)
IF (I,GT.1) GO TO 340
INTENS(I,J)=INTENS(I,J)+LI(NK)*W(J,K)
ENTENS(I,J)=ENTENS(I,J)+LE(NK)*W(J,K)
GO TO 350
340 INTENS(I,J)=INTENS(I,J)+LI(NK)*W(J,K)*DEXP(-RT(K)*TAU(I-1))
ENTENS(I,J)=ENTENS(I,J)+LI(NK)*W(J,K)*DEXP(-RT(K)*TAU(I-1))
350 INTENS(I,JJ)=INTENS(I,JJ)+LI(NK)*W(JJ,K)*AX
ENTENS(I,JJ)=ENTENS(I,JJ)+LE(NK)*W(JJ,K)*AX
360 CONTINUE
INTENS(I,J)=INTENS(I,J)+DBLE(BINTC(I))
INTENS(I,JJ)=INTENS(I,JJ)+DBLE(BINTC(I))
ENTENS(I,J)=ENTENS(I,J)+DBLE(BINTC(I))
ENTENS(I,JJ)=ENTENS(I,JJ)+DBLE(BINTC(I))
370 CONTINUE
380 CONTINUE
1EMIS=1
ICCRAD=0
NDUM=1
JOUNT=3
C
C EXTRAPOLATE 'ENTENS' (FOR EMISSIVITY) VALUES AT THETA = 00, AND 90
IUPDN=0
CALL EXTRP0(THETA,ENTENS,TVERT,NDUM,JDUM,IUPDN)
CALL EXTRP9(THETA,ENTENS,THORIZ,NDUM,JDUM,IUPDN)
IF(ICDEM.GT.0.1) EMISS=TVERT/BINTC(1)
C
C EXTRAPOLATE 'INTENS' VALUES AT THETA = 0 AND 90 DEGREES FOR
C TRANSMITTED AND REFLECTED RADIANCE USED IN DETERMINING THE CLOUD
C TRANSMISSIVITY AND REFLECTIVITY
C THE EXTRAPOLATED CLEAR COLUMN RADIANCE(UP) FOR THETA=0 IS 'CUVERT'
C
1EMIS=0
CALL EXTRP0(THETA,INTENS,TVERT,NDUM,JDUM,IUPDN)
CALL EXTRP9(THETA,INTENS,THORIZ,NDUM,JDUM,IUPDN)
IUPDN=1
NDUM=3
CALL EXTRP0(THETA,INTENS,RVERT,NDUM,JDUM,IUPDN)
CALL EXTRP9(THETA,INTENS,RHORIZ,NDUM,JDUM,IUPDN)
IF(CUVERT(JAY),EQ.0) GO TO 384
TRANS=TVERT/CUVERT(JAY)
REFLT=RVERT/CUVERT(JAY)
384 THRUPT(JAY)=THRUPT(JAY)
IF(ITER,NE.0) GO TO 385
IF(CUVERT(JAY),NE.0) GO TO 383
THRUPT(JAY)=2.0
CUVERT(JAY)=RVERT
GO TO 385
383 THRUPT(JAY)=RVERT/CUVERT(JAY)
385 WRITE (6,420) JAY,NU(JAY)
WRITE (6,430) OPTH(KTHK),TAU(NLYR)
WRITE (6,440) TVERT,RHORIZ
DO 390 J=1,NG2
JU=N6+1-J
WRITE (6,450) THETA(J),INTENS(I,J),THETA(JJ),INTENS(NLYR,JJ)
390 CONTINUE

```

```

      YYY=INTENS(1,1)
      WRITE (6,460) THOR1Z,RVERT
      WRITE (6,470) EMISS,TRANS,REFLCT
      IF(CLUEM.GT.0.1) EMISSM=INTENS(1,1)/BINTC(2)
      WRITE (6,480) EMISSM,BINTC(2)
      CALL TEMTOP(TEMP,NBASE,KTHK,JAY,EMISSM,TVERT,YYY,
      INU(JAY),REFLCT)
      IF(JAY.NE.INT) GO TO 400
      IF(IFLAG(2).EQ.0) GO TO 400
      WRITE(20,1000) LNUM,IFLAG(2),NBASE,THKNS(KTHK)
      WRITE(20,1010) ((TAUABS(I,J),I=1,LNUM),J=1,INT)
      WRITE(20,1020) (TEMP(I),I=1,LNUM)
      WRITE(20,1020) (ALT(I),I=1,LNUM)
      WRITE(20,1010) (PINI(I,J),I=1,NG),J=1,INT)
      WRITE(20,1010) (BEXT(I),I=1,INT)
      WRITE(20,1010) (PT(I),I=1,INT)
 400  CONTINUE
  DO 405 I=1,INT
    J=I+INT
    PT(I)=SAVE(I)
    BEXT(I)=SAVE(J)
 405  CONTINUE
  RETURN
C
 175 FORMAT(1H0,'REVISED SINGLE SCAT ALBEDO AND BEXT FOR CHANNEL ',I2,
   * ',', ' SINGLE SCAT ALBEDO=',F5.3,2X,',BEXT=',F5.3)
 410 FORMAT(10X,'SSSS ITERATION FAILED SSSSS FIFF =',E20.14)
 420 FORMAT(//,'----SPECTRAL REGION',I2,'---- NU=',F6.4)
 430 FORMAT(32X,'CLOUD THICKNESS=',F6.2,'(KM) OPTICAL THICKNESS=',F8.5,/,36X,'THETA',6X,'UPWARD INTENSITY',5X,'THETA',5X,'DOWNWARD I
 2NTENSITY',/)
 440 FORMAT(36X,'0.0000',5X,F13.5,7X,'90.0000',5X,F13.5)
 450 FORMAT(36X,F8.4,5X,F13.5,5X,F9.4,5X,F13.5)
 460 FORMAT(37X,'90.0000',5X,F13.5,6X,'180.0000',5X,F13.5)
 470 FORMAT(1/20X,'EMISSIVITY= ',F9.6,5X,'TRANSMISSIVITY= ',F9.6,5X,'R
 1EFLECTIVITY= ',F9.6,/)
 480 FORMAT(1/10X,'MEAN EMISSIVITY = ',F9.6,
   1' CORRESPONDING TO T = ',F7.2,'DEG K')
 1000 FORMAT(2I2,2F10.5)
 1010 FORMAT(350E15,7)
 1020 FORMAT(50F10.5)
  END

```

```

SUBROUTINE TC (LA,OPTHI,HGT,JAY,KTHK)
C ****
C THIS SUBROUTINE CALCULATES THE CLOUD LAYER TEMPERATURES FROM THE
C INPUT ATMOSPHERIC TEMPERATURE PROFILE, HEIGHT OF CLOUD BASE, AND THE
C NUMBER OF ISOTHERMAL LAYERS APPROXIMATING THE TEMPERATURE GRADIENT
C ****
C
PARAMETER LEV=40, INT=6, MZ=25, NG=16, NG2=8, NMOST=LEV+10
REAL INBASE
COMMON/INPUT/ALT(1:NMOST),TEMP(NMOST),PHE(NMOST),H2O(NMOST),
* THKNS(9),NTHICK,1:BASE,TRN(NMOST,INT),NEWLEV(10)
* ,TAUARS(NMOST,INT)
COMMON /CLOUD/ TEMPc(10)
COMMON/LAMULT/UHC,ATMD,ATMR,ATMA,SFC,THRUSV(INT),THRUPT(INT),ITER
* ,ECA,IPCHAN(INT),CLDEM
DIMENSION TEMPNT(10)

C ASSUME LINEAR TEMP GRADIENT ....MONOTONICALLY DEC W/ HEIGHT
C
IUXBOT=NEWLEV(1)
IDXTOP=NEWLEV(KTHK+1)
TEMP1=TEMP(IDXTOP)*CLDEM
TEMP(LA)=TEMP(IUXBOT)*CLDEM
LT=TEMP(LA)-TEMP1
DZ=FLOAT(LA)-1.
LA1=LA-1
DO 10 I=2,LA1
TEMPc(I)=TEMPc(1)+(LT/DZ)*(FLOAT(I)-1)*CLDEM
10 CONTINUE
IF (JAY.GT.1) GO TO 30
WRITE (6,40)
DO 20 I=1,LA
TEMPNT(I)=TEMPc(I)-273.16
IF (I.EQ.1) WRITE (6,50) I,TEMPNT(I)
IF (I.EQ.LA) WRITE (6,60) I,TEMPNT(I)
IF (I.NE.1.AND.I.NE.LA) WRITE (6,70) I,TEMPNT(I)
20 CONTINUE
30 CONTINUE
RETURN
C
40 FORMAT (//,4RX,'CLOUD LAYER TEMPERATURES')
50 FORMAT (51X,I1,F7.2,' (TOP)')
60 FORMAT (51X,I1,F7.2,' (BASE)')
70 FORMAT (51X,I1,F7.2)
END

```

```

SUBROUTINE TEMTOP(TEMP,NRASE,KTHK,JAY,EMISSM,X,Y,U,REFLCT)
C THIS SUBROUTINE FINDS THE BRIGHTEST TEMPERATURE AT
C THE SATELLITE'S POINT OF VIEW IN A CLOUDY ATMOSPHERE
C
      PARAMETER LEV=40, INT=6, NMOST=LEV+10
      REAL NRASE
      COMMON/INPUT/ALT1(NMOST), TEMP1(NMOST), PRE(NMOST), H2O(NMOST),
     * THK(N), NTHICK,I,BASE1,TRN(NMOST,INT),NEWLEV(10)
     * ,TAUAHS(NMOST,INT)
      COMMON/NEWLEV/ADDHT(10), NUMNEW,LVNUM
      DIMENSION TAU(NMOST,INT), TEMP(NMOST), TEMTOP(2), TISFC(2), ANGMOD(2)
      EQUIVALENCE (TRN(1,1), TAU(1,1))
      HULT=1.38046E-16
      C=2.497929E10
      CONVKT=2.*HULT*C*(U**2)
      ANGMUL(1)=1.0
      ANGMUL(2)=1.01110
      TISFC(1)=X
      TISFC(2)=Y
      LEV1=LVNUM
      IF(JAY.NE.1) GO TO 60
      HU ISFC=NEWLEV(KTHK+1)
      ISFCF1=ISFC+1
      DO 100 L=1,2
      H1=TEMP(ISFC)
      TAU1=TAU(ISFC,JAY)*ANGMUL(L)
      TEMTOP(L)=0.0
      DO 90 K=ISFCP1,LEV1
      H2=TEMP(K)
      TAU2=TAU(K,JAY)*ANGMUL(L)
      TEMTOP(L)=TEMTOP(L)+0.5*(H1+H2)*(TAU2-TAU1)
      TAU1=TAU2
      90 H1=H2
      H2=TISFC(L)*TAU(ISFC,JAY)
      100 TEMTOP(L)=TEMTOP(L)+H2
      WRITE(6,400) TEMTOP(1),TFMTOP(2)
      400 FORMAT (/,1UX,' VERT. R. TEMP. =',F12.6,10X,'B.TEMP.AT 8.5 =',
     * F12.6,/)
      RETURN
      END

```

```

SUBROUTINE USADA (Y,X,N)
C GENERATION OF SADA FUNCTION
C
C
      DOUBLE PRECISION Y,X,PINU,FI,YII
      COMMON /POLY/ PINU(16)
      DIMENSION Y(1)
      Y(1)=1.0D0
      IF (N) 10,10,20
10   RETURN
20   Y(2)=-(1.0D0-PINU(1))/X
      IF (N-1) 10,10,30
30   DO 40 I=2,N
      A=I
      FI=DHLE(A)
      YII=(FI-1.0D0)/FI*Y(I-1)
      Y(I+1)=-(2.0D0*(FI-1.0D0)+1.0D0-PINU(I))/(FI*X)*Y(I)-YII
40   CONTINUE
      RETURN
      END

```

```

SUBROUTINE PFILE
C WRITE ATMOSPHERE PROFILES TO FILE 20
C
      PARAMETER LEV=40, NUMCHN=6,NMOST=LEV+10
      COMMON/INPUT/H(NMCST),T(NMOST),P(NMOST),H20(NMOST),THK(9),
     *LTHICK,NHASE,TRN(NMOST,NUMCHN),NEWLLV(10)
      COMMON/FREQ/FNU(NUMCHN)
      COMMON/NELEV/ADDT(10),NUMNEW,LVNUM
      COMMON/SFCEMS/EMIS(NUMCHN)
      DIMENSION TH(NMOST,NUMCHN),HT(NMOST),TP(NMOST)

      ISTAT=NERTRN(6,'WASG,AX 20.,F/0/TRK/100 . ')
      PRINT 200,ISTAT
200  DO 50 J=LVNUM+1,-1
      K=LVNUM-J+1
      H(K)=H(J)
      T(K)=T(J)
      DO 50 J=1,7
      L=J
      IF(J.GT.4) L=4-J+J*INT(S/J)
      TR(K,L)=TH(N,J)
50   CONTINUE

      PRINT 400,(FNU(J),J=1,NUMCHN)
      DO 100 I=1,LVNUM
      WRITE(20,300),HT(I),TP(I),H20(I),(TR(I,J),J=1,NUMCHN)
      PRINT 500,HT(I),T(I),H20(I),(TR(I,J),J=1,NUMCHN)
100  CONTINUE
300  FORMAT(1H1,'STATIS OF ASSIGN FOR FILE 20. = ',I3)
300  FORMAT(F7.3,F6.1,F7.3,2X,7F13.6)
400  FORMAT(1H1,'HEIGHT TEMP H20    ',2X,7(' TAU(''F5.2,'''))
500  FORMAT(1A,F7.3,F6.1,F7.3,2X,7F13.6)
      RETURN
      END

```

BLOCK DATA

C DATA OF ANTENNA GAIN OF RADIOMETER, AND CLIMATOLOGICAL PROFILS
C OF TEMPERATURE, HUMIDITY, AND WINDS.

```
PARAMETER NUMLV=40, NMOST=NUMLV+10, NUMCHN=6
COMMON/PRES/ P(NMOST)
COMMON/FREQ/FNU(NUMCHN)
COMMON/TANOW/T(NMOST),W(NMOST)
COMMON/HANDU/H(NMOST),U(NMOST)
COMMON/GAIN/GANT(127:NUMCHN)
DATA (P(I),I=1:NUMLV)/
* .10.2,.5.1,.1.5.2,.3.4.5,.7.10.15.20.25.30.50.60. .
* 70.,45.,100.,115.,135.,150.,200.,250.,300.,350.,400.,430.,475. ,
* 500.,570.,620.,670.,700.,780.,850.,920.,950.,1000./
DATA FNU/22.235,31.65,52.85,53.85,55.45,37.00/
DATA(GANT(I,1),I=1:127)/ 63*0. ,
* 96.5, 93.7, 85.3, 78.9, 63.9, 51.7, 38.5, 28.2, 18.9,
* 11.7, 6.12, 1.53, 1.39, 3.21, 3.60, 3.64, 2.51, 1.33,
* 0.065, 0.889, 1.43, 1.31, 1.05, 0.355, 0.124, 0.707, 0.9,
* 0.846, 0.556, 0.431, 0.695, 0.875, 0.984, 0.873, 0.703, 0.455,
* 0.279, 0.364, 0.584, 0.707, 0.865, 0.733, 0.549, 0.361, 0.153,
* 0.125, 0.321, 0.539, 0.565, 0.513, 0.457, 0.309, 0.279, 0.215,
* 0.347, 0.409, 0.520, 0.544, 0.621, 0.594, 0.645, 0.539, 0.477,
* 0.422 /

DATA(GANT(I,2),I=1:127)/ 63*0. ,
* 96.5, 93.7, 85.3, 78.9, 63.9, 51.7, 38.5, 28.2, 18.9,
* 11.7, 6.12, 1.53, 1.39, 3.21, 3.60, 3.64, 2.51, 1.33,
* 0.065, 0.889, 1.43, 1.31, 1.05, 0.355, 0.124, 0.707, 0.9,
* 0.846, 0.556, 0.431, 0.695, 0.875, 0.984, 0.873, 0.703, 0.455,
* 0.279, 0.364, 0.584, 0.707, 0.865, 0.733, 0.549, 0.361, 0.153,
* 0.125, 0.321, 0.539, 0.565, 0.513, 0.457, 0.309, 0.279, 0.215,
* 0.347, 0.409, 0.520, 0.544, 0.621, 0.594, 0.645, 0.539, 0.477,
* 0.422 /

DATA(GANT(I,3),I=1:127)/ 63*0. ,
* 96.5, 93.7, 85.3, 78.9, 63.9, 51.7, 38.5, 28.2, 18.9,
* 11.7, 6.12, 1.53, 1.39, 3.21, 3.60, 3.64, 2.51, 1.33,
* 0.065, 0.889, 1.43, 1.31, 1.05, 0.355, 0.124, 0.707, 0.9,
* 0.846, 0.556, 0.431, 0.695, 0.875, 0.984, 0.873, 0.703, 0.455,
* 0.279, 0.364, 0.584, 0.707, 0.865, 0.733, 0.549, 0.361, 0.153,
* 0.125, 0.321, 0.539, 0.565, 0.513, 0.457, 0.309, 0.279, 0.215,
* 0.347, 0.409, 0.520, 0.544, 0.621, 0.594, 0.645, 0.539, 0.477,
* 0.422 /

DATA(GANT(I,4),I=1:127)/ 63*0. ,
* 96.5, 93.7, 85.3, 78.9, 63.9, 51.7, 38.5, 28.2, 18.9,
* 11.7, 6.12, 1.53, 1.39, 3.21, 3.60, 3.64, 2.51, 1.33,
* 0.065, 0.889, 1.43, 1.31, 1.05, 0.355, 0.124, 0.707, 0.9,
* 0.846, 0.556, 0.431, 0.695, 0.875, 0.984, 0.873, 0.703, 0.455,
* 0.279, 0.364, 0.584, 0.707, 0.865, 0.733, 0.549, 0.361, 0.153,
* 0.125, 0.321, 0.539, 0.565, 0.513, 0.457, 0.309, 0.279, 0.215,
* 0.347, 0.409, 0.520, 0.544, 0.621, 0.594, 0.645, 0.539, 0.477,
* 0.422 /
```

```

DATA(GANT(I,5),I=1,127)/ 63*0..
* 96.5, 93.7, 85.3, 78.9, 63.9, 51.7, 38.5, 28.2, 18.9,
* 11.7, 6.12, 1.53, 1.39, 3.21, 3.60, 3.64, 2.51, 1.33,
* 0.065, 0.8A9, 1.43, 1.31, 1.05, 0.355, 0.124, 0.707, 0.9,
* 0.846, 0.556, 0.431, 0.695, 0.875, 0.984, 0.873, 0.703, 0.455,
* 0.279, 0.364, 0.564, 0.707, 0.865, 0.733, 0.549, 0.361, 0.153,
* 0.125, 0.321, 0.539, 0.565, 0.513, 0.457, 0.309, 0.279, 0.215,
* 0.347, 0.409, 0.520, 0.544, 0.621, 0.594, 0.645, 0.539, 0.477,
* 0.422 /

DATA(GANT(I,6),I=1,127)/ 63*0..
* 96.5, 93.7, 85.3, 78.9, 63.9, 51.7, 38.5, 28.2, 18.9,
* 11.7, 6.12, 1.53, 1.39, 3.21, 3.60, 3.64, 2.51, 1.33,
* 0.065, 0.8A9, 1.43, 1.31, 1.05, 0.355, 0.124, 0.707, 0.9,
* 0.846, 0.556, 0.431, 0.695, 0.875, 0.984, 0.873, 0.703, 0.455,
* 0.279, 0.364, 0.564, 0.707, 0.865, 0.733, 0.549, 0.361, 0.153,
* 0.125, 0.321, 0.539, 0.565, 0.513, 0.457, 0.309, 0.279, 0.215,
* 0.347, 0.409, 0.520, 0.544, 0.621, 0.594, 0.645, 0.539, 0.477,
* 0.422 /

DATA (T(I),I=1,NUMLV) /
* 22h.2, 244.2, 256.7, 266.2, 262.2, 258.2, 251.2, 246.2, 242.2,
* 235.2, 231.2, 227.2, 223.2, 221.2, 219.2, 214.2, 215.2, 212.2,
* 211.2, 209.2, 216.3, 216.3, 216.3, 218.4, 225.5, 233.4, 240.4,
* 251.7, 255.4, 259.9, 262.2, 268.4, 272.4, 276.2, 278.3, 283.6,
* 247.5, 290.7, 291.8, 293.6/

DATA (W(I),I=1,NUMLV) /
* 20*0., .6669E-3,
* 0.4156E-3, .9703E-3, .4807E-2, .3021E-1, .8973E-1, .1703E-0, .2957E00,
* 0.3468E00, .5653E00, .6897E00, .1204E+1, .1808E+1, .2639E+1, .3138E+1,
* 0.5306E+1, .7582E+1, .1010E+2, .1140E+2, .1348E+2/

DATA (H(I),I=1,NUMLV) /
* 66.25, 61.28, 54.30, 48.85, 45.60, 43.35, 40.24, 38.27,
* 37.16, 34.14, 31.79, 28.93, 27.10, 25.53, 24.20, 20.89,
* 19.71, 16.73, 17.48, 16.44, 15.55, 14.54, 13.88, 12.08,
* 10.59, 9.358, 8.268, 7.465, 6.930, 6.186, 5.796, 4.773,
* 4.102, 3.472, 3.116, 2.228, 1.505, .8297, .5533, .1113/

END

```